ETHYLBENZENE DEHYDROGENATION TO STYRENE OVER MESOPOROUS MIXED OXIDE CATALYSTS: SYNTHESIS, CHARACTERIZATION AND KINETIC MODELING

BY

LUQMAN ABIOLA ATANDA

A Thesis Presented to the
DEANSHIP OF GRADUATE STUDIES

KING FAHD UNIVERSITY OF PETROLEUM & MINERALS
DHAHRAN, SAUDI ARABIA

In Partial Fulfillment of the
Requirements for the Degree of

MASTER OF SCIENCE
In
CHEMICAL ENGINEERING

MAY 2011

KING FAHD UNIVERSITY OF PETROLEUM & MINERALS
DHAHRAN 31261, SAUDI ARABIA

DEANSHIP OF GRADUATE STUDIES

This thesis, written by Atanda Luqman Abiola under the direction of his thesis advisor and approved by his thesis committee, has been presented to the Dean of Graduate Studies, in partial fulfillment of the requirement for the degree of MASTER OF SCIENCE IN CHEMICAL ENGINEERING.

Thesis Committee

Dr. Sulaiman Al-Khattaf
(Thesis Advisor)

U.A. Al-Mub

Dr. Usamah Al-Mubaiyedh
(Department Chairman)

Dr. Nabil Al-Yassir
(Member)

Dr. Salam A. Zummo
(Dean of Graduate Studies)

24/7/11

Date

Dr. Muhammed Ba-Shammakh
(Member)

DEDICATION

This work is dedicated to my late father, Atanda Adeyinka, to my mother, Atanda Serifat and the entirety of my loving family for their immeasurable love, moral and financial support.

ACKNOWLEDGEMENT

First and foremost I am grateful to Allah (SWT), the Lord of the worlds, for giving me life to accomplish this far. To Him belongs all praise in the Heavens and on Earth.

I am heartily grateful to my supervisor, Dr Sulaiman Al-Khattaf, whose encouragement, guidance and support from the initial to the final level enabled me to develop an understanding of the subject. I would like to thank other members of my committee, Dr. Nabil Al-Yassir for his numerous contributions of his expertise and Dr. Mohammed Ba-Shammakh for the assistance he provided at all levels of the research project. I would like to thank Mr. Mariano Gica who greatly helped out on the experimental work.

To my parents, brothers (Hakeem, Nurudeen), and sister (Anifat), I am deeply appreciative of your patience, encouragement and love throughout the study.

I also want to offer my regards and appreciation to all of those who supported me in any respect during the completion of the project.

In conclusion, I recognize that this research would not have been possible without the financial assistance of KACST, the Center for Refining and Petrochemicals, King Fahd University of Petroleum & Minerals Graduate Studies (Graduate Research Assistanship), and the Department of Chemical Engineering.

TABLE OF CONTENT

DEDICATION ……………………………………………………………… iii

ACKNOWLEDGEMENT ……………………………………………………… iv

TABLE OF CONTENT ………………………………………………………… v

LIST OF TABLES ……………………………………………………………….. ix

LIST OF FIGURES …………………………………………………………… xi

THESIS ABSTRACT ………………………………………………………… xiv

THESIS ABSTRACT (ARABIC) ……………………………………………….. xv

CHAPTER 1 ………………………………………………………………… 1

1.0 INTRODUCTION ………………………………………………………….. 1

1.1. BACKGROUND ………………………………………………………... 1

1.2. MAIN INDUSTRIAL TECHNOLOGIES FOR STYRENE PRODUCTION …. 4

1.2.1. Catalytic dehydrogenation of ethylbenzene ………………………. 4

1.2.2. Styrene and propylene oxide (SMPO) process ……………………. 7

1.3. OTHER TECHNOLOGIES ………………………………………………… 9

1.3.1. Styrene production from ethane and benzene ……………………... 9

1.3.2. Styrene production from methanol and toluene …………………... 9

1.4. MOTIVATION ……………………………………………………….…... 10

1.5. THESIS OBJECTIVES ……………………………………………….…... 12

1.5.1. Synthesis and characterization of hydrotalcites and mesoporous iron oxide – alumina catalysts ……………………………………….. 12

1.5.2. Catalysts test performance ………………………………………… 12

1.5.3. Kinetic Modeling ………………………………………………….. 13

1.6. THESIS OUTLINE …………………………………………………………… 13

CHAPTER 2 ……………………………………………………………………… 15

2.0 LITERATURE REVIEW ……………………………………………….. 15

2.1. INTRODUCTION ……………………………………………………………... 15

2.2. CATALYSTS FOR ETHYLBENZENE DEHYDROGENATION …………….. 17

2.3. CATALYST DEACTIVATION ………………………………………………… 19

2.4. REACTION KINETICS AND MECHANISMS ……………………………... 21

2.5. CATALYST DEVELOPMENT FOR ETHYLBENZENE DEHYDROGENATION ……………………………………………………… 23

2.5.1. Hydrotalcites ………………………………………………………. 23

2.5.2. Mesoporous alumina doped with iron …………………………….. 29

CHAPTER 3 ……………………………………………………………………… 32

3.0 EXPERIMENTAL SECTION ………………………………………….... 32

3.1. EXPERIMENTAL SET-UP …………………………………………………... 32

3.1.1. Riser simulator ……………………………………………………….. 35

3.1.2. Gas chromatography (GC) system ………………………………... 37

3.1.3. Coke Analyzer ……………………………………………………….. 39

3.2. EXPERIMENTAL PROCEDURE …………………………………………… 40

3.2.1. Materials …………………………………………………………….... 40

3.2.2. Catalyst preparation ……………………………………………….. 40

3.2.2.1. Synthesis of hydrotalcite catalysts ………………………… 40

3.2.2.2. Synthesis of mesoporous alumina doped with iron ……….. 41

3.2.3. Catalyst characterization …………………………………………... 42

3.3. GC CALIBRATION …………………………………………………………….. 44

3.3.1. Determination of retention time for the different components ……. 44

3.3.2. Correlating GC response and actual weight percentage of each compound ……………………………………………………………. 44

3.4. CATALYST EVALUATION ………………………………………………… 44

3.4.1. Testing procedure …………………………………………………. 45

3.5. COKE ANALYSIS …………………………………………………………. 46

CHAPTER 4 ……………………………………………………………………. 47

4.0 RESULTS AND DISCUSSIONS ………………………………………... 47

4.1. ETHYLBENZENE DEHYDROGENATION OVER HT PRECURSORS OF $Mg_3Fe_{0.25}Me_{0.25}Al_{0.5}$ (*Me* = Co, Mn and Ni) CATALYSTS …………….......... 47

4.1.1. Physico-chemical properties ………………………………………. 47

4.1.1.1. Chemical composition and textural properties ……………. 47

4.1.1.2. Surface analysis of the catalysts …………………………... 50

4.1.1.3. Bulk phase identification ………………………………….. 50

4.1.1.4. Reducibility of the active specie on the catalysts ………… 52

4.1.2. Catalytic activity …………………………………………………... 54

4.1.2.1. Styrene/Benzene Selectivity ………………………………. 60

4.1.2.2. Styrene/Benzene Yield ……………………………………. 63

4.1.3. Coke Content Measurement ………………………………………. 65

4.1.4. Kinetic Modeling ………………………………………………….. 67

4.1.4.1. Model development ……………………………………….. 67

4.1.4.2. Catalyst activity decay function based on reactant

conversion (RC) ………………………………………………... 68
4.1.4.3. Catalyst activity decay function based on time-on-stream (TOS) ……………………………………………………... 72
4.1.4.4. Determination of model parameters ………………………. 73
4.2. ETHYLBENZENE DEHYDROGENATION OVER Fe_2O_3/Al_2O_3 …………….. 82
4.2.1. Catalyst characterization …………………………………………... 82
4.2.1.1. N_2 adsorption-desorption isotherm ………………………... 82
4.2.1.2. X-ray diffraction patterns …………………………………. 85
4.2.1.3. Transmission electron microscopy ………………………... 87
4.2.2. Catalyst activity …………………………………………………… 89
4.2.3. Kinetic Modeling ………………………………………………….. 97
4.2.3.1. Model development ……………………………………….. 97
4.2.3.2. Determination of model parameters ………………………. 102
CHAPTER 5 ………………………………………………………………… 109
5.0 CONCLUSION AND RECOMMENDATIONS ……………………….. 109
5.1. Conclusions ……………………………………………………………. 109
5.2. Recommendations ……………………………………………………... 110
APPENDIX ………………………………………………………………….. 111
NOMENCLATURE ………………………………………………………... 113
REFERENCES ……………………………………………………………... 115
VITAE ……………………………………………………………………….. 122

LIST OF TABLES

Table 4.1 Specific surface area, metal composition, and XPS analytical data of $Mg_3Fe_{0.25}Me_{0.25}Al_{0.5}$ (Me = Co, Mn and Ni) ………………………………………. 48

Table 4.2 Product distribution at various reaction conditions for the dehydrogenation of ethylbenzene over $Mg_3Fe_{0.25}Co_{0.25}Al_{0.5}$ mixed oxides catalyst 55

Table 4.3 Product distribution at various reaction conditions for the dehydrogenation of ethylbenzene over $Mg_3Fe_{0.25}Mn_{0.25}Al_{0.5}$ mixed oxides catalyst 56

Table 4.4 Product distribution at various reaction conditions for the dehydrogenation of ethylbenzene over $Mg_3Fe_{0.25}Ni_{0.25}Al_{0.5}$ mixed oxides catalyst . 57

Table 4.5 Coke formation of Ethylbenzene dehydrogenation reaction at different reaction conditions ……………………………………………………………… 66

Table 4.6 Estimated kinetic parameters for hydrotalcite mixed oxides catalyst based on reactant conversion model ………………………………………………. 74

Table 4.7 Correlation matrix for ethylbenzene dehydrogenation over hydrotalcite mixed oxides catalyst (RC model) ……………………………………………… 75

Table 4.8 Estimated kinetic parameters for hydrotalcite mixed oxides catalyst based on time-on-stream model ………………………………………………… 77

Table 4.9 Correlation matrix for ethylbenzene dehydrogenation over hydrotalcite mixed oxides catalyst (TOS model) ……………………………………………. 78

Table 4.10 Physical and structural properties of Fe_2O_3/Al_2O_3 ……………………. 84

Table 4.11 Product distribution at various reaction conditions for the dehydrogenation of ethylbenzene over 21%Fe-meso.Al_2O_3 (one pot) catalyst …... 90

Table 4.12 Product distribution at various reaction conditions for the dehydrogenation of ethylbenzene over 21%Fe/meso.Al_2O_3 (impregnation) catalyst ………………………………………………………………………….. 91

Table 4.13 Product distribution at various reaction conditions for the dehydrogenation of ethylbenzene over 21%Fe-con.Al_2O_3 (impregnation) catalyst.. 92

Table 4.14 Effects of reaction temperature on catalytic properties of iron doped mesoporous alumina catalysts …………………………………………………….. 96

Table 4.15 Estimated kinetic parameters for all the Fe_2O_3/Al_2O_3 catalyst based on reactant conversion model (Mechanism I) ……………………………………... 103

Table 4.16 Correlation matrix for ethylbenzene dehydrogenation over all the Fe_2O_3/Al_2O_3 catalyst based on reactant conversion model (Mechanism I) ……….. 104

Table 4.17 Estimated kinetic parameters for all the Fe_2O_3/Al_2O_3 catalyst based on reactant conversion model (Mechanism II) …………………………………….. 105

Table 4.18 Correlation matrix for ethylbenzene dehydrogenation over all the Fe_2O_3/Al_2O_3 catalyst based on reactant conversion model (Mechanism II) ……… 106

Table A3.1 Retention time of different compounds in the GC …………………… 112

LIST OF FIGURES

Figure 1.1a Global styrene capacity (2008) …………………………………….. 3

Figure 1.1b Global styrene consumption (2008) ……………………………….. 3

Figure 1.2 Lummus/UOP Classic SM process of adiabatic ethylbenzene dehydrogenation plant ……………………………………………………….. 6

Figure 1.3 Simplified flow diagram of the SMPO process ……………………….. 8

Figure 2.1 Reaction scheme of catalytic dehydrogenation of ethylbenzene ……… 16

Figure 2.2 Schematic life cycle of a prototype catalyst without any promoter additives ………………………………………………………………… 20

Figure 2.3 Structure of hydrotalcite ……………………………………………….. 25

Figure 2.4 The dehydrogenation of ethylbenzene over $Mg_2Fe_xAl_{1-x}$ mixed oxides catalysts ○ethylbenzene conversion; ●styrene selectivity; ■benzene selectivity; ▲toluene selectivity ……………………………………………………… 28

Figure 3.1 Schematic diagram of the riser simulator experimental set-up ……….. 34

Figure 3.2a Schematic diagram of the riser simulator …………………………….. 36

Figure 3.2b Cross section of the riser simulator displaying the unit components … 36

Figure 3.3 Schematic diagram of the gas chromatograph ………………………… 38

Figure 4.1 Pore size distribution of $Mg_3Fe_{0.25}Me_{0.25}Al_{0.5}$, where *Me* = Co (A), Mn (B), and Ni (C) ……………………………………………………………….. 49

Figure 4.2 XRD patterns of $Mg_3Fe_{0.25}Me_{0.25}Al_{0.5}$ (*Me* = Co (a), Mn (b) and Ni (c)) after A) drying and B) calcination at 550 °C (■: Hydrotalcites; ♦: unknown and ▼: periclase) 51

Figure 4.3 H_2-TPR of $Mg_3Fe_{0.25}Me_{0.25}Al_{0.5}$ (*Me* = Co, Mn, and Ni) catalysts. a)

Mg_3Fe_1; b) $Mg_3Fe_{0.5}Al_{0.5}$; c) $Mg_3Fe_{0.25}Mn_{0.25}Al_{0.5}$; d) $Mg_3Fe_{0.25}Co_{0.25}Al_{0.5}$; and f) $Mg_3Fe_{0.25}Ni_{0.25}Al_{0.5}$ …………………………………………………………... 53

Figure 4.4 Conversion of ethylbenzene with respect to time at various temperatures over different hydrotalcite mixed oxides; A) $Mg_3Fe_{0.25}Co_{0.25}Al_{0.5}$, B) $Mg_3Fe_{0.25}Mn_{0.25}Al_{0.5}$, and C) $Mg_3Fe_{0.25}Ni_{0.25}Al_{0.5}$ ………………………………… 58

Figure 4.5 Conversion of ethylbenzene with respect to time at 500 °C, comparison between commercial and HT catalysts ………………………………. 59

Figure 4.6 Product selectivity of ethylbenzene dehydrogenation over the different catalysts at ~ 6% ethylbenzene conversion ……………………………………….. 61

Figure 4.7 Selectivity with respect to conversion and temperature for $Mg_3Fe_{0.25}Mn_{0.25}Al_{0.5}$ ………………………………………………………………. 62

Figure 4.8 Styrene (A) and benzene (B) yields vs. ethylbenzene conversion at various temperatures for $Mg_3Fe_{0.25}Mn_{0.25}Al_{0.5}$ ……………………………………. 64

Figure 4.9 Overall comparisons between the experimental results and model predictions of all HTs catalysts for scheme 1: A) RC model, B) TOS model …….. 81

Figure 4.10 N_2 adsorption-desorption isotherm …………………………………... 83

Figure 4.11a XRD pattern of pure alumina support ………………………………. 86

Figure 4.11b XRD pattern of 21%Fe doped on alumina support …………………. 86

Figure 4.12a Mesoporous alumina doped with iron ………………………………. 88

Figure 4.12b Conventional alumina doped with iron ……………………………... 88

Figure 4.13 Comparison of styrene yield for all reaction temperatures over Fe_2O_3/Al_2O_3 ……………………………………………………………………….. 93

Figure 4.14 Effect of reaction condition on ethylbenzene conversion (Mechanism

I) over: A) 21%Fe-meso.Al_2O_3 (one-pot), B) 21%Fe/meso.Al_2O_3 (impregnation), C) 21%Fe-con.Al_2O_3 (impregnation) …………………………………………….. 95

Figure 4.15 Overall comparison between the experimental results and model predictions of all the catalysts for: A) scheme 2, B) scheme 3 …………………… 108

THESIS ABSTRACT

Name: **ATANDA LUQMAN ABIOLA**

Title of Study: **ETHYLBENZENE DEHYDROGENATION TO STYRENE OVER MESOPOROUS MIXED OXIDE CATALYSTS: SYNTHESIS, CHARACTERIZATION AND KINETIC MODELING**

Degree: **MASTER OF SCIENCE**

Major Field: **CHEMICAL ENGINEERING**

Date of Degree: **May, 2011**

A steamless process for ethylbenzene dehydrogenation to styrene was studied in a fluidized bed reactor over mesoporous mixed oxides based catalysts. Experimental runs were carried out over hydrotalcite and Fe_2O_3 supported on Al_2O_3 catalysts in a riser simulator at different operating conditions. The reaction temperature was varied in the range of 350–550 °C, and the reaction time was varied from 5-20 seconds. Both catalyst systems were significantly active for the ethylbenzene dehydrogenation reaction. This behaviour is ascribed to the high surface area and porosity of the catalysts which enhaced the diffusion of reactant molecules into and the reaction products out of the catalyst pores. This is also coupled with the effective catalytic cycle due to mixed acidic-basic sites and reduction-oxidation reaction of the active specie. A kinetic model was derived to better understand the reaction behaviour. Modeling of the experimental results was based on both reactant conversion (RC) and time-on-stream (TOS) models.

THESIS ABSTRACT (ARABIC)

ملخص البحث

الاسم: لقمان اتاندا ابيولا

عنوان البحث: اعادة هدرجة ايثيل البنزين الى الاستيرين فوق الحفازات: اصطناع و نموزج حركي

الدرجة: ماجستير العلوم

المجال العام: الهندسة الكيميائية

تاريخ منح الدرجة: مايو 2011

تمت دراسة انتاج الاستيرين في مفاعل الطبقه المتميعه عن طريق اعادة هدرجة ايثيل البنزين بدون بخار الماء تم اجراء التجارب باستخدام حفازات الهيدروتالسيت و اكسيد الحديد المدعم بالالومنيا في مفاعل تجريبي رافع و تحت ظروف تشغيل مختلفه تم دراسة مدى درجة حرارة التشغيل بين 350 و550 درجه مئويه بزمن تفاعل من 5 الى 20 ثانيه تحليل ناتج التفاعل بواسطة كروماتوغرافيا الغاز اظهر ان الناتج الرئيس هو الاستيرين و وجد ان نوعي الحفاز نشطان لاعادة هدرجة ايثيل البنزين هزا النشاط يعزى لمساحة السطح الكبيره و النفازيه للعوامل الحفازه التي تساعد على تحسين انتشار جزيئات المتفاعل الداخله لمسامات الحفاز بالاضافه الى جودة دورة الحفاز نسبة لوجود نقاط نشطه حامضيه و قاعديه و تفاعل الاكسده و الاختزال الدوري للنقاط النشطه تم تطوير نموزج لحركية التفاعل لفهم ميكانيكية التفاعل بناء على معدل تحول المتفاعلات الى نواتج و نموزج زمن التفاعل الداخلي

CHAPTER 1

1.0 INTRODUCTION

1.1. Background

Styrene is one of the most important monomers in modern petrochemical industry. The market has grown from around 20 million tons in 2000 and is expected to reach around 28 million tons in 2010 [1]. However, prior to World War II, the styrene industry, which uses ethylbenzene as a starting material was relatively insignificant. The tremendous demand for synthetic styrene – butadiene rubber (SBR) during the war prompted accelerated technology improvements and capacity expansion. The styrene process was developed in the 1930s by BASF (Germany) and Dow Chemical (USA) and this effort have led to the construction of several large-scale factories, and styrene production became a significant industry.

Styrene is a basic building block in making a variety of materials, most recognizable is polystyrene. Other materials include acrylonitrile-butadiene styrene (ABS) plastic, styrene-acrylonitrile (SAN) plastic, styrene-butadiene rubber (SBR), unsaturated polyester resins and expanded polystyrene foam (EPS). These materials can further be transformed to produce variety of products across a wide range of industries as there is no direct end use for styrene. Products made from styrene are of high performance, durable, safety, value and high quality [1]. Many of these products offer very good insulation qualities and the ability to be recycled. These products range from packaging materials to a myriad of consumer electronics, construction, transportation and medical applications. Therefore, styrene production is done indeed in a large scale that follows those of ethylene, propylene and vinyl chloride. The global styrene capacity in 2008 is 26million tons per year. The global distribution of the styrene production facilities is shown in Figure 1.1a. while global distribution of styrene consumption by product is shown in Figure 1.1b [2].

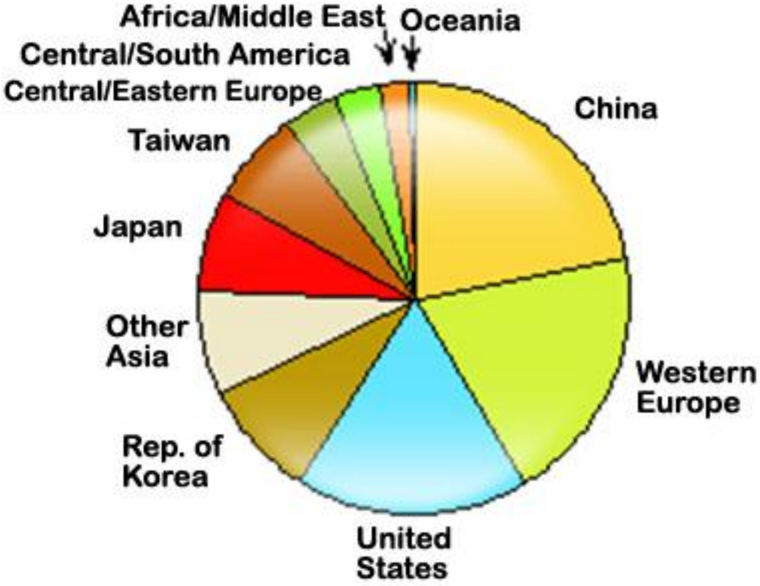

Figure 1.1a. Global styrene capacity (2008)

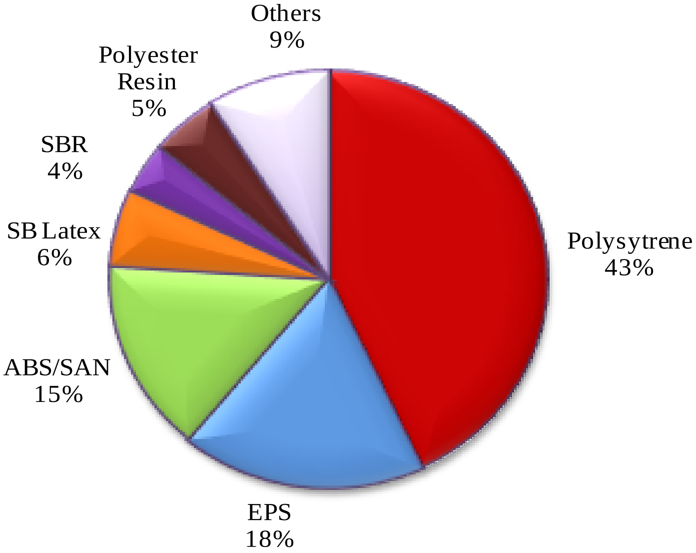

Figure 1.1b. Global styrene consumption (2008)

1.2. Main Industrial Technologies for styrene production

Industrially, styrene is produced mainly through two process routes: dehydrogenation of ethylbenzene and co-production with propylene oxide in a process known as SM/PO (Styrene Monomer/Propylene Oxide) or POSM. Both routes use ethylbenzene (EB) as the intermediate, EB is first made by the catalytic alkylation of benzene with ethylene, using either aluminium chloride or, more recently, zeolite catalysts [3]. Ethylbenzene and styrene units are almost always installed together with matching capacities because nearly all of the ethylbenzene produced commercially is converted to styrene. Alkylation is exothermic and dehydrogenation is endothermic, as a result energy economy in a typical ethylbenzene-styrene complex is achieved by integrating the energy flows of the two units.

1.2.1. Catalytic Dehydrogenation of Ethylbenzene

This route accounts for 90% of the total world production. Dehydrogenation of ethylbenzene can be run industrially using either multiple bed adiabatic or tubular isothermal reactors in which the reactants are passed over the catalyst bed employing radial or axial flow. In this process, EB is dehydrogenated to styrene in the presence of potassium promoted iron oxide catalyst and a super-heated steam was fed to supply the heat of endothermic dehydrogenation and further to suppress the coking. Formations of by-products are suppressed by reducing the partial pressure of the reaction. Generally, adiabatic dehydrogenation in multiple bed reactors is preferred but both methods are used. This process is employed by the Lummus/UOP Classic Smart [4]. Typical conversions up to 69%, styrene selectivity of more than 97 mol% and a styrene monomer purity of 99.85 wt% are achieved. Flow scheme of a typical Lummus/UOP adiabatic ethylbenzene dehydrogenation plant is shown below:

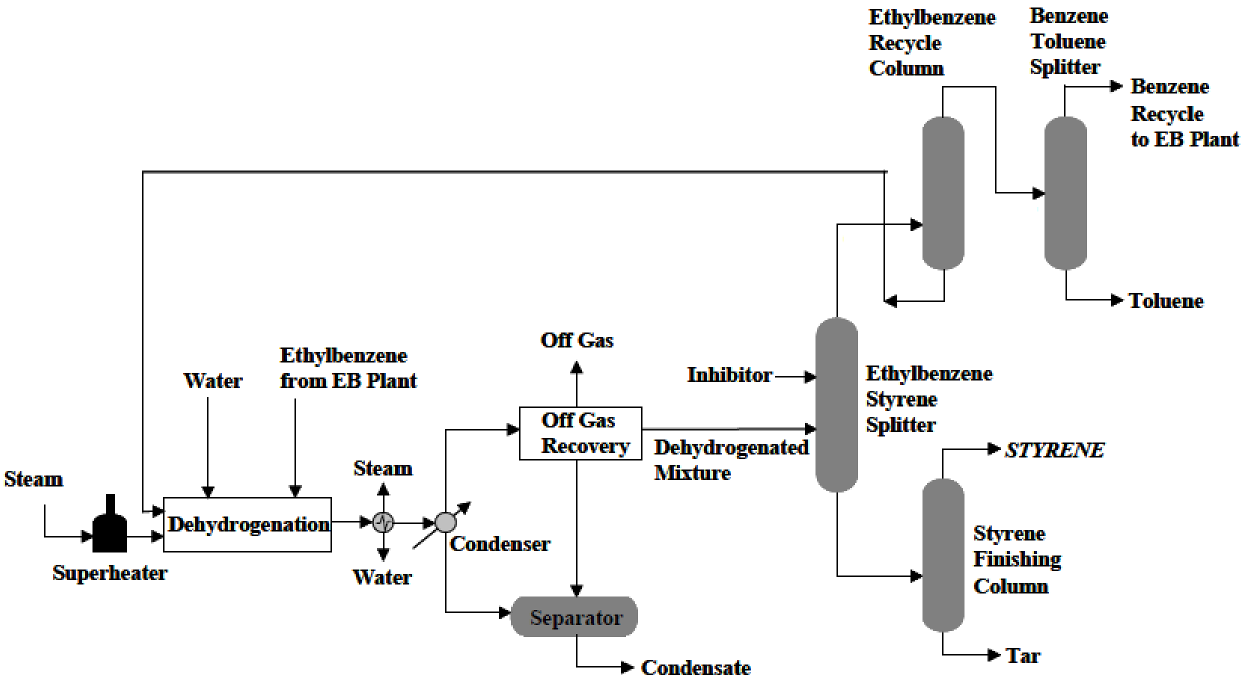

Figure 1.2. Lummus/UOP Classic SM process of adiabatic ethylbenzene dehydrogenation plant

To eliminate the costly interstage reheating and reduce superheated steam requirements, the technology has been modified and improved to Lummus/UOP Smart SM process [4]. This modified technology combines oxidative reheat technology with adiabatic dehydrogenation technology. In this approach, heat needed for the dehydrogenation reaction is generated by controlled combustion of hydrogen. By removing hydrogen from the reaction mixture, the reaction equilibrium is shifted towards higher EB conversion. Increased conversion up to 80 % is achieved without compromising the purity of the styrene monomer.

1.2.2. Styrene and Propylene Oxide (SMPO) Process

This process was discovered in the 1970's by Halcon and improved by Royal Dutch SHELL [5]. The coproduction of propylene oxide (PO) and styrene (SM) route is complex and capital-intensive in comparison to dehydrogenation of ethylbenzene. The process includes three reaction steps: oxidation of ethylbenzene to ethylbenzene hydroperoxide (EBHP), epoxidation of ethylbenzene hydroperoxide (EBHP) with propylene to form α-phenylethanol and propylene oxide, and dehydration of α-phenylethanol to styrene.

$$\mathrm{C_6H_5-CH_2CH_3+O_2\rightarrow C_6H_5-CH_2CH_2O_2H}$$

$$\mathrm{C_6H_5-CH_2CH_2O_2H+CH_3CH=CH_2\rightarrow C_6H_5-CH_2CH_2OH+CH_3CHCH_2O}$$

$$\mathrm{C_6H_5-CH_2CH_2OH\rightarrow C_6H_5-CH=CH_2+H_2O}$$

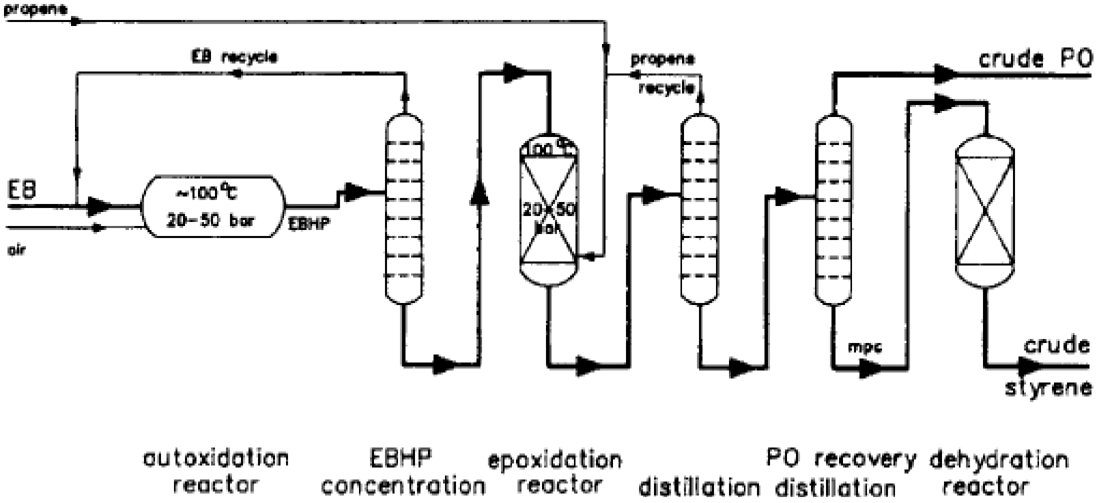

Figure 1.3. Simplified flow diagram of the SMPO process

The SMPO process is cleaner and much less energy intensive than the conventional dehydrogenation route (less by-products). Its major drawback is that production of styrene is limited by the amount of propylene oxide that can be sold [6]. The process flow diagram is shown in Figure 1.3

1.3. Other Technologies

Other technologies in the manufacture of styrene include:

1.3.1. Styrene production from ethane and benzene

This is a joint technology developed by Snamprogetti S.p.A and Dow [7, 8]. It is an alternative dehydrogenation process that use ethane rather ethylbenzene as feed to the process. Ethane and ethylbenzene from the alkylation unit is fed to a circulating fluidized bed reactor system that simultaneously produces styrene and ethylene and allows continuous catalyst regeneration. The dehydrogenation reactor effluent is cooled and separated and the ethylene stream is recycled to the alkylation unit. The catalyst composition suitable for this process consists of microspheroidal catalyst particles of Gallium/Platinum/Potassium supported on alumina with a silica binder. This novel route of styrene production integrates the processes of producing ethylene, ethylbenzene and styrene. Another advantage of the process is the recovery of commercial grade hydrogen as a by-product.

1.3.2. Styrene production from methanol and toluene

The side chain alkylation of toluene with methanol is a potential alternative technology to produce styrene. Direct side alkylation of toluene over basic zeolites is an interesting reaction, considering the industrial importance of its products, especially ethylbenzene and styrene [9]. It is generally accepted that zeolites with some basicity catalyze side-chain alkylation to styrene which is subsequently hydrogenated to ethylbenzene while those which compose of acid sites accomplish only ring alkylation. Styrene monomer production via alkylation of toluene occurs in gas phase at condition 420 °C, 4-7 bar with the presence of zeolite X and Y catalyst. The reactions occur in a two parallel reaction that produces styrene and ethyl benzene. The raw material being used are liquid toluene and liquid methanol that are preheated to 420 °C before enter the reactor. The catalyst used in this process has high styrene selectivity so that the styrene yield could reach 85%. This process has been claimed to be economically attractive offering the advantage of lower raw material cost compared with the traditional process [10].

Other processes for the production of styrene are: side-chain chlorination of ethylbenzene, styrene extraction from pyrolysis gasoline (Toray's STEX process) and oxidative conversion of ethylbenzene to a-phenylethanol via acetophenone and subsequent dehydration of the alcohol [11].

1.4. Motivation

Research and development of new catalysts, reactor designs, and process routes has been continuously pursued to achieve process improvement. Recently a good collaboration has been done between catalyst research and process development, and such collaboration evidently enabled the development of new much energy-saving catalytic process, to decrease the cost unit of raw materials and finally to enhance the production capability. BASF and DOW processes composed of multitubular fixed-bed reactor have been known as industrial processes, whereas Lummus and Badger (Stone &

Webster, Shaw group) processes composed of radial-flow type reactor are recently used due to its adiabatic character applicable for the large scale production. Now the size of reactor is increasing and new plants possessing 500,000~600,000 t/y productivity are under construction. SMART process developed by UOP is known by its unique technology combining dehydrogenation and oxidation; hydrogen formed by dehydrogenation was consumed by reacting with oxygen gas. This favors thermodynamic equilibrium to styrene production and simultaneously steam and heat are supplied to the reactor. Actually, this process is frequently adopted when the reactor is reformed to increase the productivity.

In view of this, a plausible new catalytic process of ethylbenzene dehydrogenation to improve styrene production will be developed which is going to be a steamless process without the promotional role of potassium. Development of this process depends primarily on the development of highly efficient catalysts, which will be achieved by fundamental studies of the catalyst preparations as well as the catalytic reactions involved in the process. For the dehydrogenation at a low temperature, highly dispersed Fe catalyst derived from Mg/Fe/Al ternary hydrotalcite precursors is a promising candidate due to its high activity. Alumina-supported metal oxides with well ordered mesoporosity are also a choice for the dehydrogenation process. We aim to optimize the catalysts by modifying the preparative conditions and the metal compositions in the catalysts. The catalytic process will make use of a fluidized bed reactor instead of the more commonly used fixed bed reactors. A fluid bed process can offer several potential advantages over the fixed bed process. These include enhanced reactant-catalyst contact resulting in higher reaction rates and hence shorter reaction times, uniform product quality as a result of extensive bed mixing and heat distribution. It also enhances easy and timely catalyst regeneration in contrast to the fixed bed process where catalyst regeneration is often laborious, expensive and time consuming [12]. The reaction will be studied under several conditions (reaction times and temperatures) for catalyst testing and kinetic modeling of catalytic reactions. Finally, by optimizing the reaction conditions, highly efficient process can be established in the dehydrogenation of ethylbenzene to styrene, as well as lead to an energetically and environmentally benign chemical production.

1.5. Thesis Objectives

The main objectives of this work are of two-fold; i) to develop highly efficient catalysts for dehydrogenation of ethylbenzene to styrene, and ii) kinetic studies of the reaction. The detailed specific objectives are as follows:

1.5.1. Synthesis and characterization of hydrotalcite and mesoporous iron oxide-alumina based catalysts

i. Mg/Fe/Al hydrotalcite precursor is selected as a base catalyst which is to be modified by Cobalt, Manganese and Nickel.

ii. Facile synthesis of mesoporous alumina on which iron oxide shall be doped.

iii. Determination of the physico-chemical properties of the catalysts through some characterization techniques.

1.5.2. Catalysts Test Performance

The prepared catalysts' activity and selectivity will be determined for the dehydrogenation process. Fluidized bed reactor will be used for the catalytic dehydrogenation of ethylbenzene at short reaction time (5 – 20 s) and reaction temperature (350 – 550 °C) lower than that used industrially. It is expected that the short reaction times will limit the tendencies of undesired reactions from taking place and the relatively low temperature will prevent the occurrence of thermal reactions.

1.5.3. Kinetic modeling

Key to any process development is the availability of important design parameters such as the activation energy of the reaction, rate constants, etc. This will involve the following:

i. Proposing different possible reaction models
ii. Fitting experimental data into the proposed models to check the suitability of the models
iii. Determination of kinetic parameters; apparent activation energies, apparent reaction rate constants.

1.6. Thesis Outline

Chapter 2 presents a literature review on dehydrogenation of ethylbenzene. An overview of its reaction mechanism is given, catalyst composition and deactivation. Challenges facing the commercial catalyst used for the dehydrogenation process were discussed, and what has been done so far in terms of catalysts development to tackle these challenges. Overview of the kinetic studies of the reactions involved was also reviewed.

Chapter 3 deals with the experimental section. Description of the equipment used for the experimental set-up is given as well as the procedures adopted. This chapter also explains catalyst synthesis, characterization and evaluation.

Chapter 4 focuses on the results of the experimental work. Discussion of the effects of reaction conditions (temperature and time) are given in details. In addition, a detailed kinetic modeling of the reaction over all the catalysts (hydrotalcites and mesoporous iron oxide-alumina) is presented starting first with model formulation and then estimation of the kinetic parameters using non-linear regression analysis.

Chapter 5 gives the summary of our contribution, conclusions and recommendation for future work

CHAPTER 2

2.0 LITERATURE REVIEW

2.1. Introduction

The catalytic dehydrogenation of ethylbenzene is an important reaction used commercially for the production of styrene. The dehydrogenation reaction is thermodynamically favored at high temperature and low pressure. The dehydrogenation reaction must overcome the constraint resulting from the fact that energy required to break a C-C bond (245 kJ/mol) is less than the energy necessary to break C-H bond (365 kJ/mol) [13]. Therefore, thermal reaction is not advisable, since it would lead to a predominance of cracking reactions over dehydrogenation reactions. However, in the presence of a suitable catalyst, dehydrogenation can be carried out with minimal C-C bond rupture. Therefore, typical dehydrogenation of ethylbenzene industrially is carried out on iron oxide based catalysts at temperatures above 600 °C. The reaction is highly endothermic ($\Delta H = 124.9$ kJ/mol) and reversible, therefore steam is used in large amount since; steam plays a prominent role in shifting of the reaction equilibrium towards products, prolonging the catalyst activity and most significantly acts as a heat carrier. The dilution with steam also reduces the potential for the formation of coke [14]. The conversion per pass is generally 60-70%, with styrene selectivity between 93-95%. A simplified reaction scheme of catalytic dehydrogenation of ethylbenzene is shown in Figure 2.1.

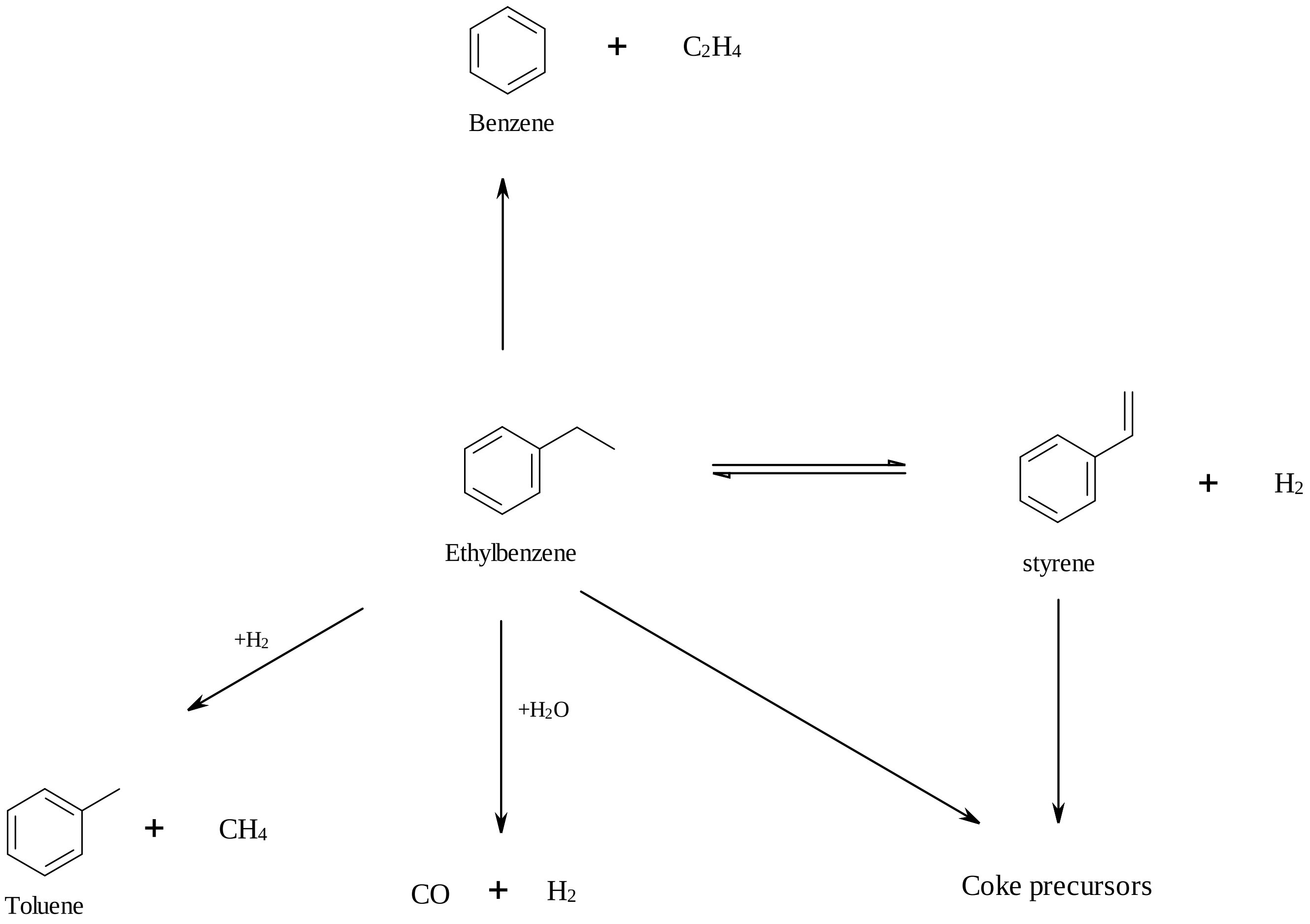

Figure 2.1 Reaction scheme of catalytic dehydrogenation of ethylbenzene [15]

The main reaction produces styrene and hydrogen.

$$C_6H_5-CH_2CH_3 \Leftrightarrow C_6H_5-CH=CH_2+H_2 \quad \text{(dehydrogenation)}$$

In addition to the main dehydrogenation reaction, some side reactions also occur. The most common side reactions are cracking to benzene and ethylene or hydrogenolysis to toluene and methane, and coke formation. Therefore, the main by-products are benzene and toluene [15].

$$C_6H_5-CH_2CH_3 \rightarrow C_6H_6+C_2H_4 \quad \text{(cracking)}$$

$$C_6H_5-CH_2CH_3+H_2 \rightarrow C_6H_5-CH_3+CH_4 \quad \text{(hydrogenolysis)}$$

However, the usage of large volume of superheated steam is one of the drawbacks of the present technology. The process involves high consumption estimated to be 1.5×10^6 kcal/styrene tone [16] because all the latent heat of condensation of steam is lost at the liquid-gas separator during the process. Therefore, efforts are underway in reducing the steam/hydrocarbon ratio to molar values less than 6, essentially through modifications in catalyst composition to save energy and reach higher styrene conversion levels.

2.2. Catalysts for Ethylbenzene dehydrogenation

The use of a suitable catalyst allows high reaction rates and, above all, high selectivity. The principal catalytic system that has dehydrogenation activity for ethylbenzene is essentially potassium promoted iron oxide, containing chromium oxide (Shell 105). Among the most common promoters added to iron oxide, the alkali oxides have the most noticeable effects on catalytic activity and selectivity. Other metals are used as supplementary promoters, such as, cerium, tin, calcium, molybdenum, magnesium, titanium and others. Potassium-promoted iron oxide is uniquely superior to any other known catalyst for the dehydrogenation of ethylbenzene in the presence of steam [17], particularly efficient with respect to both selectivity and activity. Promotion of iron oxide with potassium enhances the activity of iron oxide by an order of magnitude and reduces the formation of carbonaceous surface deposits or coke that deactivates the catalysts [14,18-19]. A study of the structure and composition of the catalysts established the promotional role of potassium to consist of the formation of $KFeO_2$, which constitutes the active phase. Muhler et. al. [20] also confirmed the active phase to be a thin layer of $KFeO_2$ supported on a solid solution of $K_2Fe_{22}O_{34}$ in Fe_3O_4. The existence of the ternary $K_2Fe_{22}O_{34}$ serves as storage medium from which the active surface is continuously supplied with a near monolayer coverage of potassium ions in an environment of Fe^{3+} ions. Lee and Holmes [21] suggested that potassium increase activity by encouraging electron transfer at the solid-gas interface. Potassium further stabilizes the catalyst against reduction [22] and supports the removal of coke. The formation of well dispersed K_2CO_3 is believed to be the active center for carbon gasification [23]. However, a major setback of potassium is its deactivation with time which is caused by migration and susceptibility to poisoning by halides and residual organic chloride impurities [14]. Small amounts of other promoters are added to favor the formation and stability of the active phase under reaction conditions at lower steam to hydrocarbon ratios. Aluminum and chromium act as structural promoters and increase the lifetime of the catalysts. Titanium increased the number of active phase $KFeO_2$ and improves the dispersion of CeO_2 [24], while the addition of both Ce and Mo improved the catalyst composition, increasing both activity and selectivity [19]. Addition of alkaline earth oxides especially MgO to the potassium promoted iron oxide catalysts improved its activity and stability [25].

2.3. Catalyst deactivation

Several forms of catalyst deactivation have been identified for this type of catalysts under ethylbenzene dehydrogenation. The catalyst slowly deactivates and typically needs to be replaced every 1-2 years. The major cause of catalyst deactivation is carbon deposition. The temperatures and low pressures necessary to achieve high equilibrium conversions are conducive to the rapid coke formation. Steam is continuously used during the reaction to aid gasification of the coke to substantially reduce coke formation, via the reaction:

$$C + H_2O \rightarrow CO + H_2$$

$$CO + H_2O \leftrightarrow CO_2 + H_2$$

Formation of CO_2 from the above reaction blocks the active sites of the catalyst leading to the second type of catalyst deactivation. These two forms of deactivation are considered reversible because both, coke and adsorbed CO_2, can be eliminated by the same steaming treatment. However, in addition to this reversible deactivation, other irreversible phenomena occur in these catalysts. The most important one is the loss or redistribution of potassium from the active phase, $KFeO_2$. This changes the composition of the catalyst leading to a potassium rich core and a potassium depleted shell in each catalyst pellet or extrudate. This deactivation phenomenon alters the catalytic activity of the catalyst by increasing its acidity [14]. This consequently favors cracking reactions to benzene and toluene. Physical degradation and reduction of the catalyst by the hydrogen formed during the reaction are other forms of catalyst deactivation [18,26]. A comprehensive investigation of the catalyst life cycle was studied by Muhler et. al. [20], and the authors proposed a model shown below:

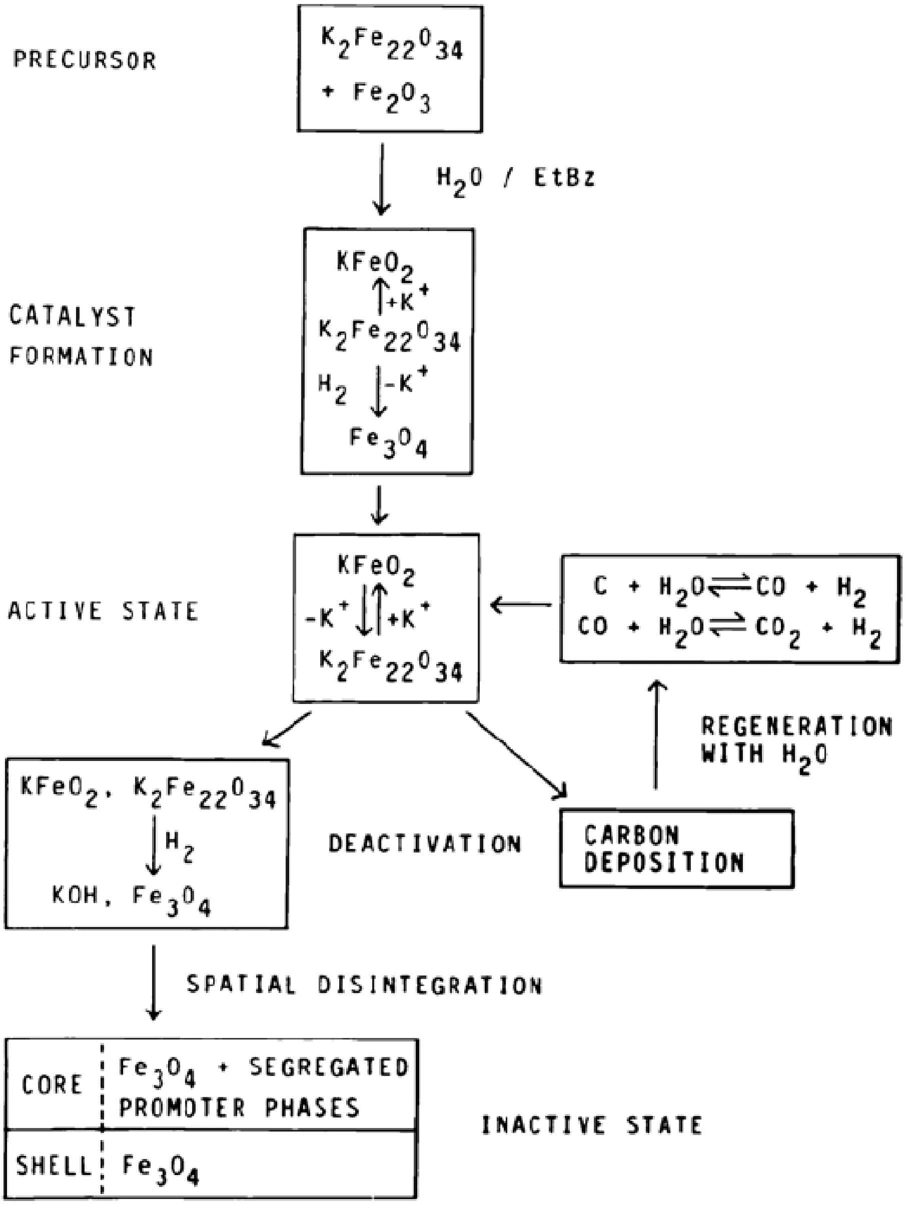

Figure 2.2. Schematic life cycle of a prototype catalyst without any promoter additives [20]

2.4. Reaction Kinetics and Mechanisms

Kinetics of ethylbenzene dehydrogenation has been extensively investigated with the aim of obtaining a kinetic model useful for both industrial application and interpretation of the reaction mechanism. Kinetic models based on pseudo-homogeneous reactor model have been used to determine intrinsic reaction rates [27,28]. A reaction scheme composed of six independent reactions: the main reaction, i.e., ethylbenzene to styrene, and five side reactions were proposed. The rate constants thus were effective but not intrinsic. Therefore, a rigorous heterogeneous model has been developed and used to extract intrinsic rate constants based on dusty gas models accounting for diffusion and reaction in the catalyst pellets [29]. Carrà and Forni [30] performed kinetic studies in the temperature range of 770–900 K over the industrial catalyst, Shell 105. The intrinsic rate of styrene formation was developed, based upon unimolecular Langmuir-Hinshelwood mechanism, where the reaction rate depends on the adsorption-desorption equilibrium of ethylbenzene and styrene. It is believed that water does not take part in the reaction itself i.e. not involved in the rate determining step of the reaction mechanism, but acts purely as inert diluents agent. Hirano [18-19, 31] investigated the kinetics over various iron oxide catalysts in a differential reactor. The rate of styrene formation was independent of the partial pressure of steam and of ethylbenzene. However, styrene addition to the ethylbenzene feed decreased the rate of styrene formation, which confirmed the earlier suggestion of Carrà and Forni that preferred adsorption of styrene can lead to site-blocking effect by the product. Dittmeyer et. al. [32] studied the reaction kinetics of ethylbenzene dehydrogenation in a gradientless recycle reactor. The rate equations were developed based on the Langmuir-Hinshelwood-Hougen-Watson (LHHW) type formula for the main reaction and the power law for the steam reforming reactions. The authors found out that the formation of styrene and toluene were suppressed due to controlled CO_2 addition and production of CO_2 was attributed to the stream reforming of ethylbenzene and CH_4. A mechanistic catalyst model neglecting side reactions towards benzene and toluene was derived by Schüle et al. [33]. The model assumes overall conversion consists of individual steps adsorption, surface reaction and desorption. Another single-step reaction considered is the gas-solid reactions related to formation of coke and phase transformation of iron oxide. More recently Lee and Froment [34] developed a set of intrinsic rate equations for a commercial potassium-promoted iron catalyst based on Hougen-Watson model. The model was applied in the simulation of the dehydrogenation in industrial multibed adiabatic reactors which accounts for thermal radical-type reactions, internal diffusion limitations, coke formation, and gasification. Kinetic studies on model catalysts by Coulter et al. [35] showed similar apparent activation energies for K-promoted and unpromoted iron oxide catalysts. They suggested that potassium only increases the number of active sites, but does not change their nature.

Several authors have investigated the reaction mechanism of dehydrogenation of ethylbenzene on the Fe-K mixed oxide catalyst. An infrared spectroscopy study by Addiego et al [36] observed that ethylbenzene dehydrogenation from which styrene is formed was bonded to the catalyst surface through the vinyl group, whereas styrene adsorbed from the gas phase was bound via the aromatic ring. Miura et al. [37] investigated dehydrogenation of alkylbenzenes over an Fe_2O_3- K_2CO_3- Cr_2O_3 catalyst by means of isotope exchange experiments. According to them, dissociation of α-hydrogen is the first step followed by dissociation of β-hydrogen, which is the rate-determining step or post rate-determining step. They concluded that the α-hydrogen is dissociated as a proton on a basic site. Dulamiţă et al. [38] proposed a mixed acid-basic and reduction-oxidation mechanism based on the kinetic study on the same catalyst as ref. 37; a formation of π-adsorbed intermediate on Fe^{3+} acid centers, followed by elimination of two hydrogen ions from two C-H ethylic groups on basic centers with electrons transfer to Fe^{3+} to form styrene and H_2. Oliveira et al. [39] proposed acid-base mechanism to operate to adsorb ethylbenzene and abstract the β-hydrogen in the ethylbenzene dehydrogenation over Fe-MCM-41.

2.5. Catalyst development for ethylbenzene dehydrogenation

Improvement of styrene production includes development of high selectivity catalyst and reactor design. The presence of several consecutive reactions is responsible for the typical trade-off between conversion and selectivity to the desired product. Therefore, the main challenges in the area of catalyst development for ethylbenzene dehydrogenation are the development of a catalyst which:

i. Stabilize the active specie in the absence of potassium promoter and superheated steam
ii. Possess high surface area
iii. Minimizes coke formation and catalyst deactivation
iv. Active and selective towards increased styrene yield

2.5.1. Hydrotalcites

Hydrotalcite-like compounds or more generally speaking layered double hydroxides (LDHs) have the general formula $[M(II)_{1-x}M(III)_x{\cdot}(OH)_2]^{x+}(A^{n-})_{x/n}{\cdot}mH_2O$ where M(II) is a divalent cation (Mg^{2+}, Ni^{2+}, Co^{2+}, Zn^{2+}, Mn^{2+}), M(III) is a trivalent cation (Fe^{3+}, Cr^{3+}, Al^{3+}), A is an anion. It is of importance to choose the appropriate ratio of cations and anions in order to obtain a pure HTlc during preparation: $0.2 \leq x \leq 0.4$ and $l/n \leq A^{n-} /M(III) \leq 1$, where $x = M(III)/[M(II)+M(III)]$ [40]. HTlcs are usually carbonate in natural minerals and belong to the class of anionic clays. They are structurally similar to brucite $Mg(OH)_2$; they are layered materials made of positively charged two-dimensional sheets of mixed hydroxides with water and exchangeable charge-compensating anions [40,41].

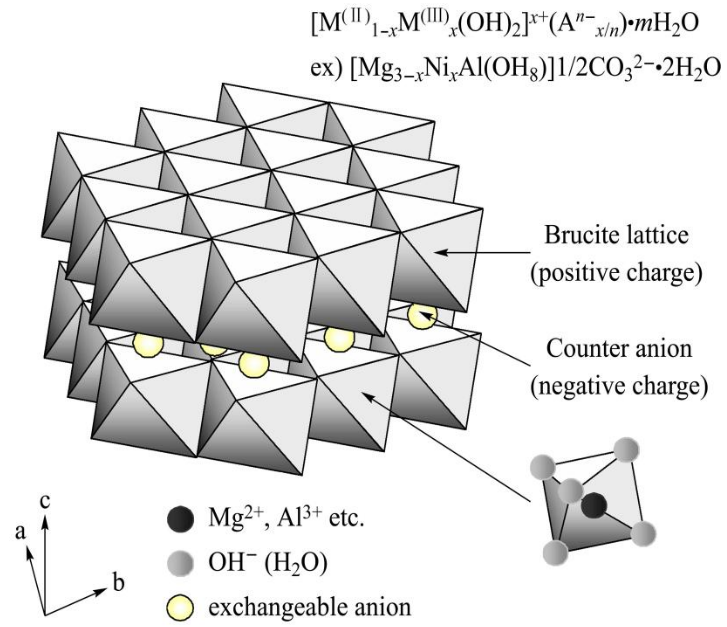

Figure 2.3. Structure of hydrotalcite

HTlcs are gaining considerable interest in several technological fields, particularly for base-catalyzed reactions. This is because the catalysts contain various transition metal cations as the catalytically active species well dispersed on the basic support materials. Their properties and applications have been the subject of detailed reviews, [40-43] and many publications have provided examples of their practical uses. Isomorphous substitution of divalent cations by trivalent ones generates positive charges on the layers, which are compensated by anions located in the interlayer region. The possibility of accommodation of cations of different natures in the sheets, atomic scale homogeneity, possibility of intercalation of several types of anions (inorganic, organic, organometallic, polyoxometalates) and formation of mixed oxides under thermal treatment makes HT applicable to wide range of applications. They are usually activated by thermal decomposition to serve as precursors for mixed oxide catalysts which offer unique basic properties that make them very attractive for catalytic applications. The resultant oxides upon calcinations exhibit high surface area, high thermal stability and highly homogeneous metal dispersion [40] which improves their catalytic performance. Moreover, they are potentially recoverable and recyclable [44]. In addition to the basic sites, acid sites or acid-base pairs on HTs also influence catalytic performance. Acid-base sites on mixed oxides are highly active sites for many reactions. Acid-base properties of Mg-Al mixed oxides are governed by the Mg/Al molar ratio, calcination temperature and preparation condition [45]. A further improvement to the catalysts has been obtained by modification of the HTlcs through the addition of other elements. Mg/Fe/Al mixed oxides prepared from Mg-Al(Fe) HTs has been reported to effectively catalyze the dehydrogenation of ethylbenzene [46]. The high catalytic performance was attributed to the formation of partially reduced iron oxides on the surface of catalyst and to the high surface area along with the porous structure, which originated from the Mg/Fe/Al hydrotalcite structure in the precursors. The main phase was identified as the formation of periclase Mg(Fe,Al)O. Catalytic tests of the $Mg_2Fe_xAl_{1-x}$ mixed oxides catalysts showed that the styrene conversion increased with increasing the iron content up to x = 0.75 and then decreased, while the selectivity was the highest at x = 0.25 (Figure 2.3). The optimum temperature for the reaction was 550 ºC, which was lower than that used in the commercial process. The ethylbenzene conversion of 60% and the styrene selectivity of 95% were kept for 3 h over $Mg_3Fe_{0.5}Al_{0.5}$ mixed oxide catalyst at 550 ºC. After the reaction for 3 h, the iron species on the catalyst was partially reduced to the valence state between Fe^{2+} and Fe^{3+}.

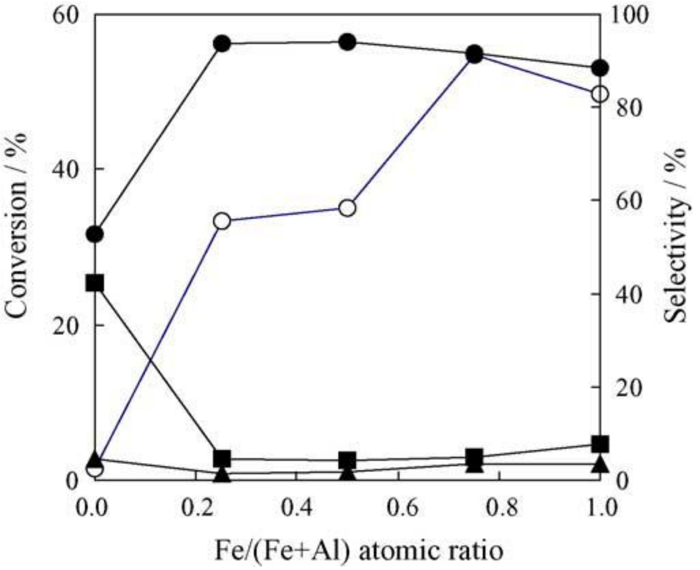

Figure 2.4. The dehydrogenation of ethylbenzene over $Mg_2Fe_xAl_{1-x}$ mixed oxides catalysts [46]: ○ethylbenzene conversion; ●styrene selectivity; ■benzene selectivity; ▲toluene selectivity.

A further study to elucidate the role of MgO as basic support for this catalyst showed that the mixed acid-basic and reduction-oxidation reaction on the Mg^{2+}-O^{2-}-Fe^{3+} active species leads to an effective catalytic cycle, responsible for its high catalytic performance [47]. MgO effectively initiated dehydrogenation by H^+ abstraction of EB on the basic site, and proceeded by the accelerated reduction-oxidation of Fe^{3+} active species. Furthermore, improvement of the activity of the $Mg_3Fe_{0.5}Al_{0.5}$ mixed oxide catalyst can be achieved by optimizing the Mg/Fe/Al metal composition and further by adding the second metal component to the Fe catalyst. This has been proven to be true from a recent study on the activity of various FeO_x-$\mathit{Me}O_y$/Mg(Al)O catalysts derived from HTs [48]. Addition of cobalt (*Me* = Co; FeO_x-CoO_y/Mg(Al)O) improved the activity of the catalyst due to the formation of Fe^{3+} - Co^{2+} (1/1) bimetallic species. This further facilitated the reduction-oxidation of Fe^{3+}/Fe^{2+} and stabilized the active Fe^{3+} species.

2.5.2. Mesoporous Alumina doped with iron

The importance of alumina as a catalyst or support has been widely recognized. As a support or co-catalyst it is used in many catalytic processes of industrial importance such as isomerization, alkylation, catalytic cracking, hydroforming, hydrodesulfurization of petroleum products [49, 50]. Transition aluminas are disordered crystalline phases formed through the thermal dehydration of aluminum hydroxides and oxyhydroxides [51]. Seven transition alumina phases have been identified which include the γ-, η-, δ-, θ-, κ-, χ-, and the stable α-alumina phase. Among these, γ-Al_2O_3 is widely used in catalysis as an active phase and is characterized by having acid sites which determines the activity and selectivity of the catalyst for specific catalytic reactions [52]. The utility of γ-Al_2O_3

as well as other transition aluminas can also be traced to a favorable combination of textural properties (i.e. surface area, pore volume and pore size). Mesoporous alumina supports with large surface areas, large pore volumes, narrow pore size and suitable surface acidic–basic properties often result in favorable enhancements in catalytic performance [53, 54]. Therefore, synthesis of organized mesoporous aluminas attracted particular research activities in the last decade, which provided new synthetic approaches using novel structure-directing agents. Synthetic approaches such as sol gel, hydrothermal, precipitation, cation-anion double hydrolysis and microemulsion templating methods [55-62], have been used to synthesize mesoporous alumina with a large surface area. However, it has been observed that relatively low thermal instability associated with as-synthesized alumina constituted a major setback. This is because phase transition often occurs during high calcinations temperatures. Recently, a facile synthesis developed by Yuan et. al. [63] has been used to develop a highly ordered mesoporous amorphous and/or crystalline γ-aluminas with high thermal stability and large amount of lewis acid sites. This method has been extended to the development of alumina-supported metal oxides with well-developed mesoporosity, relatively high surface area and crystalline pore walls through one-pot synthesis [64]. A new synthetic procedure for ordered mesoporous γ-alumina with a large surface area has been proposed by Huang et. al., suggested to be catalyst supports in high temperature reactions [65]. Few works have been reported on the use of iron doped alumina catalyst for ethylbenzene dehydrogenation. Fe_2O_3 supported on γ-alumina has been suggested to interact with each other to form $FeAl_2O_4$ spinel and stabilize the Fe_2O_3 phase [66]. This was in line with the observation of Giecko et. al. [67] and they further proposed that iron aluminates

($FeAl_2O_4$) are reducible species formed due to high temperature sintering process. Mimura and Saito [68] suggested that high activity is attainable using coprecipitation method for Fe_2O_3/Al_2O_3 catalyst and the active sites are composed of iron and aluminium which might be amorphous and/or highly dispersed. Their investigation further shows the effectiveness of Fe_2O_3/Al_2O_3 for the dehydrogenation of ethylbenzene in the presence of CO_2. Lee [14] also suggests that Al_2O_3 is effective for EB dehydrogenation in the absence of steam as diluents. However, rare works has been reported on the use of Fe_2O_3/Al_2O_3 catalyst for non-oxidative or direct ethylbenzene dehydrogenation.

CHAPTER 3

3.0 EXPERIMENTAL SECTION

3.1. Experimental Set-up

Experimental runs for the dehydrogenation process were carried out in a riser simulator reactor. The reactor was connected to a vacuum box through a four-port valve. The products were removed from the riser simulator at the end of the pre-set reaction period. A time/actuator assembly linked to the feed injection system controlled the four-port valve. The vacuum system was connected to a manually operated six-port sampling valve. This sampling valve was connected on-line to the gas chromatograph. Furthermore, the riser simulator reactor and the vacuum box were equipped with pressure transducers to monitor the pressure during and after the reaction periods. Both the reactor and the vacuum system were supplied by separated heating systems and both were well insulated.

The feed injecting system includes a gas tight syringe connected to switches to control the timer/actuator assembly on the four port valve and the data acquisition system. The data acquisition system allowed monitoring the change of pressure with time from both the reactor and the vacuum box. A four-port valve, controlled by a timer/actuator assembly, was linked to the injection system. A vacuum system was also connected to the manually operated six port sampling valve which allows for sampling injections into the gas chromatograph. Both, the reactor and the vacuum system are located in temperature controlled ovens. Connections between components are accomplished using heated and well insulated lines. The unit was also equipped with two pressure transducers which allowed for continuous pressure monitoring during the reaction and post-reaction evacuation periods. A schematic diagram of the experimental setup is given in Figure 3.1.

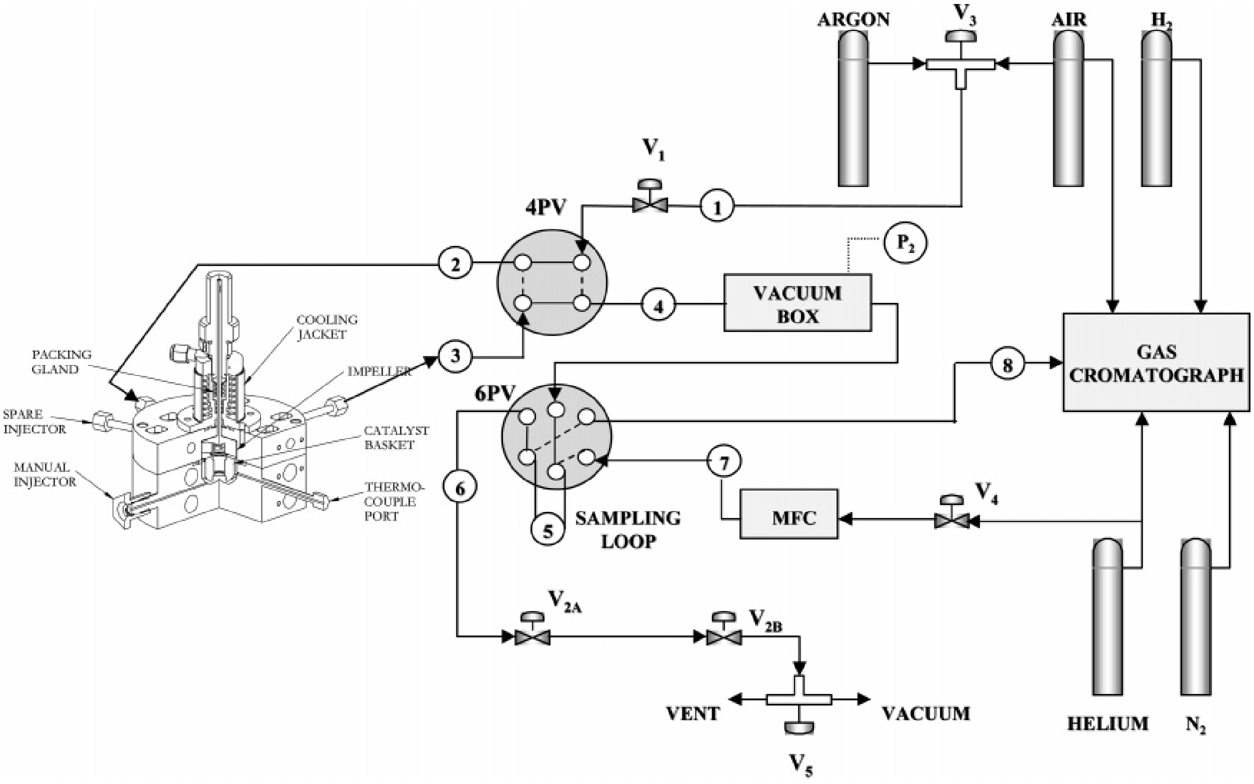

Figure 3.1. Schematic diagram of the riser simulator experimental set-up

3.1.1. Riser Simulator

This novel reactor was invented by de Lasa [69] and it was designed to provide high gas phase circulation rates as well as intense catalyst mixing. In this respect, perfect mixing with the absence of coke profiles and gas channeling can be obtained with all catalyst particles being exposed to the same reaction environment. As mentioned by Pruski et. al. [70], good fluidization is achieved under typical riser conditions and using shaft spinning rates close to 7600 rpm. The riser simulator can be used for several purposes: a) to test industrial catalysts at commercial conditions [71], b) to carry out kinetic and modeling studies for certain reactions, c) to develop adsorption studies [70], d) to use the data of this unit for assessing the enthalpy of cracking reactions. The riser simulator consists of two outer shells, the lower section and the upper section, which allow one to load or to unload the catalyst easily. The reactor was designed in such a way that an annular space is created between the outer portion of the basket and the inner part of the reactor shell. A metallic gasket seals the two chambers with an impeller located in the upper section. A packing gland assembly and a cooling jacket surrounding the shaft provide support for the impeller. Upon rotation of the shaft, gas is forced outward from the center of the impeller toward the walls. This creates a lower pressure in the center region of the impeller, thus inducing flow of gas upward through the catalyst chamber from the bottom of the reactor annular region where the pressure is slightly higher. The impeller provides a fluidized bed of catalyst particles as well as intense gas mixing inside the reactor. A schematic diagram of the riser simulator is shown in Figure 3.2

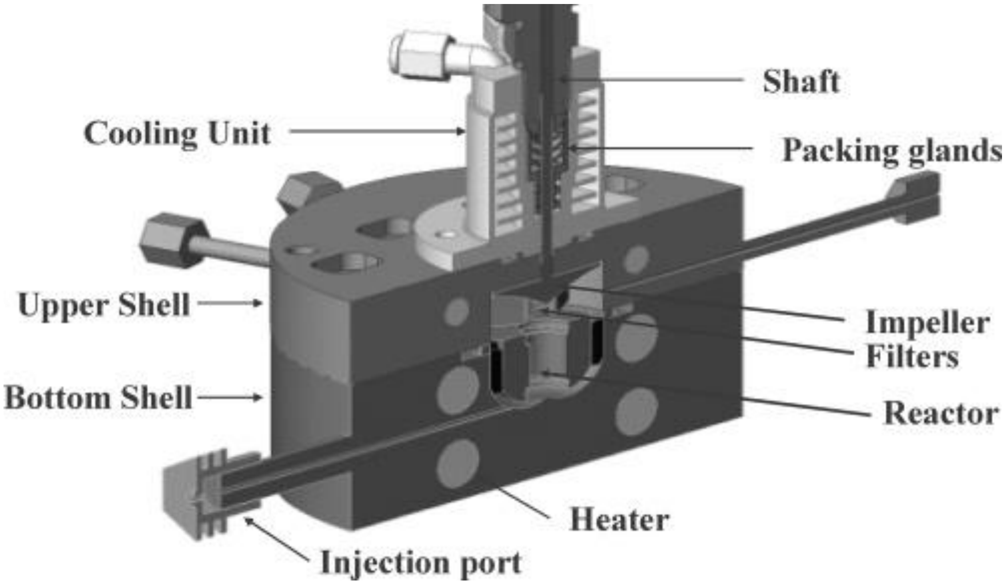

Figure 3.2a. Schematic diagram of the riser simulator

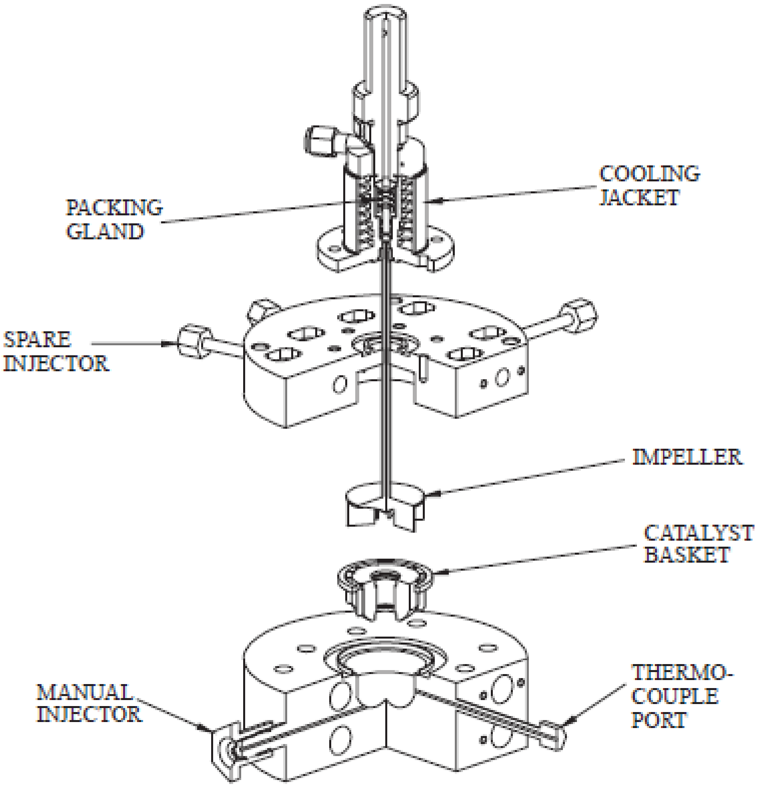

Figure 3.2b. Cross section of the riser simulator displaying the unit components

3.1.2. Gas Chromatograph (GC) System

The quantitative analysis of the reaction products were carried out online using an Agilent GC equipped with Flame Ionization Detector FID (Agilent Chromatograph Model 6890N), equipped with an HP-INNOWAX capillary column (Polyethylene glycol (PEG)) (length 60 m x internal diameter 0.32 mm x film thickness 0.50 μm). Helium is used as the carrier gas, while air and hydrogen gases are used for the FID detector. Furthermore, liquid nitrogen is used to facilitate the initial cryogenic operation of the GC temperature program. The liquid nitrogen cools the GC oven to -30 °C. The flow of liquid nitrogen is administered by a solenoid valve actuated from the GC's internal oven temperature controller. The integrator allows strip chart recording as well as integration of the GC detector signal. The integrator is connected to the GC via a HPIL instrument network cabling system.

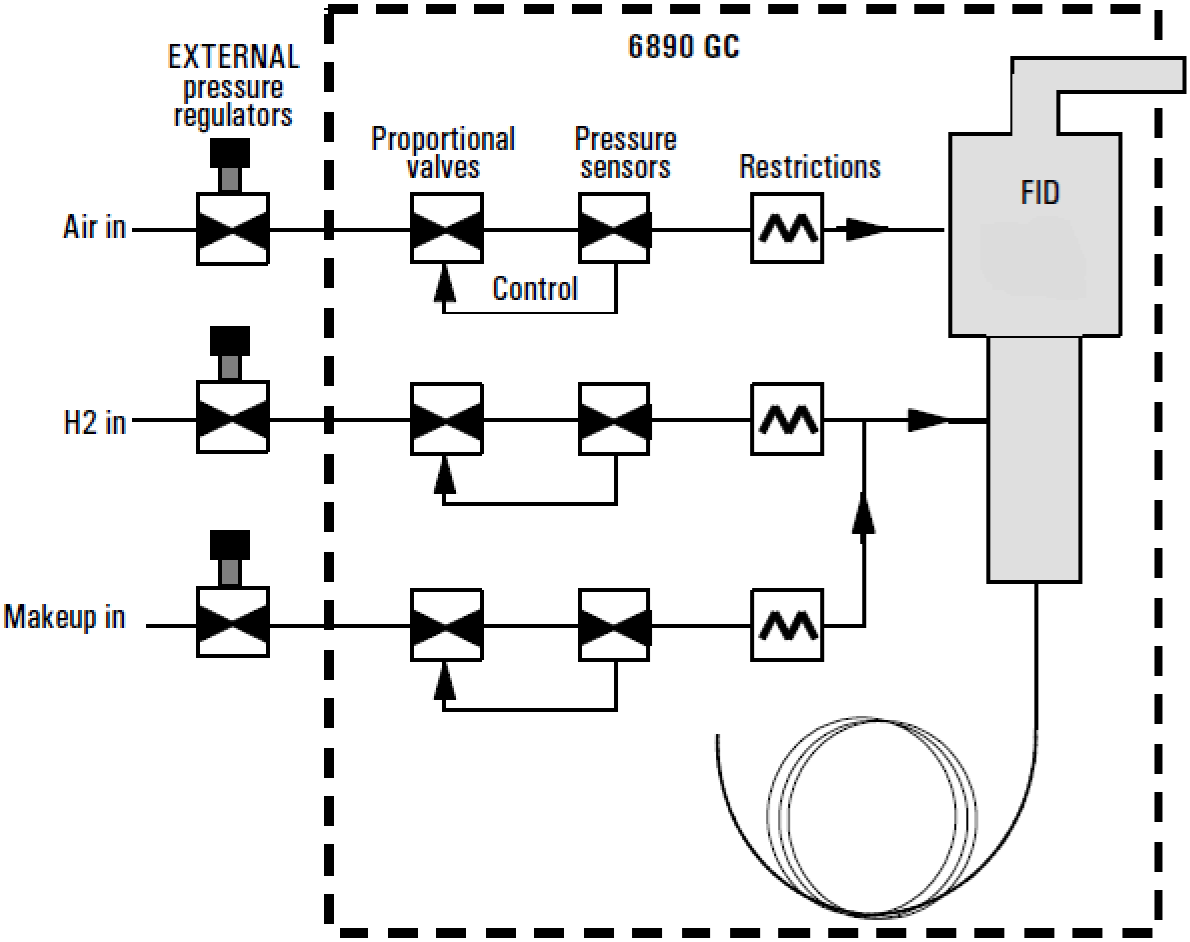

Figure 3.3. Schematic diagram of the gas chromatograph

3.1.3 Coke Analyzer

A carbon analyzer multi EA 2000 (Analytikjena) is used. This multi EA 2000 equipped with CS Module is a specially developed system which permits simultaneous or separate determination of the total carbon and total sulphur in samples of solids, pastes and liquids by means of high temperature oxidation in a current of oxygen supplied directly to the unit. It is based on special high temperature ceramics (HTC) technology which renders a catalyst superfluous. By combining the finely tuned non-dispersive infrared gas analysis (NDIR) detection which is selective to CO_2/SO_2 with the patented Verweilzeitgekoppelte Integration fur TOC-Analysen (VITA) procedure, which takes into account the dwelling time, the analysis possible is very precise. The aliquot of the sample is accurately weighed into the combustion boat and delivered complete into the hot zone of the furnace. There, pyrolysis and oxidation of the sample occurs at a high temperature in the stream of oxygen ($R + O_2 \rightarrow CO_2 + H_2O$, where R is a substance with carbon content). The gas produced in the pyrolysis is drawn through a glass tube filled with a specialist desiccant. This desiccation tube also serves as a particle filter, so that no water or dust can get into the detection system of the device. An NDIR detector is used to determine the CO_2 content in the carrier gas. Gases whose molecules are composed of different types of atom possess specific absorption bands in the infrared wavelength range. The concentration of CO_2 is signaled several times per second. An integral over time is created from the series of signals. The integral is proportional to the concentration of carbon in the sample analyzed. A calibration function is then used to calculate the amount of carbon in the sample. The calibrations allows for any changes to flow arising over time because of such factors as the ageing process, dirt getting into flow regulators, or the desiccants going lumpy, will not automatically necessitate recalibration, which is a positive factor reducing the frequency of desiccant replacement. A small amount of the spent catalyst (0.09-0.1 g) is used for the analysis.

3.2. EXPERIMENTAL PROCEDURE

3.2.1. Materials

All the precursors used in the synthesis of the HT quaternary mixed oxides $Mg_3Fe_{0.25}Me_{0.25}Al_{0.5}$ (*Me* = Co, Mn and Ni) and iron doped organized mesoporous alumina catalysts were obtained from Sigma-Aldrich and used as received. The chemical feedstock (ethylbenzene, 99%) was also supplied by Sigma-Aldrich.

3.2.2. Catalyst Preparation

3.2.2.1. Synthesis of hydrotalcite catalysts

The HT precursors of $Mg_3Fe_{0.25}Me_{0.25}Al_{0.5}$ (*Me* = Co, Mn and Ni) catalysts were prepared by co-precipitation of metal nitrates, following the method by Miyata and Okada [72] after minor modifications. An aqueous solution containing the nitrates of Mg^{2+}, Fe^{3+}, Me^{2+} (Co^{2+}, Mn^{2+} or Ni^{2+}) and Al^{3+} (200 ml) was added slowly with vigorous stirring into an aqueous solution of sodium carbonate (400 ml). The pH of the solution was adjusted at 10.0 by dropping a 1 M aqueous solution of sodium hydroxide, leading to a precipitation of heavy slurry. After the solution was aged at 60 °C for 24 h, the solution was filtrated and the precipitates were washed with de-ionized water (1000 ml), dried in air at 100 °C for 4 h, and calcined at 550 °C for 12 h using a muffle furnace in a static air atmosphere. The concentration of Na^{2+} in the catalysts after the calcination was confirmed to be less than 10 ppm by atomic absorption.

3.2.2.2.Synthesis of mesoporous alumina doped with iron-oxide

Iron doped organized mesoporous alumina was synthesized using aluminium isopropoxide (98%, Aldrich). Alumina powders were synthesized using the neutral template approach as described by Yuan et al. [63]. The procedures were modified in order to accommodate the iron. In a typical synthesis, 1.0 g of Pluronic P123 (M_{av} = 5-800, $EO_{20}PO_{70}EO_{20}$) was dissolved in 10.0 ml of ethanol at ambient temperature. Then 1.5 ml of 67 wt% HNO_3 and 2.04 g of aluminium iso-propoxide were added after 2 h into the above solution with vigorous stirring. The mixture was covered with PE film and let stir at ambient temperature for 5 h. After solvent evaporation, which was carried out at 40 °C for 72 h, samples were calcined in standing air from 25 to 550 °C (1 °C/min ramping rate, 5 h hold time). Pure organized mesoporous alumina is noted as meso.Al_2O_3.

Iron was added to organized mesoporous alumina via two different methods; direct (one-pot) synthesis and post synthesis. The direct synthesis procedures were similar to that of pure alumina powder except that the required amount of iron precursor (iron (III) nitrate hexahydrate, unless otherwise specified) that corresponds to Fe content of 21 wt% was dissolved with triblock copolymer template. Post synthesis was carried out using the conventional incipient (wetness) impregnation method. In a typical preparation, iron (III) nitrate hexahydrate was dissolved in distilled water. Subsequently, alumina powder was slowly added. The slurry was mixed at ambient temperature for 2 h, and then water was slowly evaporated while stirring. Samples were then dried at 120 °C overnight followed by calcinations treatment similar to that of pure alumina powder. Iron based samples obtained by direct and post synthesis are noted as xFe-meso.Al_2O_3, and xFe/meso.Al_2O_3, respectively (where x is 21 corresponding to Fe content in wt%).

3.2.3. Catalyst Characterization

A comprehensive catalyst characterization was done to determine the physico-chemical properties of the synthesized catalysts. The following characterization techniques were employed:

i. BET Surface Area and pore size distribution

The textural properties of synthesized samples were characterized by N_2 adsorption measurements at 77 K, using Quantachrome Autosorb 1-C adsorption analyzer. Samples were outgassed at 220 °C under vacuum (10^{-5} Torr) for 3 h before N_2 physisorption. The BET specific surface areas were determined from the adsorption data in the relative pressure (P/P_o) range from 0.06-0.2, assuming a value of 0.164 nm^2 for the cross-section of the nitrogen molecule. The pore size distribution (PSD) was calculated from the adsorption branch using the Barrett-Joyner-Halenda (BJH) method.

ii. Atomic Absorption

The chemical compositions of synthesized HT quaternary mixed oxides of Mg/Fe/*Me*/Al (*Me* = Co, Mn, Ni) and Fe_2O_3/Al_2O_3 were determined by atomic absorption spectroscopy, using the Perkin-Elmer equipment (Model AAnalyst 100).

iii. X-ray Diffraction

XRD was recorded on a Mac Science MX18XHF-SRA powder diffractometer with monochromatized CuKα radiation (λ = 0.154 nm) at 40 kV and 30 mA. The diffraction pattern was identified through comparison with those included in the

JCPDS (Joint Committee of Powder Diffraction Standards) database and literatures.

iv. X-ray Photoelectron Spectroscopy

XPS measurements were performed on a Perkin Elmer 1600E spectrometer using Mg Kα radiation as excitation source. In charge-up correction, the calibration of binding energy (BE) of the spectra was referenced to the C 1s electron bond energy corresponding to graphitic carbon at 284.5 eV. In addition, relative atomic sensitivity factors (ASF) were corrected to determine practically more accurate chemical compositions on the surface.

v. Fourier Transform Infrared Spectroscopy

Infrared spectroscopy of adsorbed pyridine was used to determine the types of acid sites present on the alumina at different extents of Fe surface coverage. The measurements were carried out using a Fourier transform infrared Nicolet spectrometer (Magna 500 model).

vi. Temperature - Programmed Desorption

Temperature-programmed desorption of NH_3 (NH_3-TPD) was carried out using Quantachrome Autosorb 1-C/TCD. Samples were pretreated at 300 °C in a flow of He (50 ml min^{-1}) for 3 h. This was followed by the adsorption of ammonia (5 vol.% in He) at 100 °C for 30 min. Samples were then purged in a He stream for 2 h at 100 °C in order to remove loosely bound ammonia (i.e. physisorbed and H-bonded ammonia). Then, the samples were heated again from 100 to 550 °C at a heating rate of 10 °C/min in a flow of He (25 ml/min) while monitoring the evolved ammonia using TCD.

3.3. GC calibration

The calibration of the gas chromatograph used in determining the product composition of the ethylbenzene dehydrogenation reaction was done as explained in sections 3.3.1 and 3.3.2 below:

3.3.1. Determination of retention time for the different compounds

The retention times of all compounds of interest in this work were determined by analyzing pure samples of each of the compounds in the GC in turns. Table A3.1 (Appendix) shows the different compounds and their corresponding retention times. These retention times were used to identify each component of the reaction products.

3.3.2. Correlating GC response and actual weight percentage of each compound

In calibrating the GC, standard samples of different compositions containing ethylbenzene and the main reaction products (styrene, benzene, toluene) were prepared. The composition of the prepared samples were carefully chosen to reflect all the possible product compositions (obtained from preliminary experimental runs) under the different reaction conditions to be investigated. 0.2µl of the first sample was then injected into the GC and the GC responses (area %) for each of the components in sample were obtained. The sample procedure was repeated for all the other samples.

3.4. Catalyst Evaluation

Ethylbenzene dehydrogenation was carried out over the synthesized hydrotalcite and Fe_2O_3/Al_2O_3 catalysts in order to test their catalytic activity. The HT catalysts were evaluated for the dehydrogenation process at reaction temperatures of 400, 450, 500 and 550 ^oC while Fe_2O_3/Al_2O_3 catalysts are tested at reaction temperatures of 350, 400, 450, 500 and 550 ^{o}C. For each reaction temperature, all catalysts were tested for reaction times of 5, 10, 15 and 20 sec. To enhance the reproducibility of the data, experimental runs for each reaction condition was repeated at least twice.

3.4.1. Testing Procedure

In a typical experiment, the reactor was charged with 0.8g of catalyst previously crushed and sieved to a particle size of ~ 60 µm diameter. The catalyst/reactant ratio was 5 (weight of catalyst = 0.81 g, weight of reactant injected = 0.162 g). The system is then sealed and tested for any pressure leaks by monitoring the pressure changes in the system. Furthermore, the reactor is heated to the desired reaction temperature. The vacuum box is also heated to around 250^{o}C and evacuated to around 0.5 psi to prevent any condensation of hydrocarbons inside the box. The heating of the riser simulator is conducted under continuous flow of inert gases (argon) and the process usually takes few hours until thermal equilibrium is finally attained. Meanwhile, before the initial experimental run, the catalyst is activated for 15 minutes at 620^{o}C with air. The temperature controller is set to the desired reaction temperature likewise the timer is set to the desired reaction time. At this point the GC is started and set to the desired conditions.

Once the reactor and the gas chromatograph have reached their desired operating conditions, 200µl of the feed stock is injected directly into the reactor via a loaded syringe while the impeller is rotating at a speed of 6000rpm. After the reaction, the four port valve opens immediately ensuring that the reaction is terminated and the entire product stream sent online to the gas chromatograph via the pre-heated vacuum box chamber. The products are then analyzed in the gas chromatograph .After each experimental run, the catalyst is regenerated at conditions similar to initial activation.

The ethylbenzene (EB) conversion is expressed as follows:

$$X_{EB} = \frac{\text{moles of converted ethylbenzene}}{\text{moles of ethylbenzene fed}} \text{ X } 100$$

The selectivity (to product i) is expressed as follows:

$$S_i = \frac{\text{Number of carbon atoms of product i}}{\text{Number of carbon atoms of converted products}} \text{ X } 100$$

The yield (to product i) is expressed as follows:

$$Y_i = \frac{S_\mathrm{i}}{\mathrm{X_{EB}}} \text{ X } 100$$

3.5. Coke Analysis

The amount of coke deposited on the spent catalysts was determined by the combustion principle of the carbon analyzer multi EA 2000 (Analytikjena). A small amount of the spent catalyst (0.09 – 0.1g) is weighed into the combustion boat and fed completely into the hot zone of the furnace. Oxygen is fed directly into the unit and the coke deposit on the spent catalyst is burned completely, converting the carbonaceous deposit into carbon dioxide. The amount of coke formed is determined by measuring the number of moles of CO_2 released. This technique however cannot be used to determine the nature of the coke formed.

CHAPTER 4

4.0 RESULTS AND DISCUSSIONS

4.1 Ethylbenzene dehydrogenation over HT precursors of $Mg_3Fe_{0.25}Me_{0.25}Al_{0.5}$ (Me = Co, Mn and Ni) catalysts.

4.1.1. Physico-chemical properties

4.1.1.1. Chemical composition and textural properties

The textural properties along with metal composition of $Mg_3Fe_{0.25}Me_{0.25}Al_{0.5}$ (Me = Co, Mn and Ni) catalysts after the calcination at 550 °C are shown in Table 4.1. It can be clearly seen from Table 4.1 that all $Mg_3Fe_{0.5}Me_{0.5}Al_{0.5}$ catalysts exhibit large S_{BET} between 150 and 200 $m^2\ g_{cat}^{-1}$. This can be mainly attributed to the ability of Mg–Al and Mg–Fe to form the hydrotalcite structure, resulting in large surface area after the calcination. The relatively low S_{BET} (158 m^2g^{-1}) of $Mg_3Fe_{0.25}Mn_{0.25}Al_{0.5}$ compared to other catalysts is probably due to plugging of the pores with segregated bulk manganese oxide particles. This was suggested by XRD and H_2-TPR, which are discussed in the following paragraphs. It is also worth mentioning that the metal compositions are in complete agreement with the nominal values. This is due to the formation of hydrotalcite structure as the precursors during the coprecipitation, which accommodates many metal cations in the structure. Furthermore, the average pore diameter of hydrotalcites based samples is in the mesopore region (2-50 nm), as suggested by the pore size distributions (Figure 4.1A-C).

Table 4.1

Specific surface area, metal composition, and XPS analytical data of $Mg_3Fe_{0.25}\mathit{Me}_{0.25}Al_{0.5}$ (*Me* = Co, Mn and Ni)

Catalyst	S_{BET}/ $m^2g_{cat}^{-1}$	Molar ratio [a]			Binding energy [b] /eV			Surface molar ratio [b,c]	
		Mg/Fe	Mg/Al	Mg/Me	Mg $2p_{3/2}$	Fe $2p_{3/2}$	Me $2p_{3/2}$	Mg/Fe	Mg/Me
$Mg_3Fe_{0.25}Co_{0.25}Al_{0.5}$	187	11.5	5.5	11.5	48.9	710.6	779.6	6.5	5.0
$Mg_3Fe_{0.25}Mn_{0.25}Al_{0.5}$	158	11.1	5.1	11.6	49.0	710.6	641.5	7.1	8.3[d]
$Mg_3Fe_{0.25}Ni_{0.25}Al_{0.5}$	197	10.2	5.8	11.3	49.0	710.6	853.8	8.0	2.4

[a] By atomic absorbance analyses

[b] By XPS analyses

[c] After ASF correction

[d] The data scattered between 6.25–12.5

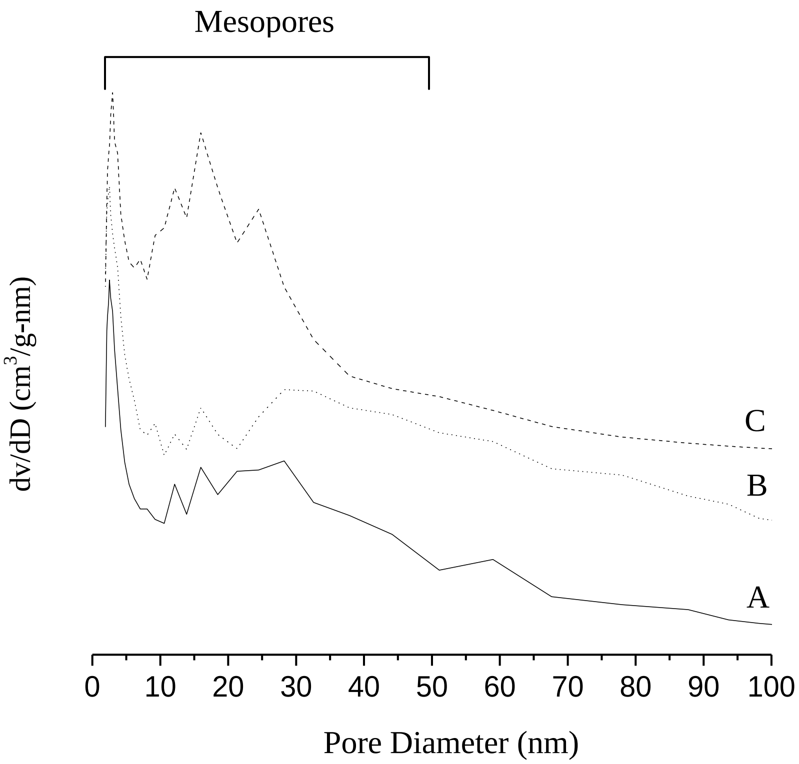

Figure 4.1. Pore size distribution of $Mg_3Fe_{0.25}\mathit{Me}_{0.25}Al_{0.5}$, where *Me* = Co (A), Mn (B), and Ni (C)

4.1.1.2. Surface analysis of the catalysts

The XPS analytical results of $Mg_3Fe_{0.25}\mathit{Me}_{0.25}Al_{0.5}$ (*Me* = Co, Mn and Ni) after calcination at 550 °C are summarized in Table 4.1. The surface molar ratios of Mg/Fe and Mg/*Me* calculated from the XPS results exhibited lower values than the bulk molar ratios obtained by AA analyses (Table 4.1). This indicates that both Fe and second component metal (*Me*) species are localized in the surface layer of the catalyst particles. On all $Mg_3Fe_{0.25}\mathit{Me}_{0.25}Al_{0.5}$ catalysts except $Mg_3Fe_{0.25}Ni_{0.25}Al_{0.5}$, Fe species showed similar surface enriched localization, i.e., almost 1.4 times higher concentration in the surface layer than the bulk phase. Surface enrichment of Fe was not so significant for $Mg_3Fe_{0.25}Ni_{0.25}Al_{0.5}$. Contrarily, some of the second component metals exhibited far enriched distribution in the surface layer, i.e., the highest concentration in the surface layer was obtained by Ni (5 times), followed by Co (2.2 times) and Mn (1.3 times). The scattered experimental values for Mn clearly suggest that Mn dispersion on the catalyst was not homogeneous.

4.1.1.3. Bulk phase identification

XRD patterns of $Mg_3Fe_{0.25}\mathit{Me}_{0.25}Al_{0.5}$ (*Me* = Co, Mn and Ni) catalysts after drying are shown in Figure 4.2a. It can be noted that all $Mg_3Fe_{0.25}\mathit{Me}_{0.25}Al_{0.5}$ showed typical hydrotalcite reflections, indicating that the second metal components were incorporated into the hydrotalcite structure except $Mg_3Fe_{0.25}Mn_{0.25}Al_{0.5}$. Mn^{2+} possesses a larger ionic radii of 0.80 Å than the other Me^{2+} [73] and requires the highest pH for its complete precipitation as hydroxides among the *Me* cations used [40]. After the calcination at 550 °C (Figure 4.2b), all samples showed the periclase reflections together with weak spinel reflections. This indicates that iron was incorporated in the periclase and the spinel.

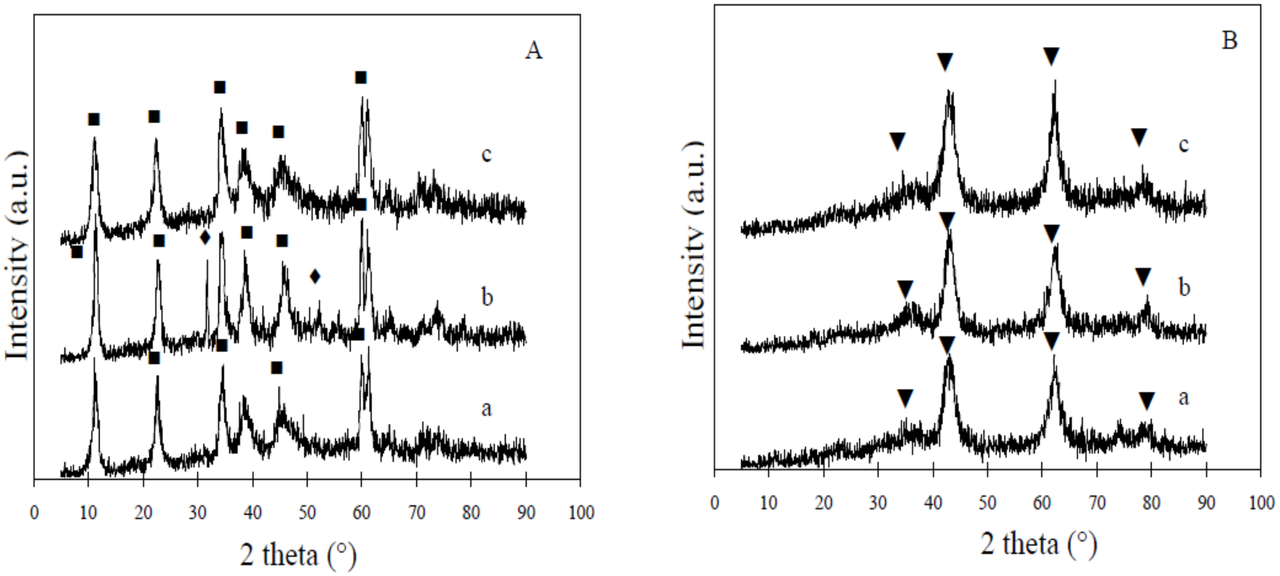

Figure 4.2. XRD patterns of $Mg_3Fe_{0.25}Me_{0.25}Al_{0.5}$ (*Me* = Co (a), Mn (b) and Ni (c)) after A) drying and B) calcination at 550 °C (■: Hydrotalcites; ♦: unknown and ▼: periclase)

4.1.1.4. Reducibility of the active specie on the catalysts

H_2-TPR data of $Mg_3Fe_{0.25}\mathit{Me}_{0.25}Al_{0.5}$ (*Me* = Mn, Ni, and Co) are shown in Figure 4.3. Mg_3Fe_1 showed a reduction peak at 418 °C and a broad peak above 650 °C (Figure 4.3a). The first peak is attributed to the reduction of spinel ($MgFe^{3+}{}_2O_4$) to periclase ($Mg_{1-x}Fe^{2+}{}_xO$) and the latter is to the reduction of $Mg_{1-x}Fe^{2+}{}_xO$ to Fe^0, as reported by Shen et al. [74], $Mg_3Fe_{0.25}Ni_{0.25}Al_{0.5}$ showed a weak reduction peak at 353 °C and broad reduction peak above 800 °C. The latter is attributed to the reduction of Ni^{2+} in the Mg(Ni)O periclase [75]. Therefore, the one observed at 353 °C can be attributed the reduction of Fe^{3+} species. $Mg_3Fe_{0.25}Mn_{0.25}Al_{0.5}$ exhibited rather strong two reduction peaks at 257 °C and 428 °C (Figure 4.3c). This catalyst exhibited unknown reflections together with those of hydrotalcite after drying (Figure 4.2b), suggesting that manganese oxides were separated from periclase after calcination. It was reported that a mixed oxide of $Mg_{0.2}Mn_{1.8}Al_1$ composition derived from hydrotalcite and cacined at 500 °C showed two reduction peaks at 333 °C and 460 °C [76]. This also suggests that manganese oxides were separated from periclase structure in $Mg_3Fe_{0.25}Mn_{0.25}Al_{0.5}$ and showed the reduction peaks at 257 °C and 428 °C.

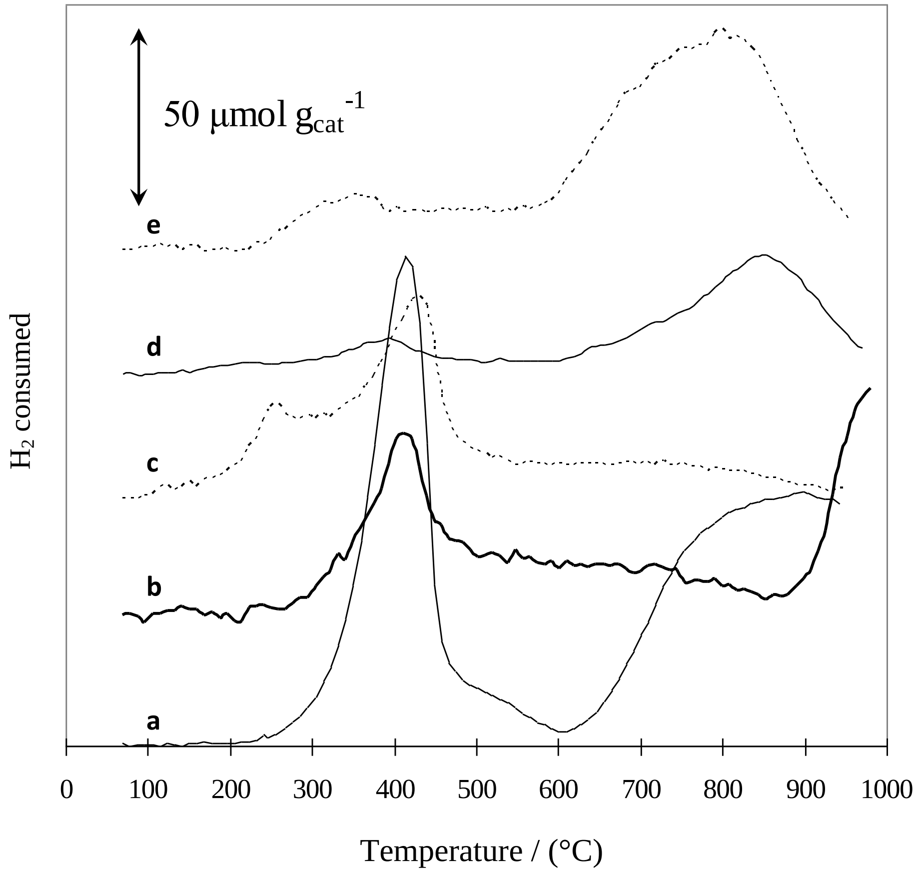

Figure 4.3. H_2-TPR of $Mg_3Fe_{0.25}Me_{0.25}Al_{0.5}$ (*Me* = Co, Mn, and Ni) catalysts. a) Mg_3Fe_1;

b) $Mg_3Fe_{0.5}Al_{0.5}$; c) $Mg_3Fe_{0.25}Mn_{0.25}Al_{0.5}$; d) $Mg_3Fe_{0.25}Co_{0.25}Al_{0.5}$; and f) $Mg_3Fe_{0.25}Ni_{0.25}Al_{0.5}$.

4.1.2. Catalytic Activity

The product distribution of the ethylbenzene dehydrogenation reaction over $Mg_3Fe_{0.25}\mathit{Me}_{0.25}Al_{0.5}$ (*Me* = Co, Mn and Ni) catalysts at different reaction temperatures and reaction times are presented in Tables 4.2–4.4. The experimental results showed styrene to be the main reaction product, although small amounts of benzene were obtained as by product. Traces of toluene, gaseous hydrocarbons, diethylbenzene (DEB) were also observed; however the yields of these products were neglected in subsequent analysis. In all the catalysts investigated, EB conversion increased with both reaction temperature and time and maximum conversion of approximately 15.5, 19.7, 18.0% was attained at 20 s of time on stream and temperature of 550 °C for $Mg_3Fe_{0.25}Co_{0.25}Al_{0.5}$, $Mg_3Fe_{0.25}Mn_{0.25}Al_{0.5}$, and $Mg_3Fe_{0.25}Ni_{0.25}Al_{0.5}$ catalysts respectively as shown in Figure 4.4(A-C). The mixed oxides catalyst consisting of Mn^{2+} gave the highest activity regardless of its low surface area. This may be accounted for by the isolation of manganese oxides from the periclase structure, as suggested by XRD, XPS and H_2-TPR. Therefore, the inhomogeneous dispersion of Mn^{2+} on the catalyst (i.e. presence of segregated (bulk) Mn oxide) is assumed to increase the active sites of the catalyst. One may suggest that the segregated manganese oxide further contributes to the basicity of MgO which has been reported to initiate H^+ abstraction [48]. The investigation of iron oxide catalysts containing various transition metal oxides by Hirano [77] also showed that increase in basicity due to reduction in electronegativity of the promoter gave rise to the dehydrogenation activity of the catalyst. As a control, a commercial catalyst was also tested. It showed a low activity as shown in Figure 4.5 which can be attributed to the absence of steam.

Table 4.2

Product distribution at various reaction conditions for the dehydrogenation of ethylbenzene over $Mg_3Fe_{0.25}Co_{0.25}Al_{0.5}$ mixed oxides catalyst

Temp (◦C)	Reaction time (s)	EB Conv. (%)	Styrene	Benzene	Toluene	Gases	DEB
400	5	3.18	2.58	0.44	0.09	-	0.12
	10	4.66	3.66	0.74	0.08	-	0.18
	15	5.19	3.85	0.89	0.11	0.06	0.22
	20	5.51	3.79	1.10	0.12	0.06	0.38
450	5	5.48	4.14	0.85	0.16	0.09	0.13
	10	6.47	4.82	1.14	0.23	0.12	0.16
	15	6.61	4.48	1.49	0.19	0.13	0.25
	20	7.12	4.44	1.58	0.18	0.14	0.41
500	5	6.99	4.89	1.45	0.23	0.19	0.15
	10	8.55	5.67	1.85	0.24	0.24	0.21
	15	10.71	6.71	2.69	0.33	0.44	0.24
	20	11.7	7.35	2.99	0.37	0.39	0.37
550	5	8.65	5.83	1.95	0.24	0.33	0.22
	10	11.38	7.11	2.83	0.36	0.48	0.17
	15	12.83	7.84	3.39	0.42	0.56	0.25
	20	15.46	8.84	4.56	0.60	0.88	0.34

Table 4.3

Product distribution at various reaction conditions for the dehydrogenation of ethylbenzene over $Mg_3Fe_{0.25}Mn_{0.25}Al_{0.5}$ mixed oxides catalyst

Temp (°C)	Reaction time (s)	EB Conv. (%)	Styrene	Benzene	Toluene	Gases	DEB
400	5	4.06	3.76	0.36	-	-	-
	10	5.82	5.19	0.49	-	-	0.04
	15	6.25	5.65	0.55	-	-	0.05
	20	6.64	5.93	0.65	-	-	0.06
450	5	5.64	4.97	0.55	0.05	-	-
	10	9.00	7.58	1.11	0.11	0.08	0.07
	15	8.98	7.44	1.12	0.09	0.08	0.13
	20	10.19	8.25	1.28	0.12	0.07	0.19
500	5	8.70	6.96	1.40	0.12	0.14	-
	10	10.65	8.33	1.77	0.18	0.15	0.07
	15	12.93	9.69	2.39	0.21	0.20	0.15
	20	17.25	12.01	3.03	0.39	0.25	0.24
550	5	11.46	8.13	2.59	0.25	0.30	-
	10	15.02	10.27	3.58	0.39	0.41	0.13
	15	18.63	11.50	4.66	0.58	0.54	0.16
	20	19.70	12.28	4.95	0.70	0.54	0.19

Table 4.4

Product distribution at various reaction conditions for the dehydrogenation of ethylbenzene over $Mg_3Fe_{0.25}Ni_{0.25}Al_{0.5}$ mixed oxides catalyst

Temp (°C)	Reaction time (s)	EB Conv. (%)	Styrene	Benzene	Toluene	Gases	DEB
400	5	2.14	1.70	0.35	0.05	-	0.06
	10	3.23	2.39	0.58	0.07	-	0.21
	15	3.86	2.64	0.76	0.08	-	0.27
	20	4.21	2.78	0.89	0.12	0.05	0.32
450	5	4.08	3.17	0.65	0.07	0.08	0.07
	10	4.82	3.36	0.88	0.13	0.07	0.23
	15	6.25	4.24	1.23	0.14	0.12	0.32
	20	7.01	4.59	1.52	0.17	0.17	0.52
500	5	5.75	4.45	0.99	0.12	0.15	0.06
	10	8.14	5.58	1.68	0.19	0.25	0.24
	15	9.74	6.26	2.23	0.25	0.31	0.40
	20	10.87	7.05	2.46	0.47	0.35	0.36
550	5	10.04	6.86	2.12	0.35	0.39	0.13
	10	13.27	8.74	3.03	0.44	0.55	0.20
	15	16.17	10.18	3.82	0.67	0.67	0.31
	20	18.04	11.16	4.31	0.86	0.76	0.37

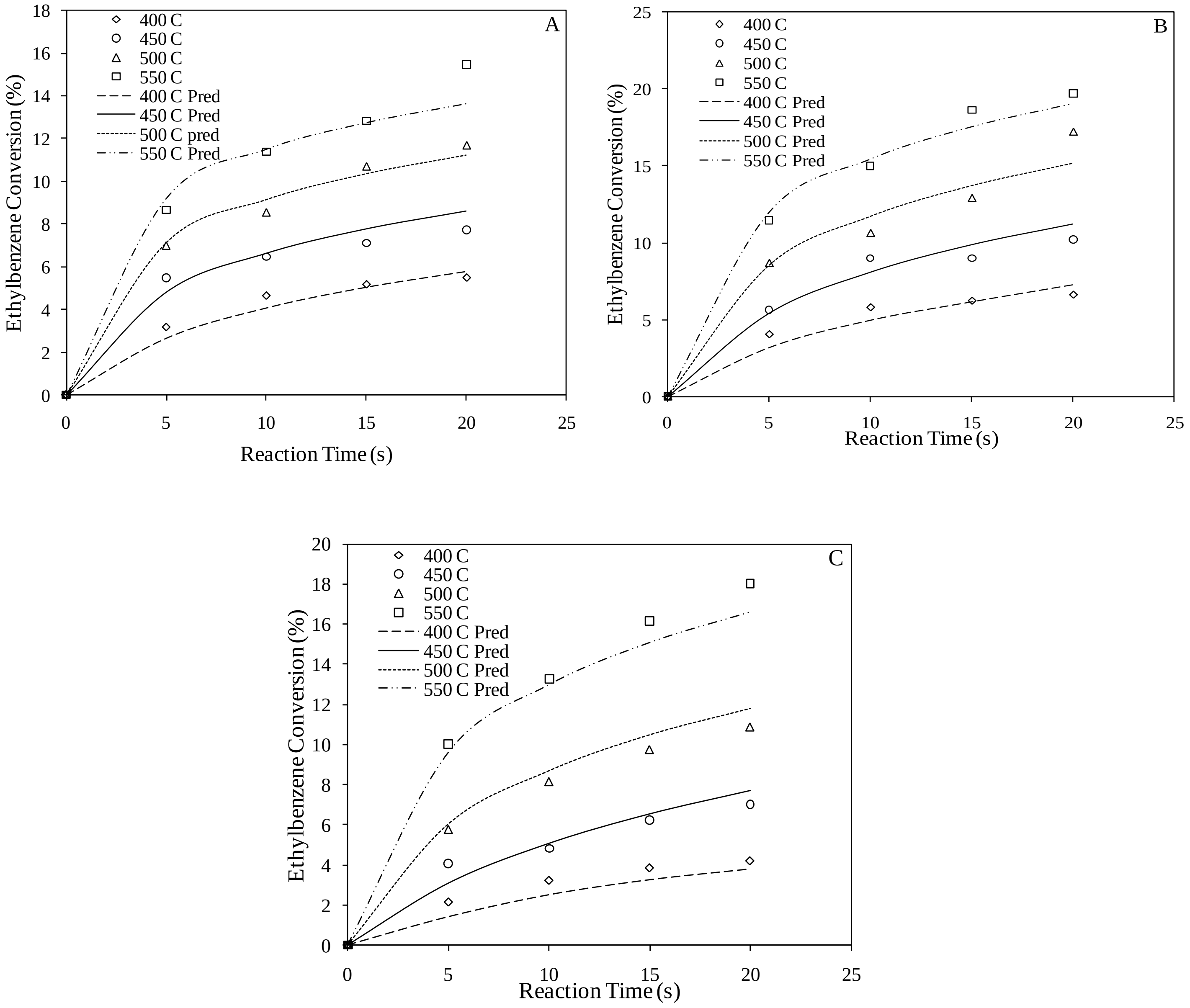

Figure 4.4. Conversion of ethylbenzene with respect to time at various temperatures over different hydrotalcite mixed oxides; A) $Mg_3Fe_{0.25}Co_{0.25}Al_{0.5}$, B) $Mg_3Fe_{0.25}Mn_{0.25}Al_{0.5}$, and C) $Mg_3Fe_{0.25}Ni_{0.25}Al_{0.5}$.

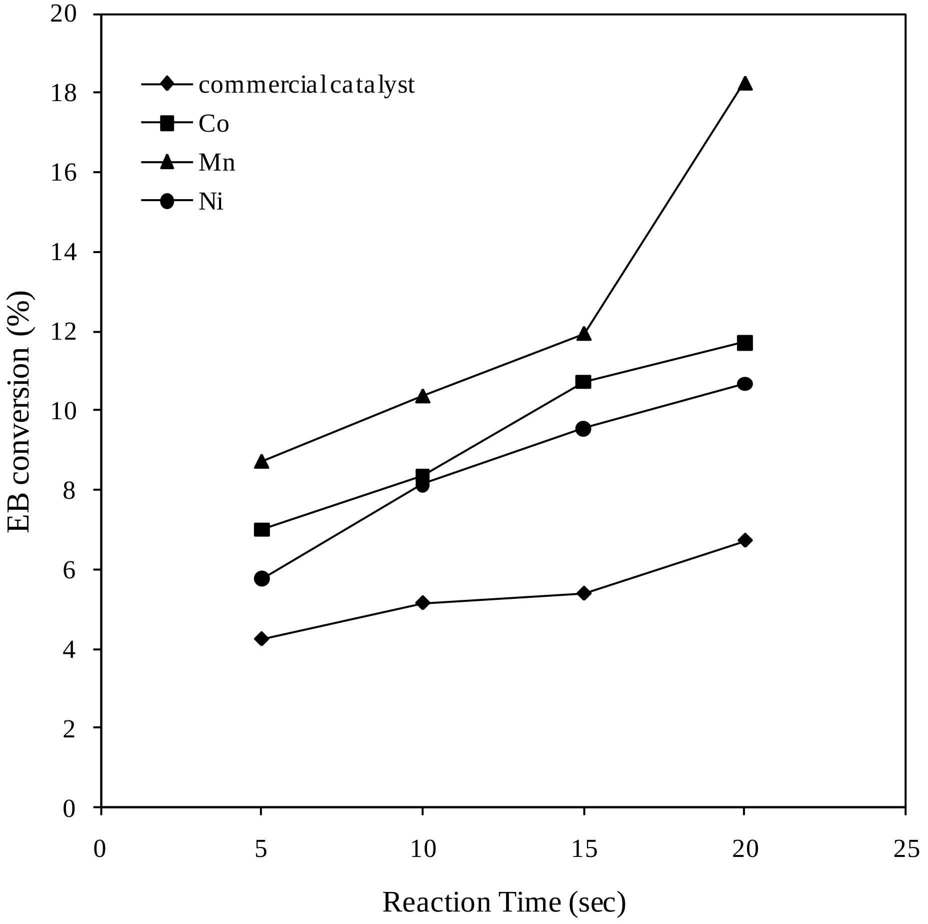

Figure 4.5. Conversion of ethylbenzene with respect to time at 500 °C, comparison between commercial and HT catalysts

4.1.2.1. Styrene/Benzene Selectivity

The product selectivity during the dehydrogenation of EB over $Mg_3Fe_{0.25}\mathit{Me}_{0.25}Al_{0.5}$ (*Me* = Co, Mn and Ni) and commercial catalysts were compared in Figure 4.6 at constant conversion level of ~ 6%. The results show that styrene is obtained as the most predominant product on all the HT catalysts with the best selectivity observed in $Mg_3Fe_{0.25}Mn_{0.25}Al_{0.5}$. The selectivity towards styrene exhibits a trend opposite to EB conversion for all the HT catalysts investigated. It decreased when the reaction temperature was raised due to cracking reaction. Figure 4.7 shows selectivity as a function of the EB conversion for all the reaction temperatures for $Mg_3Fe_{0.25}Mn_{0.25}Al_{0.5}$, showing a maximum styrene selectivity of 92.7% at reaction temperature of 400 °C which corresponds to 4.9% EB conversion. However, benzene selectivity increased as the temperature was raised. This confirmed that cracking of EB to benzene becomes pronounced at high temperature as shown in Figure 4.7. A maximum benzene selectivity of 25.1% was attained at 550 °C corresponding to 19.7% EB conversion. On the contrary, the commercial catalyst has low selectivity towards styrene which was due to significant cracking and such an occurrence has been suggested by Lee [14] to be as a result of increase in acidity of the catalyst due to loss of potassium from the catalyst surface.

It is also worth mentioning that $Mg_3Fe_{0.25}Mn_{0.25}Al_{0.5}$ catalyst exhibited much lower selectivity to diethylbenzene (DEB, three isomers) than the other two catalysts (Co^{2+} and Ni^{2+}). Therefore, it can be inferred from these results that Mn^{2+} does not favor the disproportionation reaction. For instance, the selectivity to DEB (temperature = 400 °C and residence time = 20s) over Mn^{2+}, Co^{2+}, and Ni^{2+} based oxides were 1.0 wt%, 6.9 wt% and 7.6 wt%, respectively (Tables 4.2-4.4).

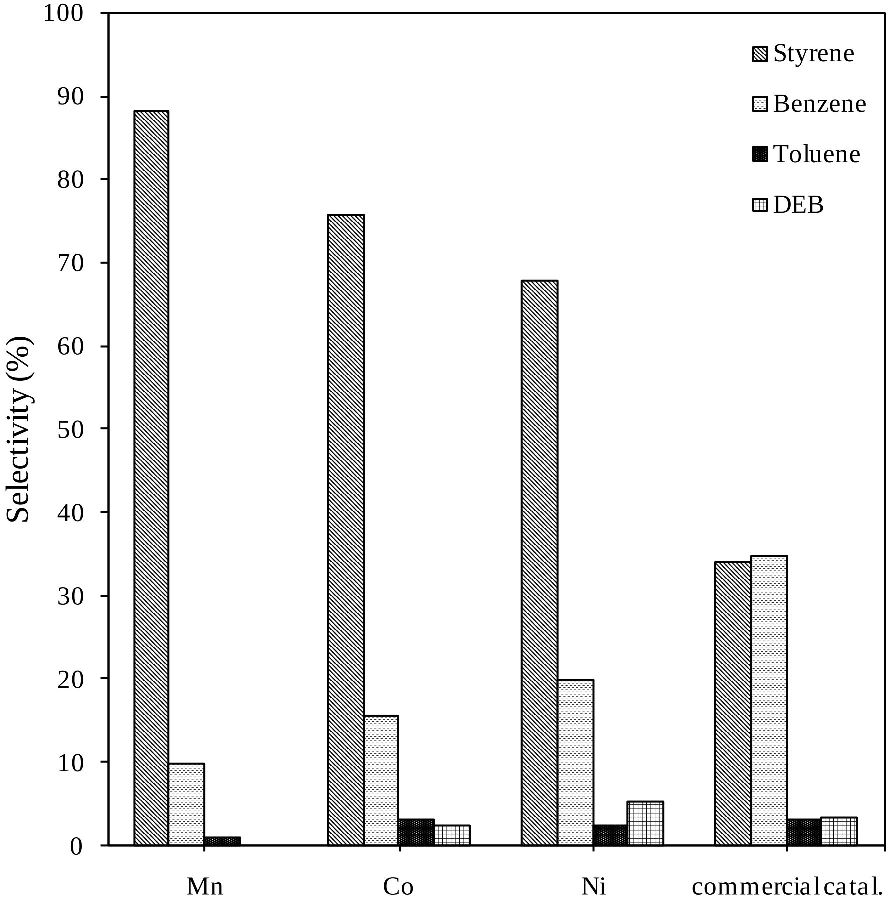

Figure 4.6. Product selectivity of ethylbenzene dehydrogenation over the different catalysts at ~ 6% ethylbenzene conversion

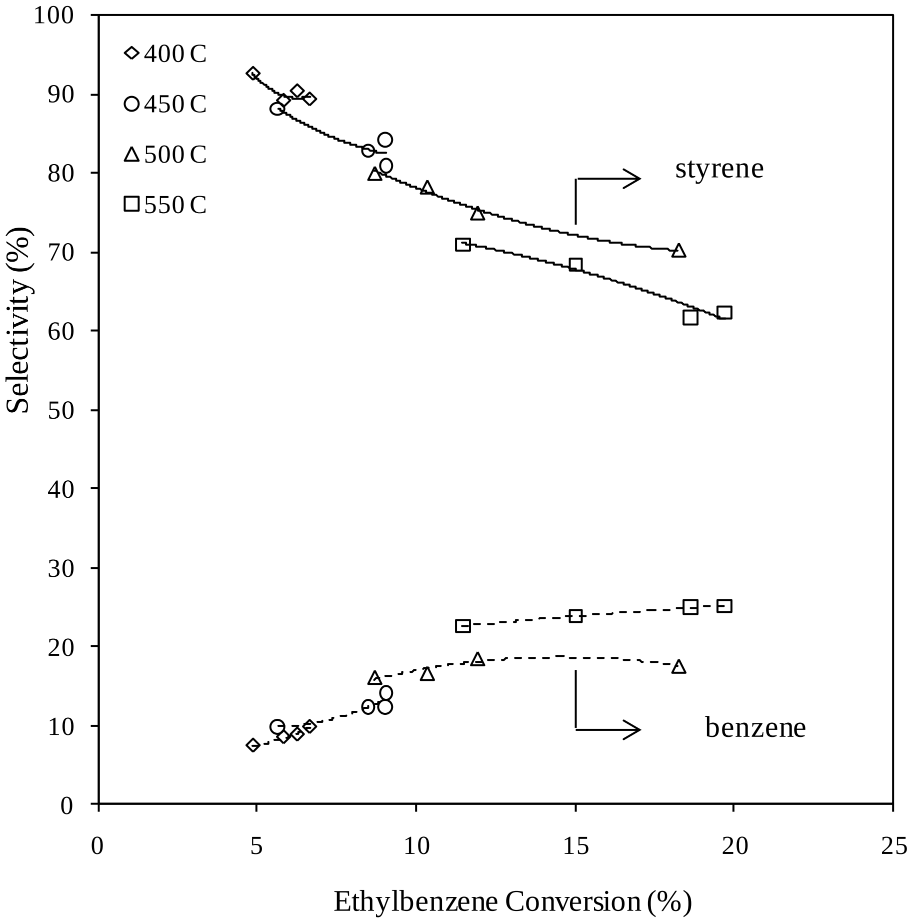

Figure 4.7. Selectivity with respect to conversion and temperature for $Mg_3Fe_{0.25}Mn_{0.25}Al_{0.5}$

4.1.2.2. Styrene/Benzene Yield

The yield of styrene was found to increase with both temperature and time, in a similar manner with EB conversion. Maximum styrene yield of approximately 8.8, 12.3, and 11.2% for $Mg_3Fe_{0.25}Co_{0.25}Al_{0.5}$, $Mg_3Fe_{0.25}Mn_{0.25}Al_{0.5}$ and $Mg_3Fe_{0.25}Ni_{0.25}Al_{0.5}$ catalysts respectively were attained at reaction temperature of 550 °C and 20 s time on stream. $Mg_3Fe_{0.25}Mn_{0.25}Al_{0.5}$ gave the maximum styrene yield, and its variation with temperature is shown in Figure 4.8A. Similarly, benzene yield was equally increasing with both temperature and time with a maximum of approximately 4.6, 4.9, and 4.3% for $Mg_3Fe_{0.25}Co_{0.25}Al_{0.5}$, $Mg_3Fe_{0.25}Mn_{0.25}Al_{0.5}$, and $Mg_3Fe_{0.25}Ni_{0.25}Al_{0.5}$ catalysts respectively at 550 °C for reaction time of 20 s. Figure 4.8B shows the variation of benzene yield with temperature for $Mg_3Fe_{0.25}Mn_{0.25}Al_{0.5}$. It can thus be concluded that for longer reaction time, EB undergoes both dehydrogenation and dealkylation reactions to give styrene and benzene respectively. It can also be seen from Tables 4.2-4.4 that both the yield of DEB (disproportionation product) and toluene (cracking product) increased with temperature.

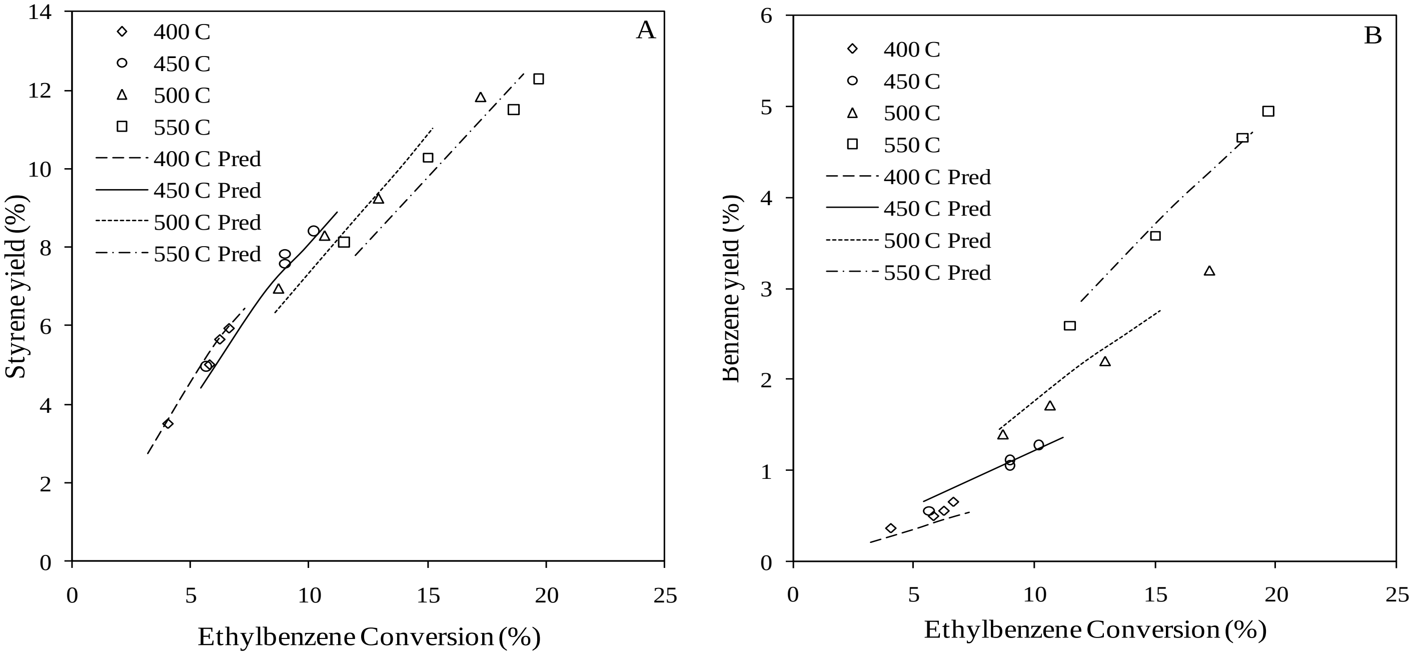

Figure 4.8. Styrene (A) and benzene (B) yields vs. ethylbenzene conversion at various temperatures for $Mg_3Fe_{0.25}Mn_{0.25}Al_{0.5}$

4.1.3. Coke Content Measurement

Table 4.5 shows the amount of coke deposited for the catalysts investigated at 550 °C. The data revealed low coke yield, and the ratio of coke weight percent to percent conversion is small. Similarly, coking on the commercial catalyst was low. This implies that dehydrogenation of ethylbenzene over the catalysts is not accompanied by substantial coke deposition. It can thus be inferred that loss of activity of this commercial catalyst in the absence of steam was not due to coking but as a result of solid state transformation, though the exact deactivation mechanism was not studied.

Table 4.5
Coke formation of Ethylbenzene dehydrogenation reaction at different reaction conditions

Catalysts	Temp (°C)	Reaction time (s)	Conversion (%)	Coke wt (% C)	Coke wt/ conversion
$Mg_3Fe_{0.25}Co_{0.25}Al_{0.5}$	550	10	11.38	0.503	0.044
		20	15.46	0.488	0.032
$Mg_3Fe_{0.25}Mn_{0.25}Al_{0.5}$	550	10	15.02	0.618	0.041
		20	19.70	0.694	0.035
$Mg_3Fe_{0.25}Ni_{0.25}Al_{0.5}$	550	10	13.27	0.582	0.044
		20	18.04	0.452	0.025
Commercial catal.	550	10	7.87	0.382	0.049
		20	11.15	0.446	0.040

4.1.4. Kinetic Modeling

4.1.4.1. Model development

In addition to the main dehydrogenation reaction (equation 4.1), the side reactions (equations (4.2) – (4.4)) are also known to take place

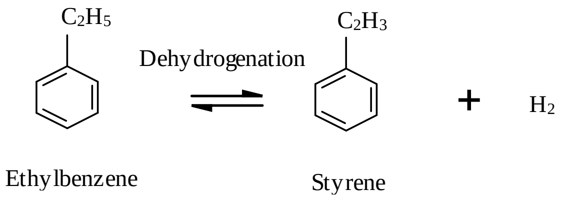

(4.1)

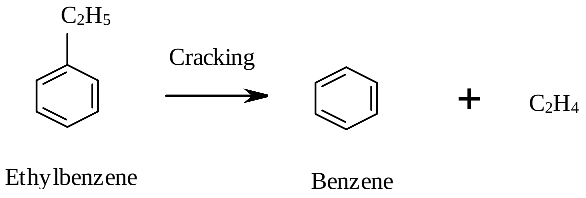

(4.2)

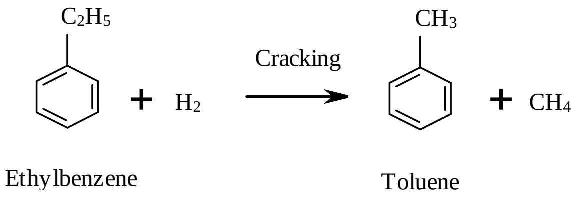

(4.3)

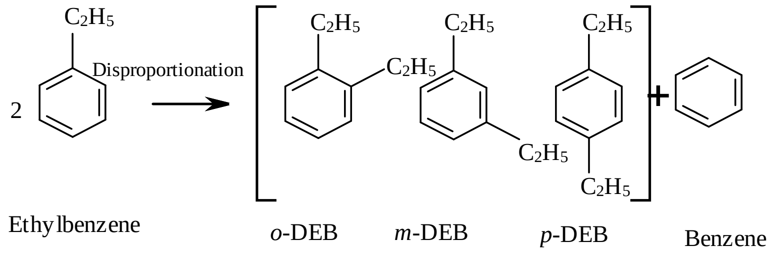

(4.4)

A reaction scheme for EB dehydrogenation is given as scheme 1, neglecting the disproportionation reaction based on the product distribution. Adapting this scheme to the model development in estimating the kinetic parameters, toluene formation was not considered owing to its very low concentration in the reaction product.

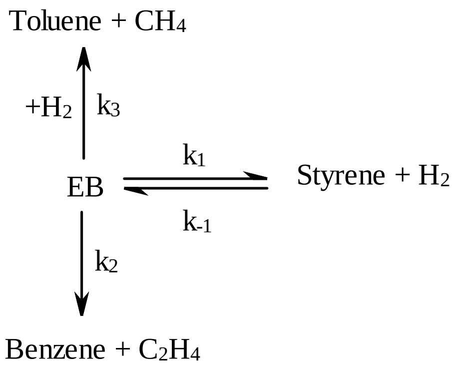

scheme 1

Scheme 1 Catalytic reaction scheme of ethylbenzene (EB) dehydrogenation

The experimental results were modeled using catalyst deactivation function model based on both reactant conversion (RC) and time-on-stream (TOS) catalyst decay function.

4.1.4.2. Catalyst activity decay function based on reactant conversion (RC)

This type of catalyst deactivation function model was developed by Al-Khattaf and de Lasa [78]. According to this model, the deactivation is based on the conversion of ethylbenzene which is directly related to coke formation. This approach is more sound than time-on-stream approach which has been widely used in literature to account for catalyst deactivation. From the reaction network shown in scheme and the assumption that toluene formation is neglected, the following set of species balances and catalytic reactions can be written:

Rate of EB disappearance, r_{EB}

$$-\frac{V}{W_c}\frac{dC_{EB}}{dt} = (k_1 C_{EB} - k_{-1} C_{ST} C_H + k_2 C_{EB})\varphi \tag{4.5}$$

Rate of styrene appearance, r_{ST}

$$\frac{V}{W_c}\frac{dC_{ST}}{dt} = (k_1 C_{EB} - k_{-1} C_{ST} C_H)\varphi \tag{4.6}$$

Rate of formation of benzene, r_B

$$\frac{V}{W_c}\frac{dC_B}{dt} = k_2 C_{EB}\varphi \tag{4.7}$$

where C_i is molar concentration of each of the species in the riser simulator, V is the volume of the riser (45 cm^3), W_c is the mass of the catalyst (0.81 g-cat), t is time (in seconds), k is the rate constant (cm^3/(g-cat·s)), and φ, the catalyst decay function, which accounts for the loss of catalytic activity as a result of deactivation due to coking. For the reactant conversion model, the catalyst deactivation function is given as:

$$\varphi = exp(-\lambda(1 - y_{EB}) \tag{4.8}$$

where λ is catalyst deactivation constant

By definition, the molar concentration C_i of each species can be written in terms of its mass fraction y_i, which are the measurable variables from our chromatographic analysis, by the following relation:

$$C_i = \frac{y_i W_{hc}}{MW_i V} \tag{4.9}$$

where W_{hc} is the weight of feedstock injected into the reactor, MW_i is the molecular weights of the individual species and V is the volume of the riser simulator.

To ensure thermodynamic consistency at equilibrium, the temperature dependent equilibrium constant for the reversible reaction was found to be:

$$K_C = \frac{k_1}{k_{-1}} \tag{4.10}$$

which has been calculated from literature as [32]:

$$K_C = \exp\left\{-\left(\frac{122700 - 126.3\mathrm{T} - 2.194 \times 10^{-3}\mathrm{T}^2}{\mathrm{RT}}\right)\right\} \times 10^5\ Pa \tag{4.11}$$

Substituting Eq. (4–6) into Eqs (1–3) and simplifying gives the following:

$$\frac{dy_{EB}}{dt} = -\left[k_1\left(y_{EB} - G_1\frac{y_{ST}y_H}{K_C}\right) + k_2 y_{EB}\right]\frac{W_c}{V}\exp(-\lambda(1 - y_{EB}) \tag{4.12}$$

$$\frac{dy_{ST}}{dt} = k_1\left(G_2 y_{EB} - G_3\frac{y_{ST}y_H}{K_C}\right)\frac{W_c}{V}\exp(-\lambda(1 - y_{EB}) \tag{4.13}$$

$$\frac{dy_B}{dt} = G_4 k_2 y_{EB}\frac{W_c}{V}\exp(-\lambda(1 - y_{EB}) \tag{4.14}$$

G_1, G_2, G_3, and G_4 are lumped constants given as:

$$G_1 = \frac{MW_{EB}W_{hc}}{MW_{ST}MW_H V}$$

$$G_2 = \frac{MW_{ST}}{MW_{EB}}$$

$$G_3 = \frac{W_{hc}}{MW_H V}$$

$$G_4 = \frac{MW_B}{MW_{EB}}$$

The activation energy, E_i, for the dehydrogenation reaction is related to temperature dependent rate constants k_i according to the Arrhenius equation given below:

$$k_i = A_i exp\left(-\frac{E_i}{RT}\right) \tag{4.15}$$

where A_i is called the pre-exponential factor. Agarwal and Brisk have suggested re-parameterization of equation above during kinetic modeling to help reduce parameter interaction. Therefore, k_i constants were re-parameterized by centering the values around k_{0i} which is the value of the rate constant for reaction i at the average temperature T_0 of the investigated temperatures [79]:

$$k_i = k_{0i} exp\left[-\frac{E_i}{R}\left(\frac{1}{T} - \frac{1}{T_0}\right)\right] \tag{4.16}$$

Since the experimental runs were done at 400, 450, 500 and 550 °C, T_o was calculated to be 475 °C.

The above reaction model equations were derived based on the following assumptions:

1. Catalyst deactivation was assumed to be a function of reactant conversion. And, a single deactivation function was defined for all the reactions.

2. The model assumes only catalytic reactions and neglects thermal conversion.

3. The reactor operates under isothermal conditions, justified by the negligible temperature change observed during the reaction.

4. Toluene yield is negligible.

5. The model also neglects the disproportionation reaction.

4.1.4.3.Catalyst activity decay function based on time-on-stream (TOS)

The catalyst activity decay model based on time-on-stream was initially suggested by Voorhies [80]. Since then, this model has been used extensively throughout the FCC literature. This model is empirically based given it does not incorporate a mechanistic description of catalyst deactivation. As a result, extrapolations of activity decay with this model are quite uncertain.

Modeling of the catalytic reactions based on TOS follows the same procedure as RC. In this case catalyst deactivation due to coke formation is related to time. Carbon deposit on catalyst increases with time, therefore the catalyst deactivation function is given as:

$$\varphi = exp(-\alpha t) \tag{4.17}$$

The model equations obtained based on similar assumptions for RC are thus:

$$\frac{dy_{EB}}{dt} = -\left[k_1\left(y_{EB} - G_1\frac{y_{ST}y_H}{K_C}\right) + k_2 y_{EB}\right]\frac{W_c}{V}\exp(-\alpha t) \tag{4.18}$$

$$\frac{dy_{ST}}{dt} = k_1\left(G_2 y_{EB} - G_3\frac{y_{ST}y_H}{K_C}\right)\frac{W_c}{V}\exp(-\alpha t) \tag{4.19}$$

$$\frac{dy_B}{dt} = G_4 k_2 y_{EB}\frac{W_c}{V}\exp(-\alpha t) \tag{4.20}$$

where G_1, G_2, G_3, and G_4 are lumped constants already defined.

4.1.4.4. Determination of model parameters

A. Reactant Conversion Model

The kinetic parameters k_{oi}, E_i and λ for the reactions were determined by fitting experimental results into the rate equations 4.12–4.14 using non-linear regression analysis with the aid of MATLAB package. The values of the model parameters along with their corresponding 95% confidence limits (CLs) are shown in Table 4.6 while the resulting cross-correlation matrices are also given in Table 4.7 for $Mg_3Fe_{0.25}Co_{0.25}Al_{0.5}$, $Mg_3Fe_{0.25}Mn_{0.25}Al_{0.5}$ and $Mg_3Fe_{0.25}Ni_{0.25}Al_{0.5}$ catalysts respectively. As shown in Table 4.7 the correlations between k_1 and E_1, E_1 and λ and k_1 and λ for all the estimated parameters of dehydrogenation reaction to produce styrene with correlations between k_2 and E_2, E_2 and λ and k_2 and λ of cracking reaction have low and moderate level of parameter interaction with only a few exceptions. From the results of the kinetic parameters, the estimated apparent energies for dehydrogenation of EB to St. for $Mg_3Fe_{0.25}Co_{0.25}Al_{0.5}$, $Mg_3Fe_{0.25}Mn_{0.25}Al_{0.5}$, and $Mg_3Fe_{0.25}Ni_{0.25}Al_{0.5}$ catalysts are 18.3, 15.6, and 20.9 kcal/mol respectively. These values are found to be lower compared to those reported in most literatures; however, the result obtained for $Mg_3Fe_{0.25}Ni_{0.25}Al_{0.5}$ is essentially the same as that reported by Addiego et al. [36], an apparent activation energy of 21 kcal/mol for 30% K-promoted Fe_2O_3. The activation energies estimated for dealkylation reactions which are 22.3, 26.7, and 22.7 kcal/mole for $Mg_3Fe_{0.25}Co_{0.25}Al_{0.5}$, $Mg_3Fe_{0.25}Mn_{0.25}Al_{0.5}$, and $Mg_3Fe_{0.25}Ni_{0.25}Al_{0.5}$ catalysts respectively, are found to be higher than that for dehydrogenation reaction. Similar trend has been reported by Hirano [18,19] both for unpromoted and promoted iron oxide catalysts. This indicates that high activation energy must be overcome for the cracking reaction to proceed.

Table 4.6

Estimated kinetic parameters for hydrotalcite mixed oxides catalyst based on reactant conversion model

Parameters	Values			r^2
	k_1	k_2	λ	
$Mg_3Fe_{0.25}Co_{0.25}Al_{0.5}$				
$E_{i\text{-}Co}$ (kJ/mol)	76.37	93.07	30.86	0.99
95% CL	7.67	9.99	3.52	
k_{0i}[a] x 10^3 [m^3 / (kg of catalyst.s)]	1.38	0.64		
95% CL	0.30	0.15		
$Mg_3Fe_{0.25}Mn_{0.25}Al_{0.5}$				
$E_{i\text{-}Mn}$ (kJ/mol)	65.2	111.8	17.18	0.99
95% CL	6.41	13.87	2.10	
k_{0i}[a] x 10^3 [m^3 / (kg of catalyst.s)]	1.24	0.32		
95% CL	0.20	0.07		
$Mg_3Fe_{0.25}Ni_{0.25}Al_{0.5}$				
$E_{i\text{-}Ni}$ (kJ/mol)	87.46	94.74	16.51	0.99
95% CL	6.24	9.63	1.9	
k_{0i}[a] x 10^3 [m^3 / (kg of catalyst.s)]	0.52	0.23		
95% CL	0.06	0.03		

[a] Pre-exponential factor as obtained from Eq. (4.16); unit for second order (m^6/(kg of catalyst).s).

Table 4.7

Correlation matrix for ethylbenzene dehydrogenation over hydrotalcite mixed oxides catalyst (RC model)

	k_1	E_1	k_2	E_2	λ
$Mg_3Fe_{0.25}Co_{0.25}Al_{0.5}$					
k_{1-Co}	1.0000	0.8342	0.9290	0.6689	0.9788
E_{1-Co}	0.8342	1.0000	0.8147	0.6937	0.8645
k_{2-Co}	0.9290	0.8147	1.0000	0.4810	0.9251
E_{2-Co}	0.6689	0.6937	0.4810	1.0000	0.6714
λ	0.9788	0.8645	0.9251	0.6714	1.0000
$Mg_3Fe_{0.25}Mn_{0.25}Al_{0.5}$					
k_{1-Mn}	1.0000	0.7903	0.6898	0.4180	0.9696
E_{1-Mn}	0.7903	1.0000	0.6074	0.4035	0.8374
k_{2-Mn}	0.6898	0.6074	1.0000	-0.2421	0.6962
E_{2-Mn}	0.4180	0.4035	-0.2421	1.0000	0.4154
λ	0.9696	0.8374	0.6962	0.4154	1.0000
$Mg_3Fe_{0.25}Ni_{0.25}Al_{0.5}$					
k_{1-Ni}	1.0000	0.6215	0.6349	0.5320	0.9260
E_{1-Ni}	0.6215	1.0000	0.6500	0.3865	0.8041
k_{2-Ni}	0.6349	0.6500	1.0000	-0.0659	0.7173
E_{2-Ni}	0.5320	0.3865	-0.0659	1.0000	0.5097
λ	0.9260	0.8041	0.7173	0.5097	1.0000

B. Time-on-stream Model

Using the experimental data for the EB dehydrogenation, the model parameters k_{oi}, E_i and α of equations 4.18–4.20 were estimated using non-linear regression in a similar manner as that of the RC model. Table 4.8 reports the values of the parameters obtained and the 95% confidence interval. Table 4.9 shows the correlation matrix indicating low to moderate parameter interaction. $Mg_3Fe_{0.25}Mn_{0.25}Al_{0.5}$ gave the best activity and selectivity based on the estimated parameters which is in accordance with the conclusion reached with RC model.

Table 4.8

Estimated kinetic parameters for hydrotalcite mixed oxides catalyst based on time-on-stream model

Parameters	Values			r^2
	k_1	k_2	α	
$Mg_3Fe_{0.25}Co_{0.25}Al_{0.5}$				
$E_{i\text{-}Co}$ (kJ/mol)	24.70	44.18	0.18	0.99
95% CL	1.75	4.75	0.01	
k_{0i}[a] x 10^3 [m^3 / (kg of catalyst.s)]	0.69	0.31		
95% CL	0.04	0.02		
$Mg_3Fe_{0.25}Mn_{0.25}Al_{0.5}$				
$E_{i\text{-}Mn}$ (kJ/mol)	24.62	67.83	0.15	0.99
95% CL	1.96	9.69	0.01	
k_{0i}[a] x 10^3 [m^3 / (kg of catalyst.s)]	0.88	0.23		
95% CL	0.06	0.03		
$Mg_3Fe_{0.25}Ni_{0.25}Al_{0.5}$				
$E_{i\text{-}Ni}$ (kJ/mol)	44.76	58.98	0.14	0.99
95% CL	1.69	4.81	0.01	
k_{0i}[a] x 10^3 [m^3 / (kg of catalyst.s)]	0.54	0.22		
95% CL	0.02	0.02		

[a] Pre-exponential factor as obtained from Eq. (4.16); unit for second order (m^6/(kg of catalyst).s).

Table 4.9

Correlation matrix for ethylbenzene dehydrogenation over hydrotalcite mixed oxides catalyst (TOS model)

	k_1	E_1	k_2	E_2	λ
$Mg_3Fe_{0.25}Co_{0.25}Al_{0.5}$					
k_{1-Co}	1.0000	-0.1634	0.4844	0.1171	0.9318
E_{1-Co}	-0.1634	1.0000	0.2283	-0.5247	-0.0048
k_{2-Co}	0.4844	0.2283	1.0000	-0.5306	0.6743
E_{2-Co}	0.1171	-0.5247	-0.5306	1.0000	-0.0023
α	0.9318	-0.0048	0.6743	-0.0023	1.0000
$Mg_3Fe_{0.25}Mn_{0.25}Al_{0.5}$					
k_{1-Mn}	1.0000	-0.1501	0.2577	0.1255	0.9362
E_{1-Mn}	-0.1501	1.0000	0.2673	-0.4480	-0.0091
k_{2-Mn}	0.2577	0.2673	1.0000	-0.7781	0.4433
E_{2-Mn}	0.1255	-0.4480	-0.7781	1.0000	-0.0024
α	0.9362	-0.0091	0.4433	-0.0024	1.0000
$Mg_3Fe_{0.25}Ni_{0.25}Al_{0.5}$					
k_{1-Ni}	1.0000	-0.3367	0.2691	0.1974	0.8862
E_{1-Ni}	-0.3367	1.0000	0.3464	-0.5360	-0.0077
k_{2-Ni}	0.2691	0.3464	1.0000	-0.6962	0.5435
E_{2-Ni}	0.1974	-0.5360	-0.6962	1.0000	-0.0040
α	0.8862	-0.0077	0.5435	-0.0040	1.0000

From the estimated activation energies, the addition of Mn^{2+} to ternary Mg/Fe/Al HT best improved its catalyst activity even though both Co^{2+} and Ni^{2+} are well incorporated into the HT structure. $Mg_3Fe_{0.25}Mn_{0.25}Al_{0.5}$ has the least activation energy to produce styrene and highest energy to be overcome to crack EB to yield Bz. This further depicts that Mn^{2+} gave the best selectivity towards styrene formation which is consistent with the experimental data. This assertion can be justified from the results of the characterization of the catalysts. Mn^{2+} has been reported to possess a higher ionic radius than the other Me^{2+} which may have led to its incomplete incorporation into the HT structure [47]. The result of XPS from Table 4.1 shows Mn^{2+} to have the least binding energy. Binding energy has being reported to be linked to the strength of basicity of a catalyst [81], the lower the binding energy, the more basic the surface of the catalyst. It can thus be suggested that the segregation of Mn^{2+} serves as additional active sites which increased the basicity of the catalyst, responsible for initiating dehydrogenation by H^+ abstraction [48]. The active specie however is still identified as the metastable Fe^{3+}.

The use of fluidized bed reactor is suggested to have improved the overall performance of this process. This same experiment (EB dehydrogenation) was conducted using a continuous gas-flow fixed bed reactor at atmospheric pressure [47] over $Mg_3Fe_{0.25}Co_{0.25}Al_{0.5}$. The reaction was carried out for 3 h of time-on-stream at 550 °C with the catalyst after been pre-treated with a He gas. Activation energy of 29.1 kcal/mol was estimated from the Arrhenius plot. It can thus be assumed that the extensive bed mixing and heat distribution within the fluidized bed enhanced reactant-catalyst contact and uniform product quality, hence reduction of activation energy towards styrene formation.

In order to ascertain the proposed models developed for the dehydrogenation process of EB in the riser simulator, validation of the estimated kinetic parameters is imperative. Therefore, the estimated parameters were substituted into the set of differential equations developed and solved numerically using fourth-order-Runge-Kutta routine. The numerical results were compared with experimental data as shown in Figure 4.4(A-C). As observed from the Figure, the model predictions compared favorably with the obtained experimental data. This demonstrates that the proposed kinetic model fits well into our experimental observations. To further determine the adequacy of the model, a reconciliation plot (Figure 4.9) showing the overall agreement of experimental data and model predictions was done. The two agrees very well as suggested by the value of regression coefficient, r^2 (0.99).

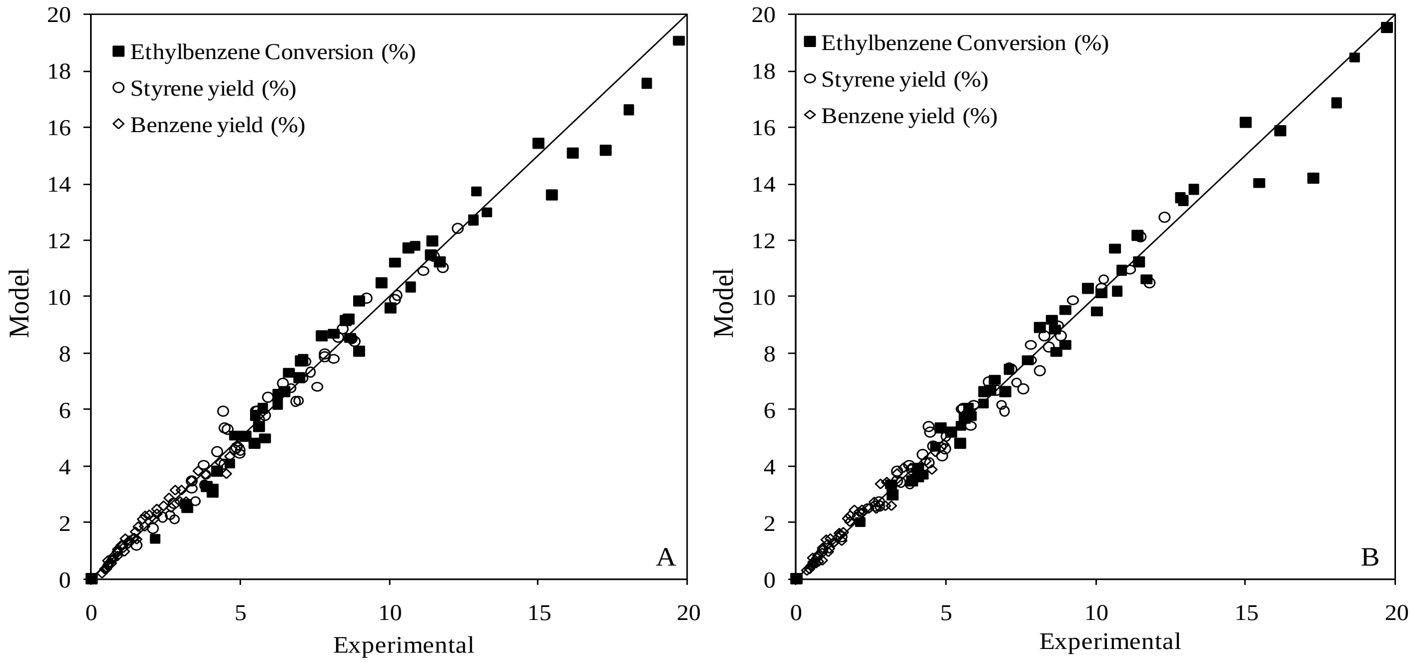

Figure 4.9. Overall comparison between the experimental results and model predictions of all HTs catalysts for scheme 1: A) RC model, B) TOS model

4.2 Ethylbenzene dehydrogenation over Fe_2O_3/Al_2O_3

4.2.1. Catalyst characterization

4.2.1.1 N_2 adsorption-desorption isotherm

The N_2 adsorption-desorption isotherm for all the Fe_2O_3/Al_2O_3 samples calcined at 550 °C is shown in Fig 4.10. All samples show typical type IV isotherms with H1 hysteresis loops characteristic of mesoporous materials suggesting their uniform cylindrical pores [82]. The condensation step observed over mesoporous alumina doped with iron is steeper and greater compared to the conventional alumina support for iron. This indicates uniformity of mesopores having a large pore volume as seen in Table 4.10. All samples possessed mesoporosity and high specific surface area, as inferred from nitrogen isotherms.

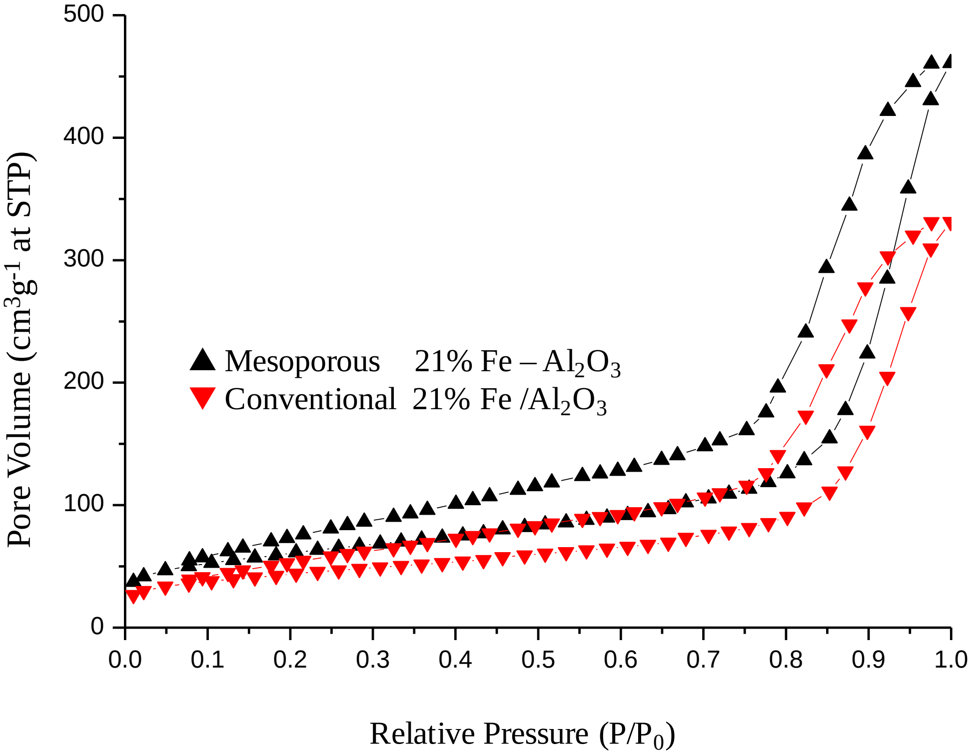

Figure 4.10. N_2 adsorption-desorption isotherm

Table 4.10. Physical and structural properties of Fe_2O_3/Al_2O_3

Sample	21% Fe /conventional alumina	21% Fe /Meso. alumina
S_{BET} (m^2/g)	116	225
Total Pore Volume (cc/g)	0.23	0.66
Average Pore Diameter (nm)	5.80	11.0

4.2.1.2 X-ray Diffraction patterns

XRD patterns of mesoporous alumina, obtained by self-induced evaporation methods reveal no evidence of crystalline alumina phase. Yuan et al. has attributed this occurrence to the presence of γ-Al_2O_3 which only crystallizes at higher calcinations temperature (> 700 °C) while peaks which are attributed to the presence of crystalline alumina phase were observed on the pure conventional Al_2O_3. When loaded with 21%Fe by both direct and post synthesis methods, the XRD patterns were similar to that of the pure alumina support, however indistinctive reflections were noticed on iron doped on alumina by post synthesis method. This depicts that the metal specie were homogeneously distributed over mesoporous alumina support irrespective of the preparation method. XRD analysis of the conventional Al_2O_3 doped with 21%Fe indicates the presence of bulk Fe_2O_3 phase. The sample exhibits well defined reflections which are assigned to Fe_2O_3.

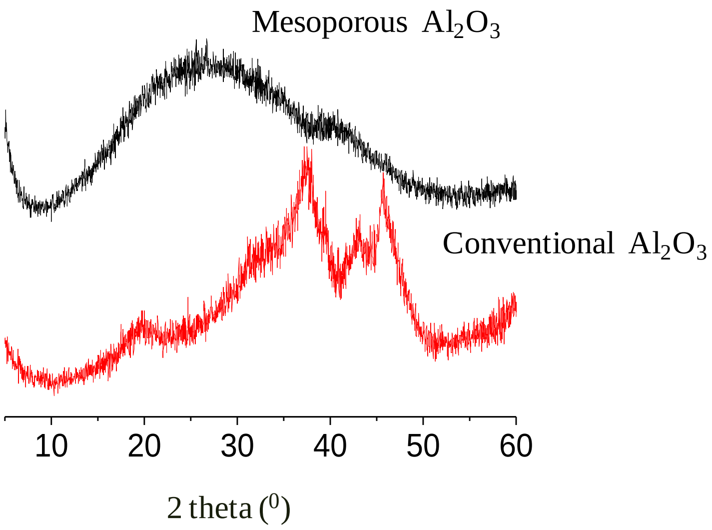

Figure 4.11a. XRD pattern of pure alumina support

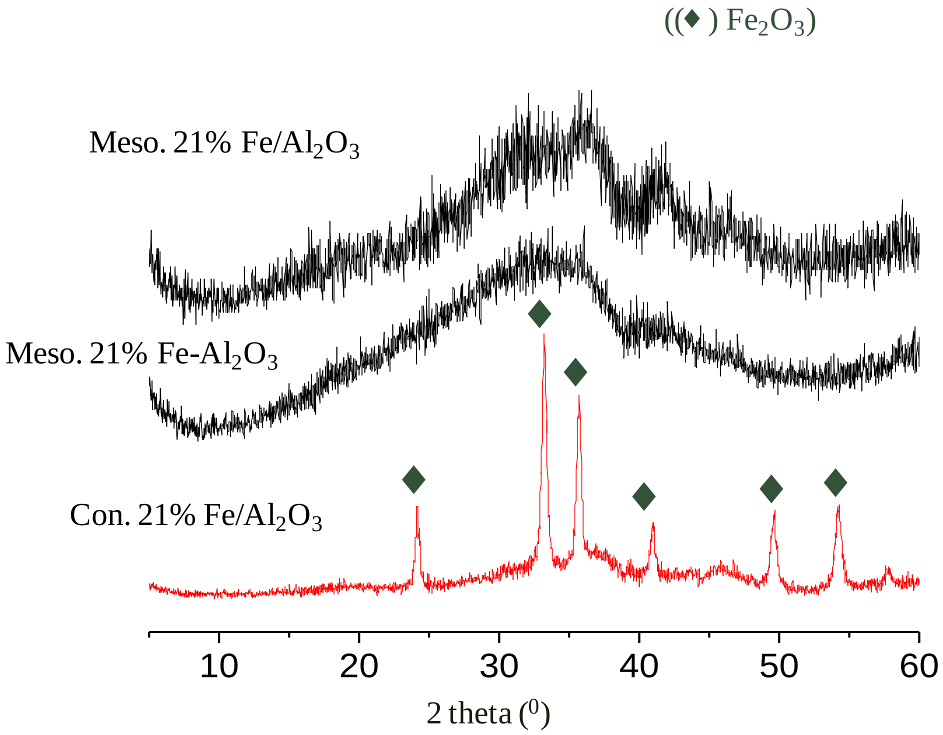

Figure 4.11b. XRD pattern of 21%Fe doped on alumina support

4.2.1.3 Transmission Electron Microscopy (TEM)

The TEM image of iron supported on mesoporous alumina reveals alternate white and dark patches which confirm the presence of high fraction of highly dispersed active iron surface species which has also been suggested from the results of the XRD. The three white diagonal lines show the particle size distance approximately to be 9 nm. This value is close to the pore diameter estimated from the N_2 adsorption isotherm. This further confirms the periodic ordering of the catalyst resulting from self assembly by the pore directing agent. In addition to the high degree of order, the supported Fe on mesoporous alumina possessed large and uniform mesopores as well as high specific surface area as obtained from nitrogen adsorption isotherm. The selective area electron diffraction (SAED) pattern (insert in Figures 4.12a & 4.12b) of the ordered mesostructure domains indicates the presence of crystalline Fe_2O_3 phase. Additional proof of the crystallinity of this specie is given by high resolution TEM image (Figure 4.12b) which reveals the existence of crystalline nanoparticles of Fe_2O_3. Bulk Fe_2O_3 phase obtained from XRD analysis of Fe supported on conventional was also confirmed by the TEM image shown in Figure 4.12b.

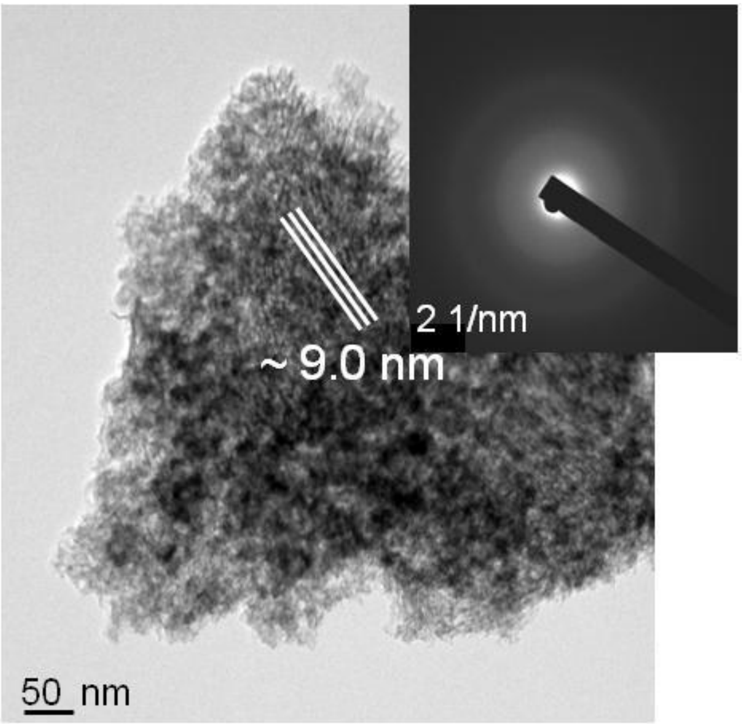

Figure 4.12a. Mesoporous alumina doped with iron

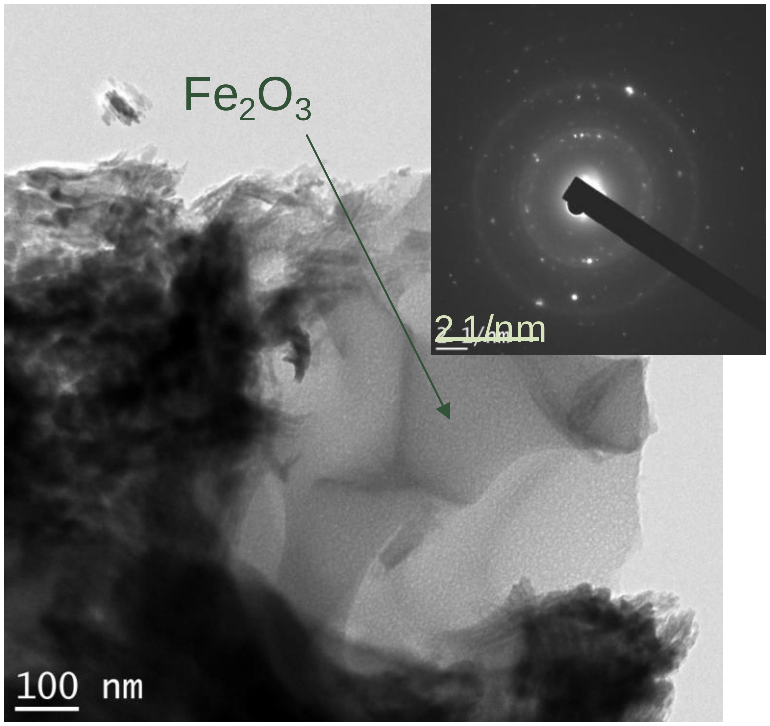

Figure 4.12b. Conventional alumina doped with iron

4.2.2. Catalyst Activity

All the catalysts examined enhanced the formation of styrene which was the major product of the reaction whereas benzene was a minor by-product. Toluene and gaseous hydrocarbons were observed in trace amounts. The catalytic activities of all the catalysts at different reaction conditions are shown in Tables 4.11 – 4.13. 21%Fe-org.Al_2O_3 (one-pot) catalyst gave the highest activity with a maximum conversion of ~22.9 % at 550 °C for a reaction time of 20 s. However, it has a maximum yield of 18.3% towards styrene at 450 °C for a reaction time of 20 s at temperatures above 450 °C, the yield of styrene decreases with increase in benzene yield. This similar trend was observed in other catalysts as depicted in Figure 4.13. Though for the iron supported on conventional alumina catalyst, at 550 °C the yield was slightly higher than 450 °C, selectivity towards styrene was better at 450 °C. Thus, it can be concluded that for all the catalysts investigated a temperature of 450 °C appears to be an optimum for maximizing the yield of styrene. From Figure 4.13, it is evident that irrespective of the method employed in preparing the iron supported on organized alumina, a better styrene yield was obtained as compared to the conventional alumina doped with iron. This was mainly attributed to the presence of high fraction of highly dispersed active iron surface species as suggested by XRD patterns, TEM and XPS measurements.

Table 4.11

Product distribution at various reaction conditions for the dehydrogenation of ethylbenzene over 21%Fe-meso.Al_2O_3 (one pot) catalyst

Temp (°C)	Reaction time (s)	EB Conv. (%)	Styrene	Benzene	Toluene	Gases	DEB
350	5	7.85	7.74	0.11	-	-	-
	10	10.46	10.34	0.12	-	-	-
	15	12.71	12.57	0.14	-	-	-
	20	16.40	16.26	0.14	-	-	-
400	5	9.34	9.18	0.14	-	-	-
	10	13.50	13.19	0.18	-	-	-
	15	16.32	16.14	0.22	-	-	-
	20	17.59	17.35	0.24	-	-	-
450	5	11.96	11.65	0.31	-	-	-
	10	16.39	15.68	0.63	0.08	-	-
	15	18.22	17.23	0.88	0.11	-	-
	20	19.50	18.28	1.07	0.15	0.05	-
500	5	9.42	8.51	0.82	0.08	-	-
	10	14.14	12.66	1.32	0.16	-	-
	15	17.41	15.35	1.83	0.22	-	-
	20	19.84	16.14	3.25	0.40	0.05	-
550	5	10.89	9.06	1.67	0.16	-	-
	10	15.11	11.62	3.01	0.39	0.09	-
	15	18.08	13.47	3.94	0.54	0.12	-
	20	22.93	14.87	6.23	0.88	0.24	-

Table 4.12

Product distribution at various reaction conditions for the dehydrogenation of ethylbenzene over 21%Fe/meso.Al_2O_3 (impregnation) catalyst

Temp (°C)	Reaction time (s)	EB Conv. (%)	Styrene	Benzene	Toluene	Gases	DEB
350	5	5.27	5.06	0.20	-	-	-
	10	7.73	7.45	0.28	-	-	-
	15	10.01	8.64	0.31	-	-	-
	20	10.03	9.75	0.29	-	-	-
400	5	7.63	7.29	0.34	-	-	-
	10	10.25	9.88	0.37	-	-	-
	15	11.61	11.16	0.45	-	-	-
	20	13.22	12.47	0.47	-	-	-
450	5	7.95	7.38	0.53	0.05	-	-
	10	11.02	10.30	0.65	0.07	-	-
	15	12.91	12.00	0.83	0.09	-	-
	20	14.44	13.03	1.07	0.12	0.06	0.05
500	5	8.37	7.08	1.01	0.12	0.08	-
	10	11.46	9.85	1.29	0.16	0.09	-
	15	13.72	11.90	1.43	0.18	0.08	-
	20	14.63	11.93	2.14	0.30	0.12	0.09
550	5	7.48	5.56	1.54	0.19	0.12	-
	10	11.82	8.96	2.34	0.32	0.14	-
	15	14.73	11.42	2.79	0.38	0.14	-
	20	20.74	14.16	5.04	0.85	0.36	0.09

Table 4.13

Product distribution at various reaction conditions for the dehydrogenation of ethylbenzene over 21%Fe-con.alumina (impregnation) catalyst

Temp (°C)	Reaction time (s)	EB Conv. (%)	Styrene	Benzene	Toluene	Gases	DEB
350	5	3.32	3.12	0.20	-	-	-
	10	3.96	3.75	0.21	-	-	-
	15	4.81	4.43	0.22	-	-	-
	20	6.17	5.06	0.25	-	-	-
400	5	6.00	5.79	0.21	-	-	-
	10	7.50	7.25	0.25	-	-	-
	15	9.20	8.92	0.27	-	-	-
	20	10.33	10.02	0.30	-	-	-
450	5	7.96	7.65	0.32	-	-	-
	10	11.81	11.23	0.52	0.07	-	-
	15	12.16	11.46	0.62	0.08	-	-
	20	14.13	13.10	0.76	0.11	0.05	-
500	5	7.25	6.66	0.52	0.07	-	-
	10	9.41	8.41	0.76	0.11	0.06	-
	15	12.34	11.03	1.05	0.17	0.09	0.04
	20	16.20	14.18	1.55	0.26	0.13	0.07
550	5	9.58	8.16	1.13	0.20	0.09	-
	10	13.96	11.54	1.81	0.34	0.14	0.05
	15	16.63	13.33	2.47	0.50	0.19	0.07
	20	22.74	18.16	3.44	0.76	0.28	0.09

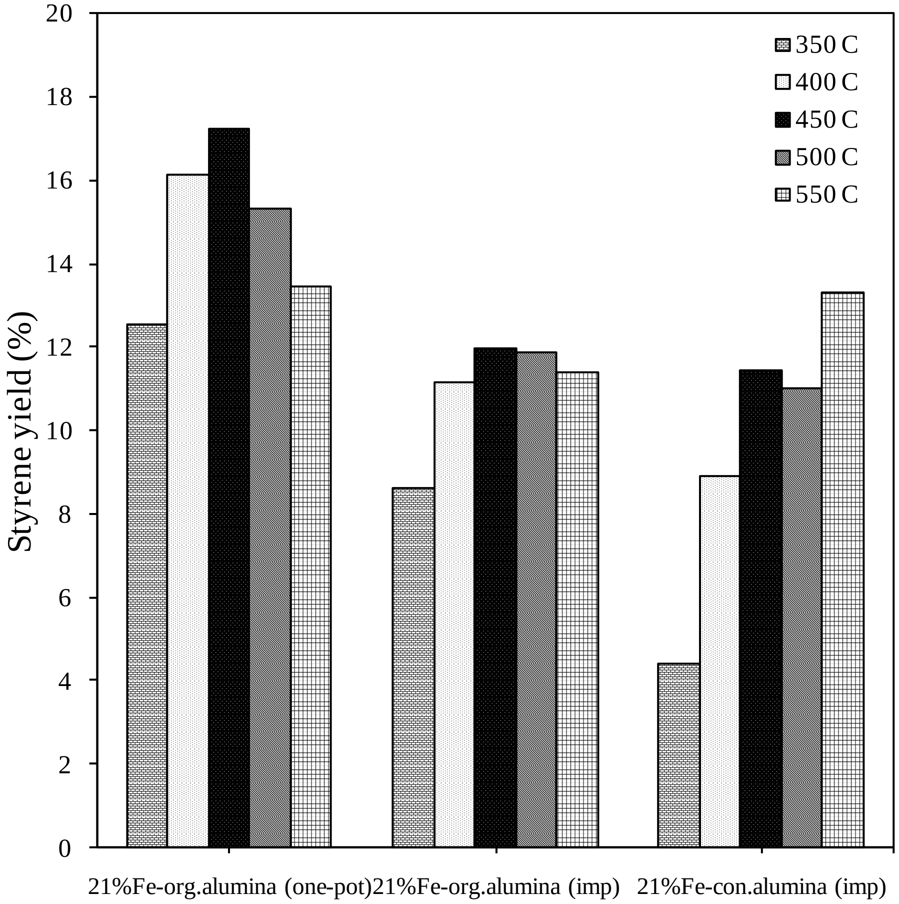

Figure 4.13. Comparison of styrene yield for all reaction temperatures over Fe_2O_3/Al_2O_3

The effect of reaction time and temperature on EB conversion over all the catalysts is shown in Figure 4.14(A – C). It is evident from the Figures that EB conversion increases with both reaction temperature and time. Table 4.14 summarizes the effect of reaction temperature on the catalytic properties of all the catalysts. The dehydrogenation activity increases significantly with the increase of temperature, but the styrene selectivity decreased. The amount of benzene in the reaction product is increased, showing that cracking reaction is favored at higher temperature. Under similar reaction conditions, iron-oxide doped on organized alumina catalysts seem even more active for EB dehydrogenation than the $Mg_3Fe_{0.25}Me_{0.25}Al_{0.5}$ (*Me* = Co, Mn, Ni) hydrotalcite catalysts reported earlier.

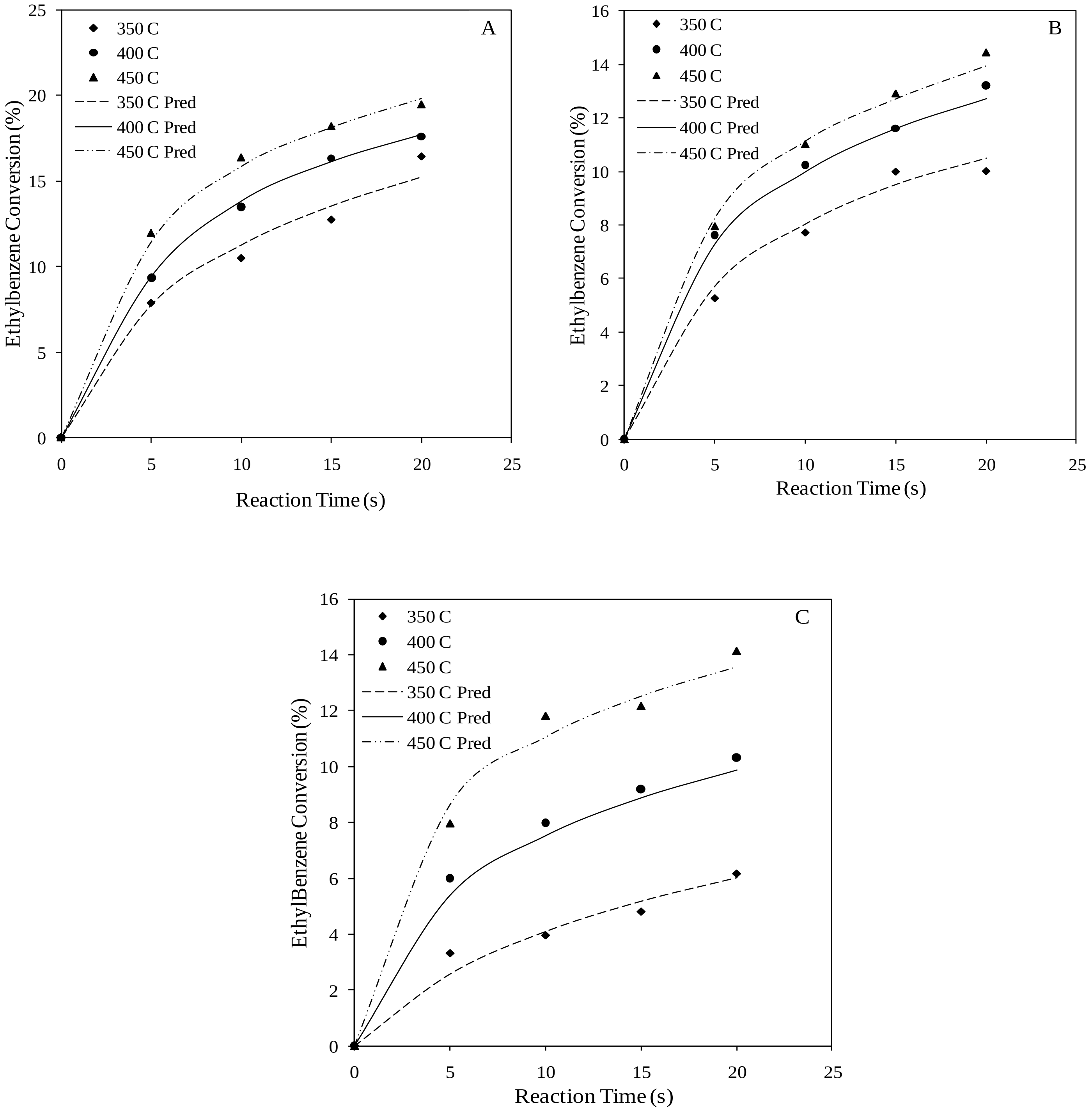

Figure 4.14. Effect of reaction condition on ethylbenzene conversion (Mechanism I) over: A) 21%Fe-meso.Al_2O_3 (one-pot), B) 21%Fe/meso.Al_2O_3 (impregnation), C) 21%Fe-con. Al_2O_3 (impregnation)

Table 4.14

Effects of reaction temperature on catalytic properties of iron doped mesoporous alumina catalysts

	21%Fe-meso.Al_2O_3 (one-pot)			21%Fe/meso.Al_2O_3 (imp)			21%Fe-con.Al_2O_3 (imp)		
Temp (°C)	EB conv. (%)	St. selectivity (%)	Bz. selectivity (%)	EB conv. (%)	St. selectivity (%)	Bz. selectivity (%)	EB conv. (%)	St. selectivity (%)	Bz. selectivity (%)
350	16.4	99.1	0.8	10.0	97.2	2.9	6.2	82.1	4.0
400	17.6	98.6	1.4	13.2	94.3	3.6	10.3	97.0	2.9
450	19.5	93.7	5.5	14.4	90.2	7.4	14.1	92.7	5.4
500	19.8	81.4	16.4	14.6	81.5	14.6	16.2	87.5	9.6
550	22.9	64.8	27.2	20.7	68.3	24.3	22.0	78.6	16.1

Reaction conditions: catalyst/feed ratio = 5; reaction time = 20 s

4.2.3. Kinetic Modeling

4.2.3.1. Model development

In addition to the main dehydrogenation reaction (equation 4.21), the side reactions (equations (4.22) – (4.23)) are also known to take place

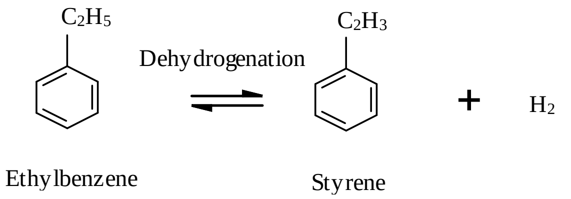

(4.21)

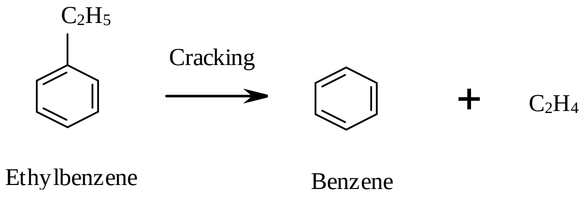

(4.22)

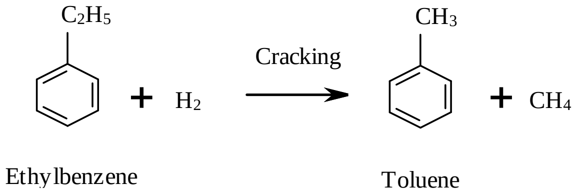

(4.23)

A reaction scheme for EB dehydrogenation is given as scheme 1. To develop a suitable kinetic model based on the product distribution, two mechanisms are postulated to represent the disappearance of EB: one mechanism for low temperature range (350 – 450 °C), and another for the complete temperature range. Scheme 2 was adapted for the low temperature range whereby formation of both toluene and benzene were negligible while overall temperature range adopts scheme 3 in which formation of benzene is considered significant, however toluene is still negligible. Reaction schemes 2 and 3 will be employed to obtain the kinetic parameters of scheme 1.

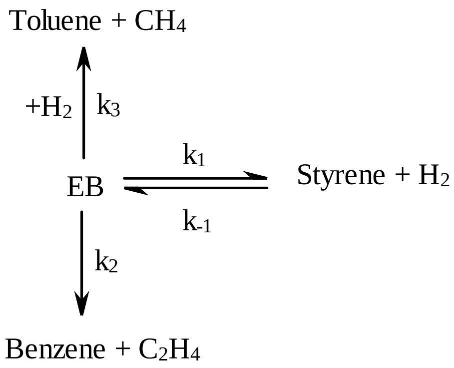

scheme 1

Scheme 1 Catalytic reaction scheme of ethylbenzene (EB) dehydrogenation

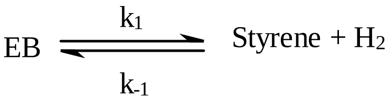

scheme 2

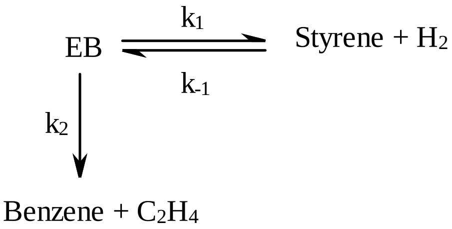

scheme 3

(a) Scheme 2: Low Temperatures. At low temperatures (350 – 450 °C), the experimental results were modeled using steady-state approximations and considering catalyst decay to be a function of reactant conversion (RC). The following catalytic reactions were utilized:

Rate of disappearance of ethylbenzene, r_{EB}

$$-\frac{V}{W_c}\frac{dC_{EB}}{dt} = (k_1 C_{EB} - k_{-1} C_{ST} C_H) exp(-\lambda(1 - y_{EB}) \tag{4.24}$$

Rate of formation of styrene, r_{ST}

$$\frac{V}{W_c}\frac{dC_{ST}}{dt} = (k_1 C_{EB} - k_{-1} C_{ST} C_H) exp(-\lambda(1 - y_{EB}) \tag{4.25}$$

(b) Scheme 3: Low and High Temperatures. This is a comprehensive model covering the complete temperature considered in the study (i.e., 350 – 550 °C). This was also modeled using the steady-state approximations and considering catalyst decay to be function of RC. This scheme takes into account cracking of ethylbenzene to benzene, however from the product distribution, toluene is negligible. Thus, the following set of species balances and catalytic reactions were utilized:

Rate of disappearance of ethylbenzene, r_{EB}

$$-\frac{V}{W_c}\frac{dC_{EB}}{dt} = (k_1 C_{EB} - k_{-1} C_{ST} C_H + k_2 C_{EB}) exp(-\lambda(1 - y_{EB}) \tag{4.26}$$

Rate of formation of styrene, r_{ST}

$$\frac{V}{W_c}\frac{dC_{ST}}{dt} = (k_1 C_{EB} - k_{-1} C_{ST} C_H) exp(-\lambda(1 - y_{EB}) \tag{4.25}$$

Rate of formation of benzene, r_B

$$\frac{V}{W_c}\frac{dC_B}{dt} = k_2 C_{EB} exp(-\lambda(1 - y_{EB}) \tag{4.27}$$

where C_{EB} is the concentration of ethylbenzene, C_{ST} is the concentration of styrene, C_H is the concentration of hydrogen, C_B is the concentration of benzene in the riser simulator, V is the volume of the riser (45 cm^3), W_c is the mass of the catalyst (0.81 g-cat), t, the time (in seconds), λ, the deactivation constant, and k is the rate constant (cm^3/(g-cat·s)). The measurable variables from our chromatographic analysis are the weight fractions of the species, y_i, in the system. By definition, the molar concentration, C_i, of every species in the system can be related to its mass fraction, y_i, by the following relation:

$$C_i = \frac{y_i W_{hc}}{MW_i V} \tag{4.28}$$

where W_{hc} is the weight of feedstock injected into the reactor, MW_i is the molecular weights of the individual specie i in the system, and V is the volume of the riser simulator.

To ensure thermodynamic consistency at equilibrium, the temperature dependent equilibrium constant for the reversible reaction was found to be:

$$K_C = \frac{k_1}{k_{-1}} \tag{4.29}$$

which has been calculated from literature as [32]:

$$K_C = \exp\left\{-\left(\frac{122700 - 126.3\mathrm{T} - 2.194 \times 10^{-3}\mathrm{T}^2}{\mathrm{RT}}\right)\right\} \times 10^5\ Pa \tag{4.30}$$

Substituting eqs 4.28 and 4.29 into eqs 4.24-4.27, we have the following first order differential equations expressed in terms of weight fractions, which are the measurable variables from gas chromatographic analysis:

$$\frac{dy_{EB}}{dt} = -k_1\left(y_{EB} - A_1\frac{y_{ST}y_H}{K_C}\right)\frac{W_c}{V}\exp(-\lambda(1 - y_{EB}) \tag{4.31}$$

$$\frac{dy_{ST}}{dt} = k_1\left(A_2 y_{EB} - A_3\frac{y_{ST}y_H}{K_C}\right)\frac{W_c}{V}\exp(-\lambda(1 - y_{EB}) \tag{4.32}$$

$$\frac{dy_{EB}}{dt} = -\left[k_1\left(y_{EB} - A_1\frac{y_{ST}y_H}{K_C}\right) + k_2 y_{EB}\right]\frac{W_c}{V}\exp(-\lambda(1 - y_{EB}) \tag{4.33}$$

$$\frac{dy_B}{dt} = A_4 k_2 y_{EB}\frac{W_c}{V}\exp(-\lambda(1 - y_{EB}) \tag{4.34}$$

A_1, A_2, A_3, and A_4 are lumped constants given as:

$$A_1 = \frac{MW_{EB}W_{hc}}{MW_{ST}MW_H V}$$

$$A_2 = \frac{MW_{ST}}{MW_{EB}}$$

$$A_3 = \frac{W_{hc}}{MW_H V}$$

$$A_4 = \frac{MW_B}{MW_{EB}}$$

The temperature dependence of the rate constants was represented with the centered temperature form of the Arrhenius equation, i.e.,

$$k_i = k_{0i} exp\left[-\frac{E_i}{R}\left(\frac{1}{T} - \frac{1}{T_0}\right)\right] \tag{4.35}$$

where T_o is an average temperature introduced to reduce parameter interaction [79], k_{oi} is the rate constant for reaction *i* at T_o, and E_i is the activation energy for reaction *i*. Since the experimental runs were done at temperature ranges 350 – 450 °C and 350 – 550 °C for both scheme 2 and scheme 3 respectively, T_o was calculated to be 400 °C and 450°C.

The above reaction model equations were derived based on the following assumptions:

1. Catalyst deactivation was assumed to be a function of reactant conversion. And, a single deactivation function was defined for all the reactions.
2. The model assumes on catalytic reactions and neglects thermal conversion.
3. The reactor operates under isothermal conditions, justified by the negligible temperature change observed during the reaction.
4. Toluene yield is negligible.

4.2.3.2. Determination of Model Parameters

The kinetic parameters in equations 4.31-4.34 were estimated using non-linear regression analysis. This was achieved using MATLAB package. The values of the preexponential factors, activation energies and deactivation constants of mechanism I with their corresponding 95% confidence limits are shown in Table 4.15 while those of mechanism II are given in Table 4.17. Correlation matrices of the regression analysis are shown in Tables 4.16 and 4.18 for mechanism I and II respectively, depicting that the interaction between the parameters is at low and moderate level.

The activation energies for styrene formation of the iron doped on organized alumina catalysts obtained by direct and post synthesis methods were apparently lower than those of iron doped on conventional alumina in both schemes 2 and 3. Consequently, it is expected that the decrease in the activation energy for styrene formation, which was observed in iron doped organized alumina catalysts, will cause an increase in the rate of styrene formation which is in agreement with the experimental results. Iron doped organized alumina catalysts obtained by direct synthesis (21%Fe-org.alumina (one-pot)) has the least values of activation energy of 28.3 kJ/mol (6.76 kcal/mol) for styrene formation for the low temperature scheme while a further reduction of activation energy to 9.4 kJ/mol (2.25 kcal/mol) was estimated for the comprehensive temperature scheme. The apparent activation energies obtained for the cracking reaction are higher compared to those of dehydrogenation of EB to St. These estimated values are consistent with the experimental data, which shows higher yields of cracking products only at elevated temperatures. Therefore, high activation energy must be overcome for EB to crack to form benzene which is more than that required for dehydrogenation to form styrene.

Table 4.15

Estimated kinetic parameters for all the Fe_2O_3/Al_2O_3 catalyst based on reactant conversion model (Mechanism I)

Parameter	Value	95% CL
21%Fe-meso.Al_2O_3 (one pot)		
E_{x1} (kJ/mol)	28.3	2.02
$k_{0i}^{a} \times 10^{3}$ [m^3/(kg of catalyst .s)]	2.47	0.21
λ	13.94	0.82
21%Fe/meso.Al_2O_3 (impregnation)		
E_{y1} (kJ/mol)	29.29	3.46
$k_{0i}^{a} \times 10^{3}$ [m^3/(kg of catalyst .s)]	2.18	0.33
λ	23.1	2.06
21%Fe-con.Al_2O_3 (impregnation)		
E_{z1} (kJ/mol)	82.46	5.12
$k_{0i}^{a} \times 10^{3}$ [m^3/(kg of catalyst .s)]	1.35	0.17
λ	25.39	2.1

[a] Pre-exponential factor as obtained from eq. (4.35); unit for second order (m^6/(kg of catalyst).s).

Table 4.16

Correlation matrix for ethylbenzene dehydrogenation over all the Fe_2O_3/Al_2O_3 catalyst based on reactant conversion model (Mechanism I)

	k_1	E_1	λ
21%Fe-meso.Al_2O_3 (one pot)			
k_{x1}	1.0000	0.4978	0.9745
E_{x1}	0.4978	1.0000	0.5139
λ	0.9745	0.5139	1.0000
21%Fe/meso.Al_2O_3 (impregnation)			
k_{y1}	1.0000	0.5127	0.9775
E_{y1}	0.5127	1.0000	0.5245
λ	0.9775	0.5245	1.0000
21%Fe-con.Al_2O_3 (impregnation)			
k_{z1}	1.0000	0.7944	0.9723
E_{z1}	0.7944	1.0000	0.8423
λ	0.9723	0.8423	1.0000

Table 4.17

Estimated kinetic parameters for all the Fe_2O_3/Al_2O_3 catalyst based on reactant conversion model (Mechanism II)

Parameters	Values		
	k_1	k_2	λ
21%Fe-org.Al_2O_3 (one pot)			
E_{xi} (kJ/mol)	9.42	105.62	12.28
95% CL	1.72	20.27	1.02
$k_{0i}^{a} \times 10^3$ [m^3 / (kg of catalyst.s)]	2.19	0.12	
95% CL	0.24	0.05	
21%Fe/org.Al_2O_3 (impregnation)			
E_{yi} (kJ/mol)	13.08	68.6	13.3
95% CL	2.21	17.1	1.58
$k_{0i}^{a} \times 10^3$ [m^3 / (kg of catalyst.s)]	1.24	0.13	
95% CL	0.16	0.04	
21%Fe-con.alumina (impregnation)			
E_{zi} (kJ/mol)	40.31	97.2	14.07
95% CL	3.78	28.75	1.87
$k_{0i}^{a} \times 10^3$ [m^3 / (kg of catalyst.s)]	1.09	0.08	
95% CL	0.15	0.04	

[a] Pre-exponential factor as obtained from eq. (4.35); unit for second order (m^6/(kg of catalyst).s).

Table 4.18

Correlation matrix for ethylbenzene dehydrogenation over all the Fe_2O_3/Al_2O_3 catalyst based on reactant conversion model (Mechanism II)

	k_1	E_1	k_2	E_2	λ
21%Fe-meso.Al_2O_3 (one pot)					
k_{x1}	1.0000	0.4653	0.2353	0.0799	0.9732
E_{x1}	0.4653	1.0000	0.1109	0.0812	0.4538
k_{x2}	0.2353	0.1109	1.0000	-0.9129	0.2210
E_{x2}	0.0799	0.0812	-0.9129	1.0000	0.0907
λ	0.9732	0.4538	0.2210	0.0907	1.0000
21%Fe/meso.Al_2O_3 (impregnation)					
k_{y1}	1.0000	0.5187	0.3316	0.1156	0.9698
E_{y1}	0.5187	1.0000	0.1942	0.0884	0.5224
k_{y2}	0.3316	0.1942	1.0000	-0.7948	0.3349
E_{y2}	0.1156	0.0884	-0.7948	1.0000	0.1126
λ	0.9698	0.5224	0.3349	0.1126	1.0000
21%Fe-con.Al_2O_3 (impregnation)					
k_{z1}	1.0000	0.7278	0.1933	0.1469	0.9648
E_{z1}	0.7278	1.0000	0.1861	0.1160	0.7848
k_{z2}	0.1933	0.1861	1.0000	-0.8790	0.2032
E_{z2}	0.1469	0.1160	-0.8790	1.0000	0.1373
λ	0.9648	0.7848	0.2032	0.1373	1.0000

From the estimated parameters for both mechanisms I and II, organized alumina favorably supports the active specie and this accounts for the low activation energies as compared to the conventional alumina as support. The activity of all the Fe_2O_3/Al_2O_3 compared to the $Mg_3Fe_{0.25}Me_{0.25}Al_{0.5}$ (Me = Co, Mn, Ni) catalysts shows better performance, which can be attributed to the orderliness of the mesopores of the alumina support. Amongst the Fe_2O_3/Al_2O_3 catalysts, iron doped organized alumina catalysts showed improvement in the dehydrogenation of EB to styrene, and the direct synthesis method best modifies the catalyst activity and selectivity.

Validity check of the estimated parameters was done by substituting the values in the developed model and then solved numerically using fourth order Runge-Kutta routine. Figure 4.15(A,B) show the reconciliation plots of the model predictions compared to experimental data for schemes 2 and 3 respectively. The plot shows an excellent fit of the experimental data and a regression coefficient, r^2 (0.99), was achieved.

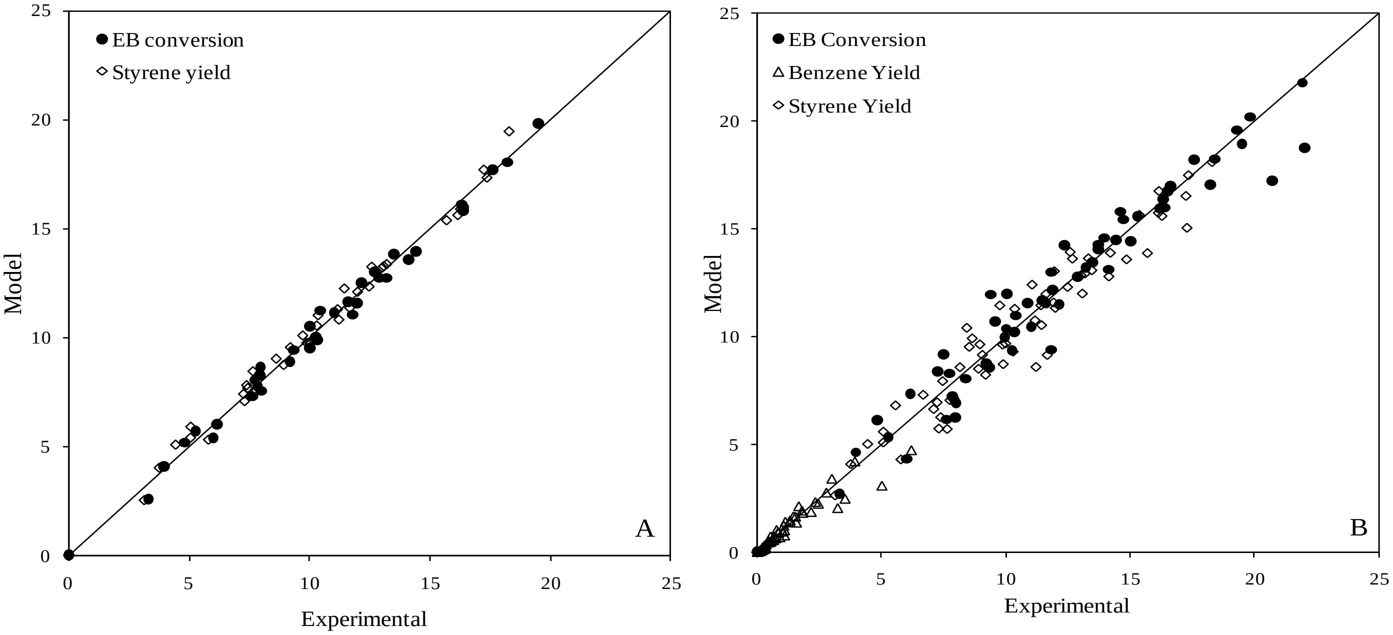

Figure 4.15. Overall comparison between the experimental results and model predictions of all the catalysts for: A) scheme 2, B) scheme 3

CHAPTER 5

5.0 CONCLUSIONS AND RECOMMENDATIONS

5.1 Conclusions

The catalytic dehydrogenation of ethylbenzene into styrene was investigated in a fluidized bed (novel riser simulator) over hydrotalcite and Fe_2O_3/Al_2O_3 catalysts in the absence of steam. These catalysts were synthesized and characterized and their activities were compared to the commercial catalyst under similar operating conditions. The synthesized catalysts exhibited high surface area and mesopore character. The finely dispersed active species on the catalyst enhanced the catalytic activity and this led to improved efficiency of the process. In addition to catalyst design, change in reactor configuration from conventionally used fixed bed reactor to fluidized bed was explored. Fluidization as a result of high gas recirculation led to a more uniform product distribution due to elimination of temperature gradient which can adversely affect the product quality. Furthermore lowering the reaction temperature and short reaction time limits considerably the occurrence of undesirable reactions due to thermal cracking and suppressed coking on the catalysts.

Among the series of catalysts synthesized for ethylbenzene dehydrogenation Fe_2O_3/Al_2O_3 catalyst prepared by direct synthesis of loading iron on mesoporous alumina support (21%Fe-meso.Al_2O_3) exhibits the highest activity and selectivity. The results of the XRD, TEM and XPS clearly attribute the presence of highly dispersed active specie over large catalyst surface area to have increased the active sites of the catalyst which play a role in H-abstraction from hydrocarbons especially β-hydrogen from ethylbenzene. Ethylbenzene conversion of 19.5% was achieved with a styrene selectivity of ~94% at reaction temperature of 450 °C and reaction time of 20 s.

Kinetic modeling of the dehydrogenation process was carried out to determine parameters such as activation energy and rate constants. The significance of the model was ascertained by the correlation matrix which indicated low and moderate parameter interaction. The estimated kinetic parameters also had a tolerable confidence limit, and an excellent fit of the experimental data was obtained. These results confirmed the observed product distribution over the catalysts which have been attributed to the catalyst composition.

5.2 Recommendations

Based on the results of this study,

i. Adsorption kinetics of ethylbenzene dehydrogenation over the hydrotalcite and Fe_2O_3/Al_2O_3 catalyst should be investigated.

ii. Oxidative dehydrogenation of ethylbenzene to styrene using CO_2 as a soft oxidant over both catalyst systems.

iii. Detailed study of catalyst deactivation mechanism.

APPENDIX

Table A3.1: Retention time of different compounds in the GC

GC conditions

Flow rate of carrier gas (Helium): 20ml/min

Oven Temperature: programmed from 40°C to 250°C in 25 mins

Compounds	*Retention time (min)
Gaseous hydrocarbons	3.019-3.45
Ethylbenzene	13.114
Styrene	15.807
Benzene	8.607
Toluene	11.217
1,2 Diethylbenzene	16.919
1,3 Diethylbenzene	16.452
1,4 Diethylbenzene	16.616

*Retention may vary slightly at different operating conditions

NOMENCLATURE

A_i	pre-exponential factor for the *i*th reaction (m^3/kg of catalyst .s)
C_i	concentration of specie *i* in the riser simulator (mol/m^3)
CL	confidence limit
E_i	apparent activation energy of the *i*th reaction (kJ/mol)
K_c	equilibrium constant
k_i	apparent rate constant for the *i*th reaction (m^3/kg of catalyst .s)
k_{oi}	pre-exponential factor for the *i*th reaction after re-parameterization (m^3/kg of catalyst .s)
MW_i	molecular weight of specie *i*
r^2	correlation coefficient
r_i	rate of reaction for species *i*
R	universal gas constant (kJ/kmol K)
t	reaction time (s)
T	reaction temperature (K)
T_o	average temperature of the experiment
V	volume of the riser (45 cm^3)
W_c	mass of the catalyst (0.81 g)
W_{hc}	total mass of the hydrocarbon injected the riser (0.162 g)
y_i	mass fraction of *i*th component

Greek Letters

λ	catalyst deactivation constant (RC model)
α	catalyst deactivation constant (TOS model)

Abbreviations

EB	ethylbenzene
Bz	benzene
cat	catalyst
con	conventional
conv	conversion
St	styrene

REFERENCES

[1] http://www.styreneforum.org/

[2]http://www.chemsystems.com/about/cs/news/items/PPE%20PCMD%20Styrenics%20 2009.cfm

[3] K. Tanabe, W. F. Hölderich, Industrial application of solid acid-base catalysts. Appl. Catal. A Gen. 181 (1999) 399-434.

[4] www.dequi.eel.usp.br/~barcza/EstirenoUOP.pdf

[5] J.P. Lange, C. M. A. M. Mesters, Mass transport limitations in zeolite catalysts: the dehydration of 1-phenyl-ethanol to styrene. Appl. Catal. A: Gen. 210 (2001) 247-255.

[6] Studies in surface science and catalysis 123 (1999) 29-80

[7] F. Buonomo, R. Iezzi, E. Micheli, D. Sanfilippo, Catalytic system and process for dehydrogenating ethylbenzene to styrene, US Patent 5,994,258, 1999.

[8] F. Buonomo, G. Donati, E. Micheli, L. Tagliabue, Process for the production of styrene, US Patent 6,031,143, 2000

[9] H. Hattori, Heterogeneous basic catalysis. Chem. Rev. 95 (1995) 537-558.

[10] Brownstein, A. M., "Chem. Indus. Ser. 5, Catalysis of Organic Reactions," Moser, New York, 1981.

[11] http://www.freepatentsonline.com/4851599.html

[12] Y. Jin, W. Liang, Z. Wang, Z. Yu, E. Min, M. He, Z. Da, Aromatic hydrocarbons alkylation and liquid-solid circulating fluidized bed for alkylation, US Patent 5,789,640 (1998).

[13] Griesbaum K. *et al.* (1989) *Hydrocarbons*, in: *Ullmann's encyclopedia of industrial chemistry*, Weinheim, VCH, 1985-1996, 37v.; v. A13, 227-281.

[14] E. H. Lee, Iron oxide catalysts for dehydrogenation of ethylbenzene in the presence of steam, Catal. Rev. Eng. Sci. 8 (1973) 285-305.

[15] F. Cavani, F. Trifirò, Alternative processes for the production of styrene. Appl. Catal. A 133 (1995) 219-239.

[16] N. Mimura, I. Takahara, M. Saito, T. Hattori, K. Ohkuma, M. Ando, Dehydrogenation of ethylbenzene over iron oxide-based catalyst in the presence of carbon dioxide. Catal. Today, 45 (1998) 61-64.

[17] Kearby, K. K. (to Standard Oil Development Company) U.S. Patent 2426829, Sept 2, 1947

[18] T. Hirano, Roles of potassium in potassium-promoted iron-oxide catalyst for dehydrogenation of ethylbenzene. Appl. Catal. 26 (1986) 65-79.

[19] T. Hirano, Dehydrogenation of ethylbenzene over potassium-promoted iron oxide containing cerium and molybdenum oxides. Appl. Catal. 28 (1986) 119-132.

[20] M. Muhler, J. Schütze, M. Wesemann, T. Rayment, A. Dent, R. Schlögl, G. Ertl. Nature of the iron oxide-based catalyst for dehydrogenation of ethylbenzene to styrene. 1. Solid-state chemistry and bulk characterization. J. Catal. 126 (1990) 339-360.

[21] E. H. Lee, L. H. Holmes Jr., Effect of alkali and alkaline earth promoters on iron oxide catalysts for dehydrogenation of ethylbenzene in the presence of steam. J. Phys. Chem. 67 (1963) 947-949.

[22] S. C. Ndlela, B. H. Shanks, Reducibilty of potassium-promoted iron oxide under hydrogen conditions. Ind. Eng. Chem. Res. 42 (2003) 2112-2121.

[23] R. L. Hirsch, J. E. Gallagher, R. R. Lessard, R. D. Wesselhoft, Science 215 (1982) 121-127.

[24] S. -J. Liao, T. Chen, C. -X. Miao, W. -M. Yang, Z. -K. Xie, Q. -L. Chen, Effect of TiO_2 on the structure and catalytic behavior of iron-potassium oxide catalyst for dehydrogenation of ethylbenzene to styrene. Catal. Comm. 9 (2008) 1817-1821

[25] T. Hirano, Dehydrogenation of ethylbenzene on potassium-promoted iron-oxide catalysts containing magnesium oxide. Bull. Chem. Soc. Jpn. 59 (1986) 2672-2674

[26] G. R. Meima, P. G. Menon, Catalyst deactivation phenomena in styrene production Applied Catalysis A: Gen. 212 (2001) 239–245

[27] J. G. P. Sheel, C. M. Crowe, Simulation and optimization of an existing ethylbenzene dehydrogenation reactor. Can. J. Chem. Eng. 47 (1969) 183-187

[28] D. E. Clough, W. F. Ramirez, Mathematical modeling and optimization of the dehydrogenation of ethylbenzene to form styrene. *AIChE* J. 22 (1976) 1097-1105.

[29] S. S. E. H. Elnashaie, B. K. Abdalla, R. Hughes, Simulation of the Industrial Fixed-Bed Catalytic Reactor for the Dehydrogenation of Ethylbenzene to Styrene - Heterogeneous Dusty Gas-Model. Ind. Eng. Chem. Res. 32 (1993) 2537-2541.

[30] S. Carrà, L. Forni, Kinetics of catalytic dehydrogenation of ethylbenzene to styrene. Ind. Eng. Chem. Process Des. Dev. 4 (1965) 281–285.

[31] T. Hirano, Active Phase in Potassium-Promoted Iron-Oxide Catalyst for Dehydrogenation of Ethylbenzene. Appl. Catal. 26 (1986) 81-90.

[32] R. Dittmeyer, V. Höllein, P. Quicker, G. Emig, G. Hausinger, F. Schmidt, Factors Controlling the Performance of Catalytic Dehydrogenation of Ethylbenzene in Palladium Composite Membrane Reactors. Chem. Eng. Sci. 54 (1999) 1431–1439.

[33] A. Schüle, O. Shekhah, W. Ranke, R. Schlögl, G. Kolios, Microkinetic Modelling of the Dehydrogenation of Ethylbenzene to Styrene over Unpromoted Iron Oxides. J. Catal. 231 (2005) 172–180.

[34] W. J. Lee, G. F. Froment, Ethylbenzene dehydrogenation to styrene: kinetic modeling and reactor simulation. Ind. Eng. Chem. Res. 47 (2008) 9183–9194.

[35] K. Coulter, D. W. Goodman, R. G. Moore, Kinetics of the Dehydrogenation of Ethylbenzene to Styrene over Unpromoted and K Promoted Model Iron-Oxide Catalysts. Catal. Lett. 31 (1995) 1–8.

[36] W. P Addiego, C. A. Estrada, D. W. Goodman, M. P. Rosynek, R. G. Windham, An infrared study of the dehydrogenation of ethylbenzene to styrene over iron-based catalysts. J. Catal. 146 (1994) 407-414.

[37] H. Miura, R. Ansai, H. Kawai. Deuterium exchange reaction of ethylbenzene over an Fe_2O_3- K_2CO_3- Cr_2O_3 catalyst. React. Kinet. Catal. Lett. 53 (1994) 323-329.

[38] N. Dulamiţă, A. Măicăneanu, D. C. Sayle, M. Stanca, R. Crăciun, M. Olea, C. Afloroaei, A. Fodor, Ethylbenzene dehydrogenation on Fe_2O_3- K_2CO_3- Cr_2O_3 catalysts promoted with transitional metal oxides. Appl. Catal. A: General 287 (2005) 9-18.

[39] A. H. de Morais Batista, F. F. de Sousa, S. B. Honorato, A. P. Ayala, J. M. Filho, F. W. de Sousa, A. N. Pinheiro, J. C. S. de Araujo, R. F. Nascimento, A.

Valentini, A. C. Oliveira, Ethylbenzene to chemcials: catalytic conversion of ethylbenzene into styrene over metal-containing MCM-41. J. Mol. Catal. A: Chemical 315 (2010) 86-98.

[40] F. Cavani, F. Trifirò, A. Vaccari, Hydrotalcite-type anionic clays: Preparation, properties and applications. Catal. Today, 11 (1991) 173-301.

[41] A. Vaccari, Preparation and catalytic properties of cationic and anionic clays. Catal. Today 41 (1998) 53-71.

[42] J. L. Atwood, J. E. Davies, J. E. D. MacNicol D. D. Vogtle, F. Eds, In Comprehensive Supramolecular Chemistry. Pergamon Press: Oxford, U.K., 1996; Vol. 7, pp 251-91.

[43] D. P. Debecker, E. M. Gaigneaux, G. Busca, Exploring, tuning, and exploiting the basicity of hydrotalcites for applications in heterogeneous catalysis. Chem. Eur. J. 15 (2009) 3920-3935.

[44] Y. Liu, E. Lotero, J. G. Goodwin, X. Mo, Transesterification of poultry fat with methanol using Mg–Al hydrotalcite derived catalysts. Appl. Catal. A Gen. 331 (2007) 138-148.

[45] M. J. Climent, A. Corma, S. Iborra, K. Epping, A. Velty, Increasing the basicity and catalytic activity of hydrotalcites by different synthesis procedures. J. Catal. 225 (2004) 316–326.

[46] Y. Ohishi, T. Kawabata, T. Shishido, K. Takaki, Q. Zhang, Y. Wang, K. Nomura, K. Takehira, Mg-Fe-Al mixed oxides with mesoporous properties prepared from hydrotalcite as precursors: Catalytic behavior in ethylbenzene dehydrogenation. Appl. Catal. A Gen. 288 (2005) 220-231.

[47] R. J. Balasamy, A. Khurshid, A. A. S Al-Ali, L. A. Atanda, K. Sagata, H Yahiro, K. Nomura, T. Sano, K. Takehira, S. S. Al-Khattaf, Ethylbenzene dehydrogenation over binary FeO_x-MeO_y/Mg(Al)O catalysts derived from hydrotalcites. Appl. Catal. A Gen. 390 (2010) 225-234.

[48] R. J. Balasamy, B. B. Tope, A. Khurshid, A. A. S. Al-Ali, L. A Atanda, K. Sagata, M. Asamoto, H. Yahiro, K. Nomura, T. Sano, K. Takehira, S. S. Al-Khattaf, Ethylbenzene dehydrogenation over FeO_x/(Mg,Zn)(Al)O catalysts derived from hydrotalcites: Role of MgO as the catalyst support. Appl. Catal. A Gen. 398 (2011) 113-122.

[49] H. Pines, W. O. Haag, Alumina: Catalyst and Support. I. Alumina, its Intrinsic Acidity and Catalytic Activity. J. Am. Chem. Soc. 82 (1960) 2471-2483

[50] C. Misra *Industrial Alumina Chemicals*; ACS Monograph 184; American Chemical Society: Washington, DC, 1986.

[51] K. Wefers, C. Misra, Oxides and Hydroxides of Aluminum. Alcoa Technical Paper No. 19, Revised; Alcoa Laboratories: Alcoa Center, PA, 1987.

[52] J. S. Valente, X. Bokhimi, F. Hermandez, Physicochemical and Catalytic Properties of Sol−Gel Aluminas Aged under Hydrothermal Conditions**.** Langmuir, 19 (2003) 3583-3588

[53] J. Cejka, Organized mesoporous alumina: synthesis, structure and potential in catalysis. Appl. Catal. A Gen. 254 (2003) 327-338.

[54] Q. Liu, A. Q. Wang, X. H. Wang, W. D. Guo, T. Zhang, Synthesis, characterization and catalytic applications of mesoporous gamma-alumina from boehmite sol. Micropor. Mesopor. Mater. 111 (2008) 323-333.

[55] H. C. Lee, H. J. Kim, C. H. Rhee, K. H. Lee, S. H. Chung, Synthesis of nanostructured γ-alumina with a cationic surfactant and controlled amounts of water. Micropor. Mesopor. Mater. 79 (2005) 61-68.

[56] V. G. Pena, I. Diaz, C. M. Alvarez, Thermally stable mesoporous alumina synthesized with nonionic surfactants in the presence of amines. Micropor. Mesopor. Mater. 44 (2001) 203-210.

[57] Q. Liu, A. Q. Wang, X. D. Wang, Mesoporous gamma-alumina synthesized by hydro-carboxylic acid as structure-directing agent. Micropor. Mesopor. Mater. 92 (2006) 10-21.

[58] L. J. Wan, H. G. Fu, K. Y. Shi, X. Q. Tian, Facile synthesis of ordered nanocrystalline alumina thin films with tunable mesopore structure. Micropor. Mesopor. Mater. 115 (2008) 301-307.

[59] S. M. Kim, Y. J. Lee, K. W. Jun, J. Y. Park, H. S. Potdar, Synthesis of thermo-stable high surface area alumina powder from sol–gel derived boehmite. Mater. Chem. Phys. 104 (2007) 56-61.

[60] R. H. Zhao, F. Guo, Y. Q. Hu, Self-assembly synthesis of organized mesoporous alumina by precipitation method in aqueous solution. Micropor. Mesopor. Mater. 93 (2006) 212-216.

[61] P. Bai, W. Xing, Z. X. Zhang, Facile synthesis of thermally stable mesoporous crystalline alumina by using a novel cation-anion double hydrolysis method. Mater. Lett. 59 (2005) 3128-3131.

[62] X. Zhang, F. Zhang, K. Y. Chan, The synthesis of large mesopores alumina by microemulsion templating, their characterization and properties as catalyst support Mater. Lett. 58 (2004) 2872-2877.

[63] Q. Yuan, A. X. Yin, C. Luo, L. –D. Sun, Y. –W. Zhang, W. –T. Duan, H. –C. Liu, C. –H. Yan, Facile synthesis for ordered mesoporous γ-aluminas with high thermal stability. J. Am. Chem. Soc. 130 (2008) 3465-3472

[64] S. M. Morris, P. F. Fulvio, M. Jaroniec, Ordered mesoporous alumina-supported metal oxides. J. Am. Chem. Soc. 130 (2008) 15210-15216

[65] F. Huang, Y. Zheng, G. Cai, Y. Zheng, Y. Xiao, K. Wei, A new synthetic procedure for ordered mesoporous γ-alumina with a large surface area. Scripta Materialia 63 (2010) 339-342

[66] P. Michorczyk, P. Kuśtrowski, L. Chmielarz, J. Ogonowski, Influence of redox properties on the activity of iron oxide catalysts in dehydrogenation of propane with CO_2. React. Kinet. Catal. Lett. 82 (2004) 121-130

[67] G. Giecko, T. Borowiecki, W. Gac, J. Kruk, Fe_2O_3/Al_2O_3 catalysts for the N_2O decomposition in the nitric acid industry. Catal. Today 137 (2008) 403–409

[68] N. Mimura, M. Saito, Dehydrogenation of ethylbenzene to styrene over Fe_2O_3/Al_2O_3 catalysts in the presence of carbon dioxide. Catal. Lett. 58 (1999) 59–62

[69] de Lasa, H. Riser Simulator for Catalytic Cracking Studies. U.S. Patent 5,102,628, 1992

[70] J. Pruski, A. Pekediz, H. de Lasa, Catalytic cracking of hydrocarbons in a novel riser simulator. Lump adsorption parameters under reaction conditions, Chem. Engng. Sci. 51 (1996) 1799-1806.

[71] D.W. Kraemer, U. Sedran, H.I. de Lasa, Catalytic cracking kinetics in a novel riser simulator, Chem. Engng. Sci. 45 (1990) 2447–2452.

[72] S. Miyata, A. Okada, Synthesis of hydrotalcite-like compounds and their physicochemical properties-the systems Mg^{2+}-Al^{3+}-$SO^{2-}{}_4$ and Mg^{2+}-Al^{3+}-$CrO^{2-}{}_4$. Clays Clay Miner. 25 (1977) 14–18.

[73] R.D. Shannon, Revised effective ionic radii and systematic studies of interatomic distances in halides and chalcogenides. Acta Crystallogr. A 32 (1976) 751–767.

[74] X. Ge, M. Li, J. Shen, The reduction of Mg-Fe-O and Mg-Fe-Al-O complex oxides studied by temperature-programmed reduction combined with in situ mössbauer spectroscopy. J. Solid State Chem. 161 (2001) 38-44.

[75] D. Li, I. Atake, T. Shishido, Y. Oumi, T. Sano, K. Takehira, Self-regenerative activity of Ni/Mg(Al)O catalysts with trace Ru during daily start-up and shut-down operation of CH_4 steam reforming. J. Catal. 250 (2007) 299-312.

[76] A. Chen, H. Xu, Y. Yue, W. Hua, W. Shen, Z. Gao, Hydrogenation of methyl benzoate to benzaldehyde over manganese oxide catalysts prepared from Mg/Mn/Al hydrotalcite-like compounds. Appl. Catal. A 274 (2004) 101-109.

[77] T. Hirano, Dehydrogenation of ethylbenzene on potassium-promoted iron-oxide catalysts containing various transitional-metal oxides. Bull. Chem. Soc. Jpn. 59 (1986) 1653-1655.

[78] S. Al-Khattaf, H. de Lasa, Catalytic Cracking of Cumene in a Riser Simulator: A Catalyst Activity Decay Model. Ind. Eng. Chem. Res 40 (2001) 5398-5404.

[79] A. K. Agarwal, M. L. Brisk, Sequential experimental design for precise parameter estimation. 1. Use of reparameterization. Ind. Eng. Chem. Process Des. Dev. 24, (1985) 203-207.

[80] A. Voorhies, Carbon formation in catalytic cracking, Ind. Eng. Chem. Res. 37 (1945) 318–322.

[81] J. S. Valente, F. Figueras, M. Gravelle, P. Kumbhar, J. Lopez, J. P. Besse, Basic properties of the mixed oxides obtained by thermal decomposition of hydrotalcites containing different metallic compositions. J. Catal. 189 (2000) 370-381.

[82] M. Kruk, M. Jaroniec, Gas adsorption characterization of ordered organic-inorganic nanocomposite materials. Chem. Mater. 2001 13 (10) 3169-3183.

VITAE

NAME: **Luqman Abiola Atanda**

NATIONALITY: **Nigerian**

DATE OF BIRTH: **March 15, 1985**

PLACE OF BIRTH: **Ogun State, Nigeria**

EDUCATION:
B.Sc. Metallurgical and Materials Engineering (First Class)
University of Lagos, Akoka,
Nigeria, November 2007

M.Sc. Chemical Engineering (Distinction)
King Fahd University of Petroleum & Minerals, Dhahran,
Kingdom of Saudi Arabia, May 2011.

EMAIL ADDRESS:
abiola2kng@yahoo.com
abiolaxl@gmail.com

CONTACT ADDRESS:
7/9 Olabode Tomori Close, Idi-Aba, Abeokuta,
Ogun State, Nigeria

PHONE NUMBER: **+966535443431**